Vesicular trafficking dynamics enable context-dependent regulation of ErbB receptor activity and signaling

Dissertation

Zur Erlangung des akademischen Grades eines

Doktors der Naturwissenschaften

(Dr. rer. nat.)

der Fakultät Chemie und Chemische Biologie

der Technischen Universität Dortmund

vorgelegt von

Yannick Brüggemann

Juli 2018

Vorgelegt im Juli 2018

von Yannick Brüggemann

Gutachter:

Prof. Dr. Philippe I.H. Bastiaens

Prof. Dr. Andrea Musacchio

The work presented in this dissertation was performed in the laboratory of Prof. Dr. Philippe I.H. Bastiaens at the Max Planck Institute of Molecular Physiology, Dortmund, (Germany).

Eidesstattliche Versicherung (Affidavit)

Name, Vorname
(Surname, first name)

Matrikel-Nr.
(Enrolment number)

Belehrung:

Wer vorsätzlich gegen eine die Täuschung über Prüfungsleistungen betreffende Regelung einer Hochschulprüfungsordnung verstößt, handelt ordnungswidrig. Die Ordnungswidrigkeit kann mit einer Geldbuße von bis zu 50.000,00 € geahndet werden. Zuständige Verwaltungsbehörde für die Verfolgung und Ahndung von Ordnungswidrigkeiten ist der Kanzler/die Kanzlerin der Technischen Universität Dortmund. Im Falle eines mehrfachen oder sonstigen schwerwiegenden Täuschungsversuches kann der Prüfling zudem exmatrikuliert werden, § 63 Abs. 5 Hochschulgesetz NRW.

Die Abgabe einer falschen Versicherung an Eides statt ist strafbar.

Wer vorsätzlich eine falsche Versicherung an Eides statt abgibt, kann mit einer Freiheitsstrafe bis zu drei Jahren oder mit Geldstrafe bestraft werden, § 156 StGB. Die fahrlässige Abgabe einer falschen Versicherung an Eides statt kann mit einer Freiheitsstrafe bis zu einem Jahr oder Geldstrafe bestraft werden, § 161 StGB.

Die oben stehende Belehrung habe ich zur Kenntnis genommen:

Official notification:

Any person who intentionally breaches any regulation of university examination regulations relating to deception in examination performance is acting improperly. This offence can be punished with a fine of up to EUR 50,000.00. The competent administrative authority for the pursuit and prosecution of offences of this type is the chancellor of the TU Dortmund University. In the case of multiple or other serious attempts at deception, the candidate can also be unenrolled, Section 63, paragraph 5 of the Universities Act of North Rhine-Westphalia.

The submission of a false affidavit is punishable.

Any person who intentionally submits a false affidavit can be punished with a prison sentence of up to three years or a fine, Section 156 of the Criminal Code. The negligent submission of a false affidavit can be punished with a prison sentence of up to one year or a fine, Section 161 of the Criminal Code.

I have taken note of the above official notification.

Ort, Datum
(Place, date)

Unterschrift
(Signature)

Titel der Dissertation:
(Title of the thesis):

Ich versichere hiermit an Eides statt, dass ich die vorliegende Dissertation mit dem Titel selbstständig und ohne unzulässige fremde Hilfe angefertigt habe. Ich habe keine anderen als die angegebenen Quellen und Hilfsmittel benutzt sowie wörtliche und sinngemäße Zitate kenntlich gemacht.
Die Arbeit hat in gegenwärtiger oder in einer anderen Fassung weder der TU Dortmund noch einer anderen Hochschule im Zusammenhang mit einer staatlichen oder akademischen Prüfung vorgelegen.

I hereby swear that I have completed the present dissertation independently and without inadmissible external support. I have not used any sources or tools other than those indicated and have identified literal and analogous quotations.

The thesis in its current version or another version has not been presented to the TU Dortmund University or another university in connection with a state or academic examination.*

*Please be aware that solely the German version of the affidavit ("Eidesstattliche Versicherung") for the PhD thesis is the official and legally binding version.

Ort, Datum
(Place, date)

Unterschrift
(Signature)

Table of Contents

Abstract

The ErbB signaling network comprises a complex dynamic system, which regulates a diverse set of cellular behaviors. In this thesis, we examined how regulating the distribution of ErbB receptors between the plasma membrane and different endosomal compartments enables contextual regulation of receptor activity and signaling.

In the first part of this work, we investigated how spatial regulation of EGFR controls its autocatalytic activity. We found that autonomously activated and EGF activated receptors are processed differently by the endocytic machinery. Constitutive vesicular recycling through perinuclear areas with high PTP1B phosphatase activity suppresses autonomous receptor activation in the absence of ligand, while maintaining EGFR abundance at the PM. In contrast, EGF binding enhances EGFR self-association and phosphorylation of the c-Cbl docking tyrosine Y1045, which results in receptor ubiquitination, internalization and lysosomal degradation. The coupling of EGFR self-association state, ubiquitination and vesicular dynamics thereby allows for the coexistence of a continuous safeguard cycle, while maintaining sensitivity to growth factor stimulation.

In the second part of this work, we examined how ligand-specific ErbB receptor trafficking determines Erk signaling dynamics and localization. We found that EGF or heregulin (HRG) differentially modulate ErbB receptor trafficking to generate distinct spatiotemporal patterns of receptor activities, leading to the activation of Erk from different subcellular compartments (plasma membrane and endosomes). The subcellular localization of Erk activation influences its interaction with different effector proteins and thereby generates ligand-specific cellular responses. Proliferative Erk signals are transmitted to the nucleus, irrespective of their spatial origin, while the Erk dependent phosphorylation of pro-migratory effectors relies on membrane proximal Erk activity.

Collectively our findings highlight how vesicular dynamics enable context dependent spatial regulation of ErbB activity and downstream signaling events.

Zusammenfassung

Das ErbB-Rezeptor Signalnetzwerk umfasst ein komplexes dynamisches System, welches vielfältige zelluläre Verhaltensweisen reguliert. Im Rahmen dieser Arbeit wurde untersucht, wie die Regulation der Verteilung von ErbB-Rezeptoren zwischen der Plasmamembran und verschiedenen endosomalen Kompartimenten, eine kontextabhägige Regulation der Rezeptoraktivität und Signalweiterleitung, ermöglicht. Im ersten Teil dieser Arbeit wurde untersucht, wie die räumliche Regulation von EGFR seine autokatalytische Aktivität steuert. Es wurde gezeigt, dass autonom aktivierte und EGF-aktivierte Rezeptoren unterschiedlich durch die endozytische Maschinerie transportiert werden. Konstitutives vesikuläres Recycling durch perinukleäre Bereiche mit hoher PTP1B-Phosphatase-Aktivität unterdrückt autonome Rezeptoraktivierung in Abwesenheit von Liganden, bei gleichzeitiger Aufrechterhaltung der Membranlokalisation von EGFR. Im Gegensatz dazu verstärkt die Bindung von EGF die EGFR-Selbstassoziation und Phosphorylierung der c-Cbl-Bindestelle Y1045, was zur Ubiquitinierung, Internalisierung und zum lysosomalem Abbau des Rezeptors führt. Die Kopplung des EGFR-Selbstassoziationszustands, der Rezeptor-Ubiquitinierung und der vesikulären Dynamik, ermöglicht somit die Koexistenz eines kontinuierlichen, suppressiven vesikuläreren Transportkreislaufes, während die Empfindlichkeit für die Stimulierung mit Wachstumsfaktoren erhalten bleibt. Im zweiten Teil dieser Arbeit wurde untersucht, wie der Liganden-spezifische ErbB-Rezeptor Transport die raumzeitliche Organisation der Erk-Signalgebung steuert. Es wurde gezeigt, dass EGF oder Heregulin (HRG) den ErbB-Rezeptor Transport unterschiedlich modulieren und so unterschiedliche raumzeitliche Muster von Rezeptoraktivitäten erzeugen. Dies führt zur Aktivierung von Erk aus verschiedenen subzellulären Kompartimenten (Plasmamembran und Endosomen). Die subzelluläre Lokalisation der Erk-Aktivierung beeinflusst die Interaktion von Erk mit verschiedenen Effektorproteinen und erzeugt dadurch unterschiedliche zelluläre Antworten. Proliferative Erk-Signale werden unabhängig von ihrem räumlichen Ursprung an den Zellkern übertragen, während die Erk-abhängige Phosphorylierung pro-migratorischer Effektoren auf membrannaher Erk-Aktivität beruht.

Zusammenfassend zeigen unsere Ergebnisse, wie die Regulation der vesikulären Dynamik von ErbB-Rezeptoren eine kontextabhängige räumliche Regulation ihrer Aktivität und Signalweiterleitung ermöglicht.

1 Introduction

Cells are constantly exposed to a wide range of extracellular cues and growth factors which they need to sense and interpret. The ability of cells to adapt their behaviour with regard to their environment is an essential aspect of tissue development and homeostasis[1,2]. Cells use signalling networks to process extracellular information and translate these into distinct responses (e.g. proliferation, differentiation, movement or death)[3]. These signalling networks are highly dynamic, often reconfigurable and can generate context-dependent function, instead of being static, linear and hardwired[4–6]. Although the identity of numerous central components of many signaling pathways has been determined and ample studies have addressed their inherent molecular properties, how they collectively process information to generate a defined cellular response to extracellular signals is still poorly understood. A growing number of studies supports that cells send and receive information about their environment by controlling the spatial and temporal dynamics of signaling molecules[7–10]. A systems level understanding how different stimuli can be encoded in spatial and temporal patterns and how these dynamics are interpreted and shape cellular behaviour could provide new insights into how cells generate higher-order emergent behavior and may reveal new pharmacological strategies for the treatment of disease[11,12].

1.1 ErbB receptors

Cell surface receptors function as sensory organs, which enable cells to sense their environment and convert extracellular signals into intracellular signaling events, employing a plethora of different posttranslational modifications[13]. Mechanisms that regulate the spatial and temporal activity of these receptors can influence their sensitivity to stimuli, duration of activity and bias their interactions with effectors, providing different levels of regulation that can influence the cellular response to receptor activation. Based on their structure, cell surface receptors are grouped into different families.

The ErbB/HER family of cell surface receptors form a subgroup of receptor tyrosine kinases which includes four family members: EGFR (HER1/ErbB1), ErbB2 (HER2/Neu), ErbB3 (HER3) and ErbB4 (HER4)[14]. ErbB receptors are ubiquitously expressed in epithelial, cardiac, mesenchymal, and neuronal cells and mediate fundamental, often opposing cellular responses including proliferation, differentiation, migration, survival and/or apoptosis[15,16]. ErbB receptors consist of an extracellular

ligand-binding domain, followed by a single transmembrane helix and an intracellular module composed of a juxtamembrane segment, a tyrosine kinase domain and a C-terminal tail (**Fig.1**)[17]. The canonical scheme of ErbB receptor activation relies on ligand-induced receptor homo- or heterodimerzation, followed by allosteric activation of their intrinsic kinase activity and the phosphorylation of tyrosine residues within the C-terminal tail of the receptor which can act as effector docking sites[14,17–20]. Subsequent recruitment of PTB- or SH2-containing effector proteins relays the extracellular signal inside the cytoplasm[21,22]. Notably, the activation of ErbB2 and ErbB3 relies on the formation of receptor heterodimers, since for ErbB2 no ligands have been identified yet, while ErbB3 is kinase impaired[15,23]. To date, seven different ligands of EGFR have been identified: Epidermal growth factor (EGF), transforming growth factor alpha (TGF-α), betacellulin (BTC), heparin-binding EGF-like growth factor (HB-EGF), amphiregulin (ARG), epiregulin (EPR), and epigen (EGN). BTC, HB-EGF and EPR as well as neuregulins (e.g. heregulins) can also bind and activate ErbB4, whereas the latter also binds to ErbB3 and promotes its heterodimerization with ErbB2[16]. Individual ligands can induce qualitatively and quantitatively different responses of downstream signaling molecules and thereby promote different cellular behaviours[24].

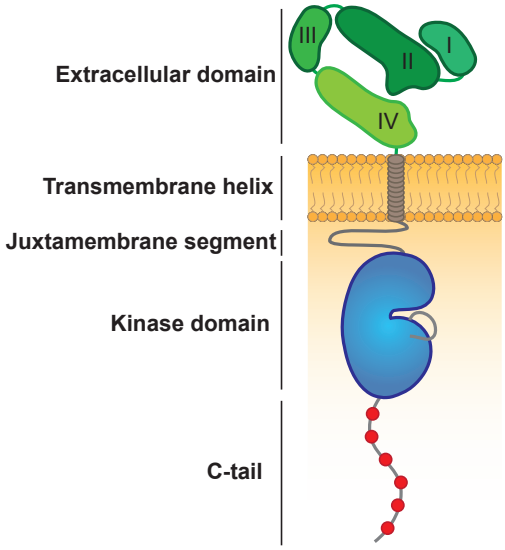

Figure 1: Domain structure of ErbB receptors. The N-terminal extracellular domain is composed of four subdomains (I – IV), which participate in ligand binding and receptor dimerization. A single transmembrane (TM) spanning alpha-helix is followed by a juxtamembrane segment, the kinase domain and the C-tail containing tyrosine autophosphorylation sites (depicted in red), serving as docking sites for the recruitment of downstream signaling molecules[17].

1.2 Epidermal growth factor receptor (EGFR)

EGFR belongs to the ErbB family of receptor tyrosine kinases. Signaling initiated by EGFR is implicated in the regulation of cellular growth, survival, proliferation and differentiation and is therefore vital during development and maintenance of tissue homeostasis[25,26]. Since EGFR can elicit potent mitogenic responses, dysregulation of its activity due to mutations and/or overexpression has been causally linked to tumor development and progression in different of types of cancer[27,28]. Elevated EGFR expression/activity is a hallmark of several cancers and EGFR therefore has emerged as an attractive therapeutic target for the use of small molecule or antibody-based approaches[29]. EGFR regulates a complex signaling network, increasing the activity of many intracellular signaling effectors, including phosphatidylinositol 3-kinase (PI3K) and its downstream kinase Akt (PKB), the Ras/Raf/Mek/Erk1/2 signaling cascade and phospholipase C (PLCγ), among others[15,30].

1.3 EGFR structure and activation

The activation of most RTKs requires trans-autophosphorylation of regulatory tyrosine residues in the activation loop, the juxtamembrane segment, and/or the C-terminal tail[14]. In contrast, EGFR family members are activated through the allosteric interaction between two kinase domains within a receptor dimer and do not rely on trans-autophosphorylation events[17,19]. The extracellular module (ECM) of EGFR is composed of four domains, denoted domains 1, 2, 3, 4. The domains 1 and 3 form the ligand binding side, while the domains 2 and 4 have regulatory functions[31]. Crystal structures showed that in the absence of ligand the ECM adopts an autoinhibited (“tethered’’) conformation through interactions between a β-hairpin of domain 2 (dimerization arm) with domain 4 (**Fig.1**)[32]. This configuration constrains the domains 1 and 3 to a distant orientation, which prevents an EGF molecule to contact both domains simultaneously[32]. Ligand binding results in conformational rearrangement and converts the ECM to an extended conformation, releasing the dimerization arm and thereby enabling `back-to-back` dimerization with the corresponding element of second a receptor molecule (**Fig.2**)[31]. On the intracellular site the kinase domains of a receptor dimer interact in an asymmetric fashion. One kinase domain (termed “activator”) allosterically locks the second kinase domain (termed “receiver”) in an activated conformation (**Fig.2**)[19]. This involves interactions between the αH helix in the C-lobe of the activator kinase and the αC helix in the N-

lobe of the receiver kinase, causing a switch from the "αC-out inactive'' conformation to an "αC-in active'' conformation[33,34]. This configuration enables the formation of a catalytically important salt bridge between Lys721 and Glu738, to co-ordinate the α- and β-phosphates of ATP bound to the active site and thereby allows the activated receiver kinase to phosphorylate the C-tail of the activator kinase[35]. Structural coupling between the extracellular and intracellular module further enables specific interactions between the trans- and juxtamembrane segments of a receptor dimer required for the formation of an asymmetric kinase dimer[36,37]. In particular, ligand binding removes steric constraints in the ECM and allows the transmembrane segments to associate through their N-terminal GxxxG dimerization motifs. This configuration promotes membrane release of the intracellular module from the plasma membrane and allows the formation of an antiparallel dimer between the N-terminal residues of the juxtamembrane segment (JM-A Segment)[38]. In addition, the C-terminal half of the juxtamembrane segment (JM-B segment) of the receiver kinase forms a latch along the C-lobe of the activator kinase and thereby further stabilizes the asymmetric kinase dimer[38]. Notably, ligand binding to EGFR has also been reported to generate higher-order multimers, which have been suggested to cooperatively enhance auto-phosphorylation in trans between neighboring dimers[39,40].

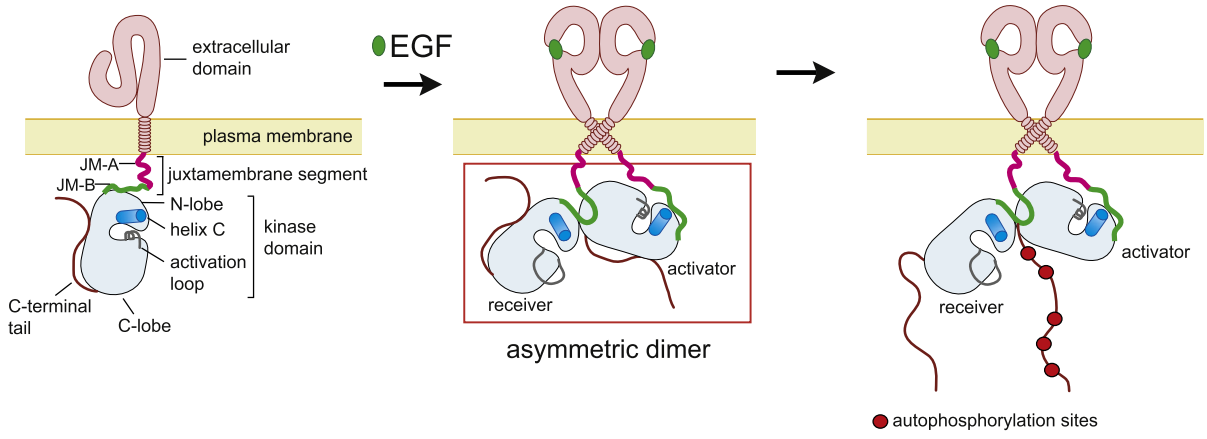

Figure 2: Ligand-induced dimerization and allosteric activation of EGFR. Ligand binding (e.g. EGF) to the extracellular domain of EGFR promotes receptor dimerization, the formation of an asymmetric kinase dimer and subsequent trans-autophosphorylation of the C-tail of activator kinase via the allosterically activated receiver kinase (adapted from [38]).

1.4 Autonomous EGFR activation

EGFR dimerization, which enables allosteric activation of its intrinsic kinase activity and triggers trans-autophosphorylation is primarily driven by the binding of growth

factors to the ECM of the receptor. However, due to thermal fluctuations ligandless EGFR can also attain an active conformation and, via the formation of short-lived dimers, trigger spontaneous autonomous phosphorylation events[14,41,42]. Moreover, it has been suggested that phosphorylation of tyrosine 845 within the activation loop establishes an autocatalytic feedback by stabilizing the active conformation of the receptor and thus triggering autonomous ligand-independent signal propagation[43]. In accordance with this, previous studies showed that local EGF stimulation promoted lateral propagation of EGFR activation at high EGFR expression levels[44,45]. Growth factor stimulation further promotes the recruitment and activation of reactive oxygen species (ROS) producing enzyme systems such as NADPH oxidase to the plasma membrane[46–48]. Due to their short half live time, the presence of ROS remains spatially constrained to the plasma membrane. Local ROS production transiently inhibits inhibitory protein tyrosine phosphatases (PTP), through reversible oxidation of a catalytic cysteine residue, and thereby lowers the activation threshold of neighbouring receptors[41,49]. Coupling of EGFR activation with PTP inhibition at the plasma membrane thereby exemplifies a double-negative feedback loop, which together with the autocatalytic kinase activity, establishes a bistable reaction network with switch like response properties[41,46]. Analogous to a toggle switch, this reaction network converts growth factor stimuli into threshold-activated responses[41,50]. However, the autocatalytic kinase activity also amplifies spurious receptor activation in the absence of growth factor stimuli, necessitating additional regulatory mechanisms to control EGFR activity in the presence and absence of growth factors.

1.5 Structural auto-inhibitory features of EGFR

The activity of EGFR and its phosphorylation dynamics are regulated via different intrinsic structural features and extrinsic cellular regulatory machineries. Multiple auto-inhibitory structural mechanisms create an energy barrier for EGFR self-association and thereby antagonize its activation in the absence of growth factors. Recent NMR and molecular dynamics simulations showed that in the ligand-free state the ECM is highly dynamic and forms an ensemble of different conformations, but generally adopts compact conformations over the extended conformation[37,51]. In ligand-free receptor dimers, the compact configuration of the ECM favors C-terminal over N-terminal dimerization of the transmembrane helices, dissociation and membrane burial of the juxtamembrane segments and the formation of symmetric,

inactive kinase dimers[37]. In addition, tethering of the intracellular module through electrostatic interactions between the negatively charged plasma membrane and positively charged patches obstruct the active site of the kinase domain[37]. The dimerization of two kinase domains is further hindered through local intrinsic disorder of the αC-helix region[34]. Activation loop phosphorylation of Tyr845 or the L834R mutation often found in lung cancer suppresses the disordered state, thereby enhancing receptor dimerization affinity, and suggesting a potential mechanism for autonomous, ligand-independent signal propagation[34]. The C-tail of EGFR has further been shown to form autoinhibitory interactions which interfere with the formation of an asymmetric kinase dimer[31,38].

In addition to these intrinsic auto-inhibitory mechanisms, the endocytic machinery and protein tyrosine phosphatases (PTP) comprise extrinsic regulatory layers of EGFR activity[46,52].

1.6 Protein tyrosine phosphatases (PTP)

The spatially distributed superfamily of cysteine-based PTPs regulates EGFR phosphorylation dynamics though the removal of phosphate groups from tyrosine residues. The overall level of EGFR phosphorylation is the product of a continuous and rapid cycle of phosphorylation and de-phosphorylation events[46,53]. Pan-specific PTP inhibition using the thiol reactive compound pervanadate has been shown to cause rapid EGFR phosphorylation in the absence of ligand, demonstrating the critical opposing role of PTPs to suppress ligand-independent EGFR activation[54,55]. Since the catalytic activity of certain PTPs (e.g. PTP1B and TCPTP) exceeds EGFR kinase activity by up to two orders of magnitude, spatial regulation of their activity is a prerequisite to permit EGFR phosphorylation[56–58]. Previous studies showed a PTP1B activity gradient emanating from the perinuclear area and declining towards the plasma membrane[59]. The relatively low membrane-proximal PTP activity has been suggested to be sufficient to shift the kinase-phosphatase balance in favor of the phosphatase in the absence of growth factor stimulation, while ligand binding shifts it in favor of the kinase[46].

1.7 Endocytic trafficking of EGFR

The spatial localization of signaling molecules is a critical parameter determining their response properties and functional output. The endocytic machinery is composed of

functionally distinct intracellular membrane compartments and regulates the internalization, re-localization and fate (i.e. endosomal-plasma membrane recycling versus lysosomal degradation) of signaling molecules from the plasma membrane. Members of the Rab small GTPase family act as multifaceted organizers of vesicular trafficking and control vesicular biogenesis, budding, delivery and fusion by the coordinated recruitment of various effector proteins[60]. Through hydrophobic geranylgeranyl groups, different Rab proteins are localized to distinct intracellular membranes and/or microdomains, organizing a modular system in which each Rab protein performs different functions (**Fig.3**)[61]. Rab5 participates during early stages of the endocytic pathway and mediates cargo entry and fusion of primary endocytic vesicles to form early endosomes (EE)[62]. The fate of endocytic cargo is determined by sorting events to subsequent endosomal compartments. Endosomal maturation from EE to late endosomes (LE) involves the replacement of Rab5 with Rab7, which mediates fusion of LE and/or multivesicular bodies with lysosomes[61,63]. In contrast, recycling of internalized cargo to the plasma membrane occurs via two routes: Rab4-mediated recycling directly from the EE to the plasma membrane or via Rab11-positive vesicles which mediate recycling through perinuclear recycling endosomes (RE, **Fig3**)[64,65]. Vesicular membrane dynamics enable different contextual modes of EGFR regulation by modulating its spatial distribution between the plasma membrane and different endosomal compartments[66,67]. The balance between internalization and recycling determines the density of EGFR at the plasma membrane. In the absence of ligand, EGFR is continuously internalized and recycled back to the plasma membrane, maintaining a steady state spatial distribution with the majority of EGFR located at the plasma membrane[68,69]. In contrast, ligand binding enhances EGFR internalization, resulting in its endosomal accumulation (**Fig.3**)[67]. Internalization of ligand-activated receptors extends the axial reach and the duration of plasma membrane initiated signaling events throughout the cytoplasm and can further create reaction platforms with distinct signaling repertoires[46,70]. Depending on the cellular context and ligand concentration, EGFR can be internalized through clathrin-mediated endocytosis (CME) or several other mechanisms (globally referred to as non-clathrin endocytosis, NCE)[71]. Internalization via CME in the absence or at low-to-intermediate ligand concentrations mainly results in receptor recycling to plasma membrane, thereby extending the duration of its signaling capacities[72]. In contrast, high ligand concentrations trigger NCE pathways and promote receptor

ubiquitination, which targets the receptor for lysosomal degradation[73]. Ubiquitination of EGFR is mediated by members of the of the Cbl family of E3-ubiquitin-ligases that interact either directly with a phosphorylated tyrosine residue (pY1045) or indirectly through the adaptor protein Grb2, which binds to pY1068 and pY1086[74–76]. Endocytosis of ligand bound receptors has further been shown to enable interaction of EGFR and the ER-bound phosphatase PTP1B, thereby contributing to the termination of receptor activity[77,78].

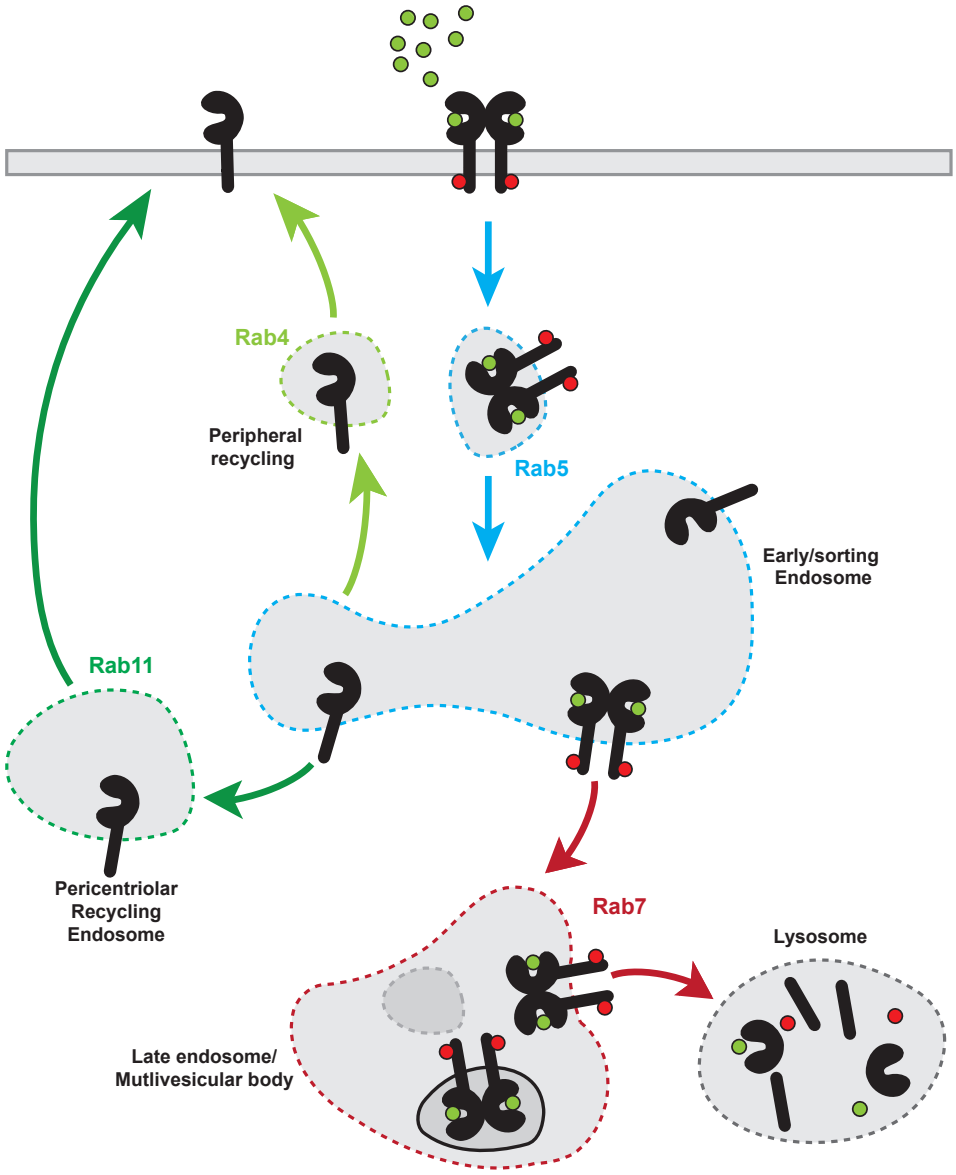

Figure 3: Vesicular dynamics of EGFR. EGF stimulation promotes EGFR internalization via Rab5-positive endosomes. Internalized EGFR is either recycled back to the plasma membrane via the peripheral or perinuclear recycling endosomes or trafficked to the lysosome for degradation. Rab GTPases localized to distinct intracellular membranes and/or microdomains are indicated by colors.

1.8 Mitogen activated protein kinases (MAPK)

Phosphorylated tyrosine residues within the C-tail of EGFR recruit a variety of signaling molecules such as Shc or Grb2, which trigger the activation of various signal-transducing proteins[15,79–81]. Among these, extracellular regulated kinase 1/2 (Erk1/2) functions as an important regulator to integrate external cues into intracellular signalling events. Erk belongs to the evolutionary conserved superfamily of mitogen activated protein kinases (MAPKs), which mediate numerous cellular responses including cellular proliferation, differentiation, and survival[82]. MAPKs form three-tiered modules, which are activated by sequential phosphorylation events: a MAPK kinase kinase (MAPKKK) phosphorylates a MAPK kinase (MAPKK), which in turn activates a MAPK[83] (**Fig.4**). So far six different MAPK modules have been identified in mammalian cells: Erk1/2, Erk3/4, Erk5, Erk7/8, Jun N-terminal kinase (JNK) and the p38 isoforms α/β/γ(ERK6)/δ[84,85]. Activated MAPKs function as proline (P) directed serine/threonine (S/T) selective protein kinases which phosphorylate a plethora of substrate proteins on selected S/T residues followed by P and thereby regulate numerous cellular responses[85,86]. This process is further thought to be mediated via docking interactions that occur outside of the active site between MAPKs and their substrates[87]. Dysregulation of MAPK activity has been implicated in various forms of human disease and developmental disorders[88–90].

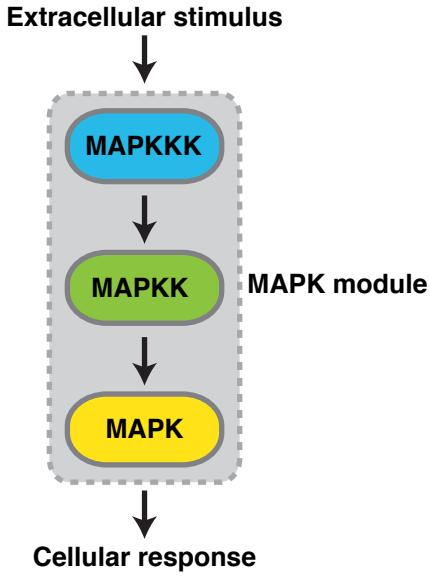

Figure 4: Scheme of the three-tiered MAPK module in eukaryotic cells. External signals sensed by growth factor receptors induce the sequential phosphorylation and activation of the three MAPKs (MAPKKK, MAPKK and MAPK), with the terminal MAPK directing the cellular response[83].

1.9 Extracellular regulated kinase (Erk)

The Erk1/2 MAPK-module further involves the MAPKKK Raf and the MAPKK Mek1/2. Activation of this module is frequently initiated via Ras-family GTPases[91]. Plasma membrane activated growth factor receptors promote Ras activation via recruitment of the Ras-guanine nucleotide exchange factor (GEF) son-of-sevenless (SOS), which promotes the GDP to GTP exchange of Ras proteins[92]. Activated RasGTP in turn serves as a reactivity-enhancing recruitment factor which concentrates effector proteins such as Raf at the plasma membrane (**Fig.5**)[93]. Recruitment of Raf family kinases (A-, B-, and C-Raf) to the plasma membrane enables their allosteric activation via homo- or heterodimerization[94]. Activated Raf kinases further promote the phosphorylation and activation of Mek1/2, which then activate Erk1/2 via phosphorylation of threonine and tyrosine residues within their activation loop (Thr202/Tyr204 for Erk1 and Thr185/Tyr187 for Erk2)[95,96]. Dephosphorylation and thereby inactivation of Erk is catalysed by dual-specificity phosphatases (DUSPs), that can dephosphorylate both tyrosine or serine/threonine residues[97]. Erk is known to interact with over 170 proteins, including many substrates and regulators[98]. These interactions are further facilitated by two distinct docking domains: a common docking (CD/ED) domain which interacts with D site motifs (also called DEJL motifs), and a F Recruitment Site (FRS), which interacts with an FXF (DEF) motif on substrate proteins[96]. In resting cells, Erk is primarily located in the cytoplasm due to interactions with anchoring proteins; however, upon activation Erk can translocate to the nucleus where it promotes gene expression and DNA replication[99]. Different growth factors are thought to promote distinct cellular responses through dynamic changes of Erk interaction partners[100]. Different mechanisms have been suggested to cooperatively direct Erk signals to different downstream targets, including the duration and signal strength of Erk activation, its interaction with scaffold proteins, spatial compartmentalization, and crosstalk with other signalling molecules (**Fig.6**)[101]. Aberrant regulation of Erk activity further contributes to various forms of cancer and other human diseases, most commonly due to mutations in EGFR, RAS, BRAF, CRAF, or MEK1/2[102].

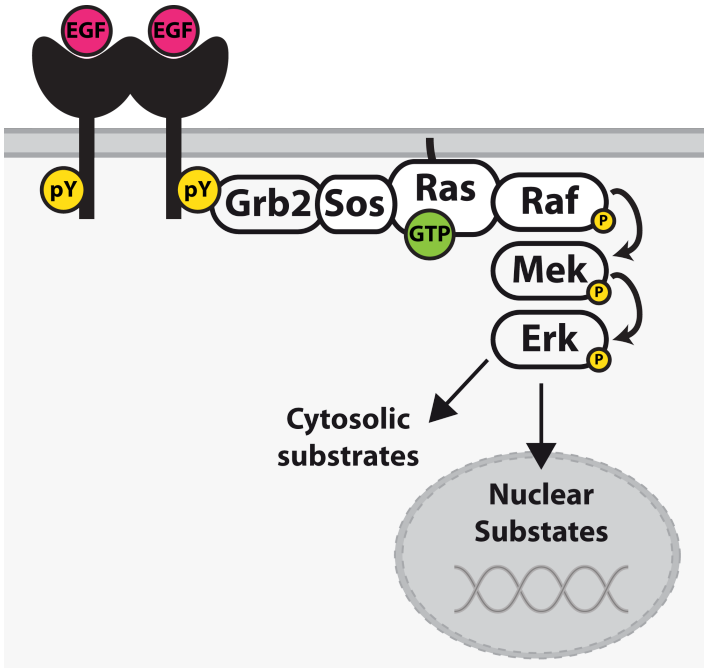

Figure 5: EGFR mediated Erk activation at the plasma membrane. EGF induced activation of EGFR induces the recruitment of a GEF complex (Grb2-SOS) to the plasma membrane to activate the membrane-bound GTPase Ras to recruit Raf to the plasma membrane. Raf promotes Mek phosphorylation, which subsequently catalyzes Erk phosphorylation. Activated Erk phosphorylates various cytosolic effectors and also translocates to the nucleus, where it phosphorylates different transcription factors to regulate gene expression[92].

1.10 Regulation of Erk signaling specificity

Given its ubiquitous role during numerous different and even opposing cellular responses, Erk acts as multifunctional signalling hub, which receives and integrates inputs from various stimuli. This functional plasticity represents a conundrum in regard to how the promiscuous activation of a shared signalling molecule can generate a specific cellular response to a given stimulus. The spatial and temporal organization of Erk activity are considered mechanisms that can encode variable extracellular signals into distinct cellular responses (**Fig.6A, C**)[101,103,104]. Different growth factors have been shown to induce distinct temporal patterns of Erk activation, which have been linked to different cellular fates[105]. Network motifs such as feed-forward loops allow decoding of Erk signal duration and thereby the induction of specific gene expression patterns that drive different cellular responses[106–108]. Furthermore, recent studies using constitutively active Ras mutants artificially targeted to specific subcellular locations established that the subcellular localization of Erk activation can influence its substrate pool[104,109,110]. Since Erk interacts with a plethora of substrate and effector proteins, the context-dependent formation of different protein complexes can further specify cellular responses[100]. Differences in

the spatial and temporal dynamics of Erk activity are determined by the underlying causal interactions within the MAPK signalling network (**Fig.6D**)[3]. The topology of the network depends on the cellular context and the resulting dynamics of Erk govern the cellular response. In PC12 cells, for example, the signal-dependent wiring of causal interactions within the network has been shown to result in different temporal Erk dynamics which determine cellular fate: proliferation (EGF, transient Erk response) and differentiation (NGF, sustained Erk response, **Fig.6A**)[4]. In this regard, it has been demonstrated that cellular responses can be rewired through targeted perturbation of causal interactions governing Erk dynamics[4].

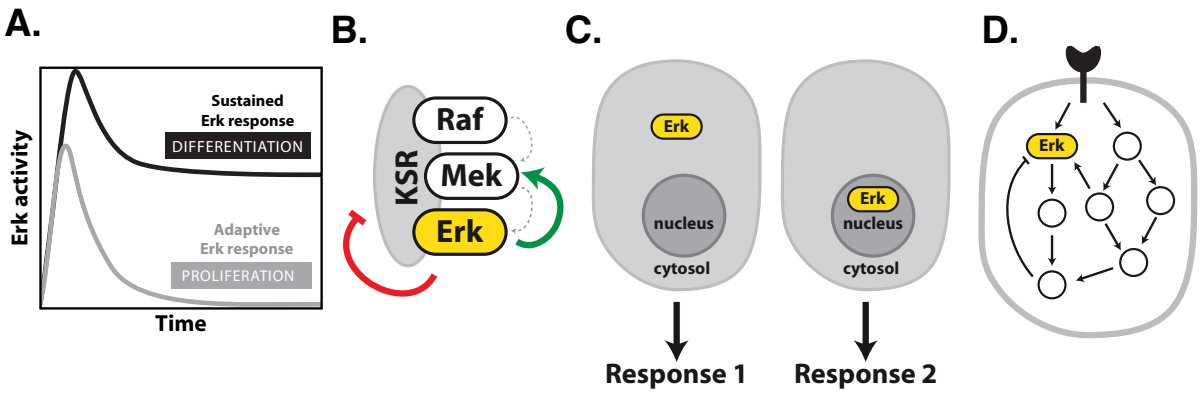

Figure 6: Mechanisms determining Erk signaling specificity and signaling dynamics. (A) Duration and strength of Erk activation. **(B)** Assembling the molecular components on scaffold proteins can facilitate their interaction and further provide positive (green arrow) and negative (red arrow) mechanisms of regulation, tuning the response dynamics. **(C)** The subcellular localization of Erk (nucleus or cytoplasm) can promote different cellular responses. **(D)** Crosstalk and conditional causal interactions can manifest in different dynamics of Erk activity[3,9,111,112].

2 Objectives

Vesicular trafficking allows the cell to dynamically regulate the spatial distribution of ErbB receptors between the plasma membrane (PM) and different endosomal compartments, however the signaling repertoire of endosomal and plasma membrane localized receptors can differ if biochemical components of the signal transduction machinery are not equally accessible within the different compartments. Changes in vesicular trafficking dynamics can alter the spatial distribution of ErbB receptors and therefore form an important layer of regulation of receptor activity and signaling that could enable context-dependent regulation. The ensuing study is divided into two parts, addressing the following questions:

Autocatalytic amplification of ligand-induced EGFR activation coupled to local PTP inhibition establishes a bistable reaction network with switch like response properties. While this feature ensures robust receptor activation to extracellular signals, it also creates the potential to amplify spontaneous phosphorylation events in the absence of growth factors[41,46]. Thus, the question arises of how the cell suppresses uncontrolled autonomous EGFR activation, while maintaining responsiveness to ligand stimulation. Endocytosis of ligand-activated EGFR has been shown to promote its interaction with spatially distributed PTPs to suppress its activity[78]. In this thesis, the role of EGFR vesicular dynamics in the regulation of autonomous receptor activity will be examined, as well as how endosomal trafficking differentially controls the activity of autonomously and ligand-activated EGFR.

Intriguingly, different ErbB ligands can induce distinct cell fates within a single cell type, despite the promiscuous activation of shared signal transducing proteins, such as the Ras/Erk mitogen-activated protein kinase (MAPK) cascade. In this regard, it has been suggested that dynamic changes in Erk-interacting proteins represent a key mechanism specifying the cellular response. Although receptor endocytosis attenuates receptor activation and signaling at the plasma membrane, active EGFR can continue to signal from endosomes. The second part of this thesis will examine how differences in the spatial and temporal distribution of active ErbB receptors within the endosomal system influence the subcellular localization of Erk activity, thereby modulating its interaction with different pools of substrates to generate specific cellular responses.

3 Material and Methods

3.1 Materials

3.1.1 Chemicals and Reagents

2-Mercapto-ethanol	SERVA Electrophoresis GmbH
2'-deoxyadenosine-5'-triphosphate (dATP)	Invitrogen™ Life Technologies
2'-deoxycytidine-5'-triphosphate (dCTP)	Invitrogen™ Life Technologies
2'-deoxyguanosine-5'-triphosphate (dGTP)	Invitrogen™ Life Technologies
2'-deoxythymidine-5'-triphosphate (dTTP)	Invitrogen™ Life Technologies
40 % (29:1)	Carl Roth GmbH
Ammonium persulfate (APS)	SERVA Electrophoresis GmbH
Ampicillin sodium salt	SERVA Electrophoresis GmbH
Bromophenolblue	Sigma-Aldrich®
Cell Lysis buffer, 10x	Cell Signaling Technology
Cocktail Tablets cOmplete, Mini, EDTA-free Protease Inhibitor	Roche
Dimethyl sulfoxide (DMSO)	SERVA Electrophoresis GmbH
Dithiothreitol (DTT)	Fluka® Analytical
Epidermal growth factor (EGF)	Sigma-Aldrich®
Erlotinib	Selleckchem
Ethanol	J.T.Baker
Ethylenediaminetetracetic acid (EDTA)	Fluka® Analytical
Glycerol	GERBU Biotechnik GmbH
Glycine	Carl Roth GmbH
Heregulin-β3	Millipore, Merck KGaA
Histofix	Carl Roth GmbH
Hydrogenperoxid (H_2O_2)	Merck
Isopropanol	J.T.Baker

Kanamycin sulfate	GERBU Biotechnik GmbH
Lapatinib	Selleckchem
Magnesium chloride ($MgCl_2$)	Merck KG/J.T.Baker
Methanol	AppliChem GmbH
N,N,N',N'-Tetramethylene-diamine (TEMED)	Sigma-Aldrich®
PD0325901	Selleckchem
Phosphatase Inhibitor Cocktail 2	Sigma-Aldrich®
Phosphatase Inhibitor Cocktail 3	Sigma-Aldrich®
Poly-L-Lysine	Sigma-Aldrich®
RedSafe, DNA Stain	Chembio Ltd, Hertfordshire, UK
Rotiphorese® NF-acrylamide/bis-solution	
Sodium chloride (NaCl)	Fluka® Analytical
Sodium dodecyl sulfate (SDS)	SERVA Electrophoresis GmbH
sodium orthovanadate	Sigma-Aldrich®
Tris-base	Carl Roth GmbH
Tris-HCl	J.T.Baker
Triton X-100	SERVA Electrophoresis GmbH
Tween 20	SERVA Electrophoresis GmbH
UltraPureTM Agarose	Invitrogen™ Life Technologies

3.1.2 Commercial Solutions

100 mM dNTP mix	Invitrogen™ Life Technologies
100x BSA	New England Biolabs Inc.
10x Lysis Buffer	Cell Signaling Technology
2-log DNA ladder	New England Biolabs Inc.
50 mM Magnesium Sulfate	Invitrogen™ Life Technologies
5x T4 DNA Ligation Buffer	Invitrogen™ Life Technologies
blocking buffer	LI-COR Biosciences GmbH

CutSmart™ Buffer	New England Biolabs Inc.
DPBS	PAN^{TM} Biotech GmbH
Dulbecco's Modified Eagle's Medium (DMEM)	PAN^{TM} Biotech GmbH
Fetal calf serum (FCS)	PAN^{TM} Biotech GmbH
Fugene® 6 transfection reagent	Roche Applied Science
Imaging medium	PANT^{M} Biotech GmbH
L-Glutamine	GIBCO®/Invitrogen^{TM}
Lipofectamine^{TM} 2000.	Invitrogen^{TM}
Odyssey Infrared Imaging System	
Precision Plus Protein^{TM} standards	Bio-Rad Laboratories, Inc.
T4 DNA ligase reaction buffer, 10×	New England BioLabs

3.1.3 Buffers and Media

LB medium	10 g/l Bacto-Trypton, 5 g/l bacto-yeast extract, 10 g/l NaCl and finally autoclave
LB agar plates	add 15 g agar per litre LB medium, pour plates when the autoclaved medium has approximately 55 °C, add antibiotic of choice at desired concentration
SOC medium	20 g/l Bacto-Trypton, 5 g/l bacto-yeast extract, 0.5 g/l NaCl, 2.5 mM KCl, 10 mM MgCl2 (SOB medium), autoclave and before usage add 20 mM glucose to obtain SOC
1x PBS (pH 7.4)	138 mM NaCl, 10 mM Na_2HPO_4, 2.7 mM KCl, 1.8 mM KH_2PO_4
5x SDS sample buffer	60 mM Tris-HCl (pH 6.8), 25 % glycerol, 2 % SDS, 14.4 mM 2-mercapto-ethanol, 0.1 % bromo-phenolblue
SDS running buffer	25 mM Tris-base, 192 mM glycine, 0.1 % SDS
Separating gel buffer	1 M Tris-HCl (pH 8.8)

Stacking gel buffer	0.375 M Tris-HCl (pH 6.8)
1x TAE buffer	40 mM Tris/Acetate (pH 7.5), 20 mM NaOAc, 1 mM EDTA
1x TBS	100 mM Tris-HCl (pH 7.4), 150 mM NaCl
1x TBST	100 mM Tris-HCl (pH 7.4), 150 mM NaCl, 0.1 % (v/v) Tween
Transfer buffer	25 mM Tris-base, 192 mM glycine, 20 % (v/v) methanol.
Modified RIPA buffer	50 mM Tris–HCl, 150 mM NaCl, 1 mM EDTA, 1 mM EDTA, 1 % Triton X-100, 1 % sodium deoxycholate, 1 % SDS

3.1.4 Bacterial Strains

XL10 Gold	Stratagene (regrown in-house)

3.1.5 Enzymes

Calf Intestinal Phosphatase (10,000 U/ml)	New England Biolabs Inc.
High-Fidelity (HF®) Restriction Endonucleases	New England Biolabs Inc.
PlasmidSafe ATP-dependent DNase	Epicentre
Q5® High-Fidelity DNA Polymerase	New England Biolabs Inc.
T4-DNA ligase	Invitrogen™ Life Technologies

3.1.6 Kits

High Pure endotoxin-freeNucleoBond®	
Micro BCA™ Protein Assay Kit	Thermo Scientific
Q5® Site-Directed Mutagenesis Kit	New England Biolabs Inc.
Roti®-Prep Plasmid MINI	Carl Roth GmbH
SiiR-DNA kit	Spirochrome
Xtra Midi EF	MACHEREY-NAGEL
Zymoclean™ Gel DNA Recovery Kit	Zymo Research

3.1.7 Antibodies

Primary antibodies

tRFP (AB234)	Evrogen
Akt (pan) (2920)	Cell Signaling Technology
anti-EGF Receptor (pY845) (558381)	BD Biosciences
c-Fos (9F6) (2250)	Cell Signaling Technology
Cbl Antibody (C-15) (SC-170)	Santa Cruz Biotechnology
Cyclin D1 (92G2) (2978)	Cell Signaling Technology
EGF Receptor (D38B1) (4267)	Cell Signaling Technology
EGFR/ErbB1 (AF231)	R&D Systems
EphA2 (AF-3035)	R&D Systems
ErbB-3 (C-17) (sc-285)	Santa Cruz Biotechnology
ErbB2 (9G6) (sc-08)	Santa Cruz Biotechnology
Erk1/2 (L34F12) (4696)	Cell Signaling Technology
Erk1/2 [9B3] (ab36991)	Abcam
GAPDH (6C5) (CB1001)	Calbiochem, Merck
HA-antibody (MMS-101P)	Covance Inc.
HER2/ErbB2 (29D8) (2165)	Cell Signaling Technology
HER4/ErbB4 (111B2) (4795)	Cell Signaling Technology
KSR1 [EPR2421Y] (ab68483)	Abcam
KSR2 (K75) (sc-100421)	Santa Cruz Biotechnology
Living colors® GFP AB (632381)	Clontech
Living colors® GFP AB (632593)	Clontech
Paxillin (610051)	BD Biosciences
Phospho- Erk1/2 (Thr202/Tyr204) (4370)	Cell Signaling Technology
Phospho- Erk1/2 (Thr202/Tyr204) (9101)	Cell Signaling Technology
Phospho-Akt (Ser473) (9271)	Cell Signaling Technology

Phospho-EGF Receptor (Tyr1068) (2234)	Cell Signaling Technology
Phospho-EGFR (Tyr1045) (2237)	Cell Signaling Technology
Phospho-EGFR (Tyr845) (558381)	BD Biosciences
Phospho-EGFR(Tyr1068) (D7A5) (3777)	Cell Signaling Technology
Phospho-EphA2 (Ser897) (D9A1) (6347)	Cell Signaling Technology
Phospho-HER2/ErbB2 (Tyr1221/1222)	Santa Cruz Biotechnology
Phospho-HER3/ErbB3 (Tyr1289) (21D3) (4791)	Cell Signaling Technology
Phospho-Rb (Ser807/811) (D20B12) (8516)	Cell Signaling Technology
Rab11 Antibody (3539)	Cell Signaling Technology
Rab11A (ab65200)	Abcam
Rab11a Antibody (2413)	Cell Signaling Technology
WAVE2 (3659)	Cell Signaling Technology
α-Tubulin (T6074)	Sigma Aldrich

Secondary antibodies for Western blots and In Cell Western

IRDye 680 donkey anti-mouse IgG	LI-COR Biosciences
IRDye 800 donkey anti-rabbit IgG	LI-COR Biosciences
IRDye 800 donkey anti-mouse IgG	LI-COR Biosciences
IRDye 680 donkey anti-rabbit IgG	LI-COR Biosciences
IRDye 680 donkey anti-goat IgG	LI-COR Biosciences

Secondary antibodies for immunofluorescence

Alexa Fluor® 647 chicken anti-rabbit IgG	Life Technologies
Alexa Fluor® 647 donkey anti-mouse IgG	Life Technologies
Alexa Fluor® 555 donkey anti-goat IgG	Life Technologies
Alexa Fluor® 488 donkey anti-mouse IgG	Life Technologies
Alexa Fluor® 546 goat anti- rabbit IgG	Life Technologies
Alexa Fluor® 546 goat anti-mouse IgG	Life Technologies

3.1.8 Oligonucleotides

siRNA

Rab11a 5´(AATGTCAGACAGACGCGAAAA)-3´	Qiagen
Rab11b 5´(AAGCACCTGACCTATGAGAAC)-3´	Qiagen
Control siRNA (1027281)	Qiagen
Rab11a siRNA (sc-36340)	Santa Cruz Biotechnology
Control siRNA (sc-37007)	Santa Cruz Biotechnology
ErbB2 siRNA (L-003126-00-0005)	Dharmacon
ErbB3 siRNA (L-003127-00-0005)	Dharmacon
ErbB4siRNA (L-003128-00-0005)	Dharmacon

DNA

Desalted DNA-oligonucleotides were purchased from Sigma-Aldrich Chemie GmbH.

3.1.9 Plasmids

EGFR-mCitrine	Encoding human EGFR with C-terminally fused mCitrine
EGFR-mCherry	Encoding human EGFR with C-terminally fused mCherry
EGFR-Y1045F-mCitrine	Encoding human EGFR-Y1045F with C-terminally fused mCitrine
EGFR-Y1045/1068/1086F-mCitrine	Encoding human EGFR-Y1045/1068/1086F with C-terminally fused mCitrine
EGFR-L834R-mCitrine	Encoding human EGFR-L834R with C-terminally fused mCitrine
ErbB2-mCitrine	Encoding human ErbB2 with C-terminally fused mCitrine
ErbB3-mCitrine	Encoding human ErbB3 with C-terminally fused mCitrine
pcDNA3.1+	Empty vector
tagBFP-Rab11a	Encoding human Rab11a with N-terminally fused tagBFP

c-Cbl-mCherry	Encoding human c-Cbl with C-terminally fused mCherry
mCherry-PTP1B-D181A	Encoding PTP1B D181A mutant with N-terminally fused mCherry
EGFR-QG-mCitrine	Encoding human EGFR with linker inserted mCitrine between Q958 and G959
pHR SFFVp PHAkt Cerulean	Encoding PH domain of Akt with C-terminally fused mCerulean
pSpCas9(BB)-2A-GFP (PX458)	Encoding Cas9 from S. pyogenes with 2A-EGFP
tagBFP-PTP1B	Encoding human PTP1B with N-terminally fused tagBFP
PTP1B-RFP-tKRas	Encoding human PTP1B with C-terminally fused RFP and tKRas
EGFR-paGFP	Encoding human EGFR with C-terminally fused paGFP
PTB-mCherry	Encoding PTB domain from Shc with C-terminal mCherry
HA-Ubiquitin	Encoding HA-Ubiquitin
eGFP-ERK	Encoding Rat ERK2 N-terminally fused to eGFP

3.1.10 Instruments and equipment

Eppendorf Research® plus pipettes	Eppendorf
Falcon tubes (15/50 ml)	BD Falcon™
Eppendorf safe lock tubes (0.5/1.5/2/5 ml)	Eppendorf
Heatable magnetic stirrer “IKMAG®RCT”	IKA®Labortechnik
Heating block ”QBD4”	Grant Instruments
Nanodrop® ND-1000 spectrophotometer	Peqlab Biotechnologie GmbH
Parafilm®	Pechiney Plastic Packaging
PFE powder-free latex exam gloves (S)	Kimberly-Clark
Pipetboy accu	Integra Biosciences

Safegrip® nitril gloves (S)	Süd-Laborbedarf GmbH
Sarstedt serological pipettes (5/10/25 ml)	Sarstedt
Surgical disposable scalpel (No. 11, No.21)	Braun Melsungen AG
Thermomixer comfort	Eppendorf
“Vortex Genie 1” touch mixer	Scientific Industries
BioRad Power Pac 300	Bio-Rad Laboratories, Inc.
BioRad Power Pac HC	Bio-Rad Laboratories, Inc.
Centrifuge 5415R	Eppendorf
Centrifuge 5810R	Eppendorf
1.5 mm cassettes for western blots	Invitrogen™ Life Technologies
1.5 mm 10-well combs	Invitrogen™ Life Technologies
1.5 mm 15-well combs	Invitrogen™ Life Technologies
Incubation box for western blots	Li-Cor® Biosciences
Incubator Shaker Series I26	New Brunswick Scientific
Odyssey Infrared Imager	Li-Cor® Biosciences
Immobilon-FL PVDF	Millipore, Merck KGaA
Sonicator needle (MS 73)	Bandelin Electronic GmbH
Ultraschall HD 2200	Bandelin Electronic GmbH
XCell SureLock™ Mini-Cell Electrophoresis System	Invitrogen™ Life Technologies
XCell II™ Blot Module	Invitrogen™ Life Technologies
Cell scraper	BD Falcon™
75 mm filter unit	Nalge Nunc International
Glass Pasteur pipettes (150 mm, 230 mm)	Brand GmbH & Co. KG
4-well LabTek® chambers No. 1.0	Nalge Nunc International
8-well LabTek® chambers No. 1.0	Nalge Nunc International
35-mm MatTek petri dishes No. 1.5	MatTek Corporation
NUAIRE™ Cellgard class II biological safety	Integra Biosciences

cabinet	
Tissue culture plate (6 well)	BD Falcon™
Vacusafe comfort	Integra Biosciences
AutoFlow NU-4750 Water Jacket CO_2 Incubator	Integra Biosciences
96 well dishes	Corning, Merck

3.1.11 Software

Adobe Illustrator	Adobe Systems Inc.
FV10-ASW Fluoview Software	Olympus
Fiji	Schindelin et al., 2012[113].
Microsoft Office 2011	Microsoft Corporation
Odyssey® Infrared Imaging System	LI-COR Biosciences GmbH
Leica LAS-AF	Leica Microsystems
GraphPad Prism 6	GraphPad Software, Inc.
Leica Application Suite X	Leica MICROSYSTEMS
Python	Python Software Foundation
CellProfiler	Kamentsky et al., 2011[114].
ImageJ64 v1.44	http://rsbweb.nih.gov/
NanoDrop ND-3300 2.6.0	Coleman Technology Inc.
DNASTAR Navigator v2.2.1.1	DNASTAR Inc.
Quantity One 4.6.9	Bio-Rad Laboratories, Inc.
Application software Version 2.1	
Multiscan Ascent Software Version 2.6	ThermoElectron Coorperation
IgorPRo v6.12	WaveMetrics

3.2 Molecular Biology

3.2.1 Polymerase chain reaction (PCR)

PCR reactions to amplify target DNA sequences using specific primer pairs were performed using the Q5® High-Fidelity DNA Polymerase. The following reaction setup and thermocycling Conditions were used:

Component	Volume [µl]
5X Q5 Reaction Buffer	10
10 mM dNTPs	1
FW Primer (10 µM)	2.5
BW Primer (10 µM)	2.5
1-10 ng template DNA	X
Q5 High-Fidelity DNA Polymerase	0.5
H_2O	30.75 – X

Table 1: 50 µl PCR batch for Q5® High-Fidelity DNA Polymerase. The volume X of the template naturally depends on its concentration.

Cycle	Temperature [°C]	Time [s]	Cycles
Initial denaturation	98	30	1
Denaturation	95	10	30
Annealing	*50–72 °C	20	
Elongation	72	30 s/kbp	
Final elongation	72	120	
-	8	hold	

Table 2: PCR-protocol for Q5® High-Fidelity DNA Polymerase. *The annealing temperature, depends on the used primers.

3.2.2 Agarose gel electrophoresis

DNA strands were separated according to their size using agarose gels with concentrations in the range of 1.2 – 2.0 % (w/v) as matrix. Gels were prepared with TAE buffer supplemented with the DNA binding dye RedSafeTM (50 µl/l). The size of the observed strands was determined by comparison with marker fragments of known size using the GelDoc XR System. Designated DNA-fragments were cut out of the gel and purified using the "ZymocleanTM Gel DNA Recovery Kit" from Zymo Research following the manufacturer's instructions.

3.2.3 Restriction digestion

Restriction digestion was performed using High-Fidelity (HF®) Restriction Endonucleases (New England Biolabs). Restriction batches of 50 µl were prepared and incubated at 37 °C for 3 h.

Component	Volume [µl]
CutSmart™ Buffer	5
Restriction Endonucleases	1 each
5µg template DNA	X
H_2O	46 – X

Table 3: 50 µl restriction batch. The volume X of the template naturally depends on its concentration.

3.2.4 Dephosphorylation of 5'-Phosphorylated DNA fragments

In order to prevent self-ligation resulting in false positive vector background, linearized plasmids were treated with 1 µl calf intestinal phosphatase (CIP) for 15 min at 37 °C.

3.2.5 Ligation of DNA Fragments

Ligation of DNA fragments and plasmids, was performed using the Quick Ligation™ Kit (New England Biolabs). The starting ligation conditions required 50 ng vector DNA and threefold excess of the insert DNA. The vector/insert ratio was calculated according to the following equation:

$$\frac{ng(\text{vector}) \cdot kB(\text{insert})}{kB(\text{vector})} \cdot 3 = ng(\text{insert})$$

The calculated amount of vector/insert DNA was supplemented with 10 µl 2x Quick Ligation Buffer, 1 µl of Quick T4 DNA Ligase and H_2O to a total reaction volume of 20 µl. The mixture was incubated for 1 h at room temperature and afterwards for 10 min at 65 °C to inactivate the ligase

3.2.6 Site-Directed Mutagenesis

Site-specific mutagenesis of double-stranded plasmid DNA was performed using the Q5® Site-Directed Mutagenesis Kit according to the manufactures instructions. Custom mutagenic primers to create insertions, deletions and substitutions were designed using the NEBaseChanger tool (https://nebasechanger.neb.com/).

3.2.7 Transformation of chemically competent E. coli cells

For transformation 50 µl of chemical competent XL 10-Gold cells were used. The cells were thawed on ice and 1.75 µl of 2.25 M DTT and 5 µl ligation-reaction mix or 1 µl plasmid for re-transformation were added and left on ice for 30 min. Afterwards cells were heat-shocked for 30 - 60 s at 42 °C and immediately placed on ice for 2 min. 125 µl SOC medium were added and the cells were incubated at 37 °C for 1 h while shaking. In case of a ligation mix, the whole cell suspension was plated on LB agar plates containing an appropriate antibiotic for selection. For re-transformation 50 µl cell suspension were used for plating.

3.2.8 Plasmid preparation

Single colonies from LB agar plates were transferred into 5 ml LB-medium containing the appropriate antibiotic and incubated overnight at 37 °C and 225 rpm. For MIDI preps a pre-culture of 5 ml was grown for approximately 6 h and afterwards used to inoculate an overnight culture of 200 ml. Plasmids were purified using the Using Roti®-Prep Plasmid MINI kit (Carl Roth GmbH) or the High Pure endotoxin-freeNucleoBond® Xtra Midi EF kit (MACHEREY-NAGEL) according to the manufacturers' instructions.

3.2.9 Determination of DNA concentration

The DNA concentration was determined with the Nanodrop® ND-1000 spectrophotometer from Peqlab by measuring the absorption at 260 nm. The concentration was calculated using the approximation that an OD_{260} of 1 corresponds to a double stranded DNA concentration of 50 ng/µl.

3.2.10 DNA Sequencing

DNA sequences were evaluated using the light-speed Sanger sequencing service from GATC (Eurofins GATC Biotech GmbH). Therefore 5 µl of purified plasmid DNA (80 - 100 ng/µl) or purified PCR fragments (20 – 80 ng/µl) were premixed with 5 ul of the respective sequencing primer (5 µM).

3.3 Protein biochemistry

3.3.1 Preparation of cell lysates

Cells were lysed on ice in ready-made Cell Lysis Buffer (9803, Cell Signaling Technology) supplemented with Complete Mini EDTA-free protease inhibitor (Roche Applied Science) and phosphatase inhibitor cocktail 2 and 3 (P5726 and P0044, Sigma Aldrich). Samples were collected in precooled 1.5 ml tubes and cleared by centrifugation for 10 min, 13,000 rpm at 4 ˚C and the supernatant was transferred to a fresh precooled 1.5 ml tube.

3.3.2 Immunoprecipitation

For immunoprecipitation cell lysis was performed in modified RIPA buffer on ice. Following lysis, the samples were subjected to sonication for 12 s and then cleared by centrifugation for 15 min, 13,000 rpm at 4 ˚C. Equal amounts of protein lysates were incubated with an anti-EGFR antibody (AF231 1:200) over night at 4 ˚C followed by incubation for 2 h with Protein-G Sepharose beads. Afterwards the beads were incubated with 20 ul 1x SDS sample buffer and incubated for 5 min at 95 °C and centrifuged at 16100 g for 1 min. The supernatant was loaded on an SDS gel. All wash steps of the Protein-G Sepharose beads were performed with modified RIPA.

3.3.3 BCA assay

The protein concentration of whole cell lysates was determined using the Micro BCA™ Protein Assay Kit. The assay was performed in a 96-well plate, using 4 µl whole cell lysate or BSA standard and 80 µl BCA working reagent (25:24:1, Reagent A: B: C). The plate was incubated for 30 min at 37 °C. For calibration, a BSA dilution series starting with 0.1 µg/ml up to 20 µg/ml (0.1; 0.2; 0.4; 0.5, 1; 2; 5; 10; 20) was measured. Protein concentrations of whole cell lysates were then determined by mapping their absorbance values at 562 nm with regard to the standard curve.

3.3.4 SDS PAGE

SDS–PAGE was performed using the X-cell II mini electrophoresis apparatus (Life Technologies) according to the manufacturer's instructions. Cell lysates were mixed with 5x SDS sample buffer and incubated for 5 min at 95 °C. Prior loading on a SDS polyacrylamide gel samples were centrifuged at 16100 g for 1 min. A molecular weight standard was used to assess the correct size of the protein of interest. Electrophoresis was performed at a constant voltage of 130 V until for approximately 90 min. According to the size of the protein of interest different SDS polyacrylamide gel compositions were chosen.

3.3.5 Western blotting

Following size separation by SDS PAGE, proteins were transferred on a PVDF membrane via electroblotting using the XCell II™ Blot Module according to the manufacturer's instructions. The transfer was performed at a constant voltage of 40 V for 75 min. Afterwards membranes were blocked for 1 h at room temperature using Odyssey infrared imaging system blocking buffer (blocking buffer). Membranes were then incubated with the respective primary antibodies diluted in blocking buffer in an antibody dependent ratio (1:200 - 1:5000) at 4 °C overnight. For detection membranes were incubated with species-specific secondary IR-Dye 800 CW and IR-Dye 680 CW antibodies (LI-COR Biosciences) for 1 h at room temperature and subsequently scanned with the Odyssey Infrared Imaging System (LI-COR Biosciences). All wash steps following primary or secondary antibody incubation were performed with TBS/T. Following background subtraction, integrated intensities of the protein bands of interest were obtained in FIJI and used for further calculations.

3.4 Cell biology

3.4.1 Cell culture

COS-7 and MCF7 cells were maintained in Dulbecco's Modified Eagle's Medium (DMEM) supplemented with 10 % fetal bovine serum (FBS), 2 mM L-glutamine (L-Glu) and 1 % nonessential amino acids (NEAA) at 37 °C and 5 % CO_2. Prior growth factor stimulation cells were starved for at least 6 h in DMEM supplemented with 0.5 % FBS, 2 mM L-Glu and 1 % NEAA.

3.4.2 Transient Transfection

COS-7 and MCF7 cells were transiently transfected using the Fugene® 6 transfection reagent, according to the manufacturer's instructions and subsequently incubated at 37 °C and 5 % CO_2 for at least 6 h before starvation.

3.4.3 RNA interference

Transfection of Rab11a siRNA was performed using siRNA transfection reagent and transfection medium according to the manufacturer's instructions. Both Rab11a siRNA or scrambled non-targeting control siRNA were used at a final concentration of 50 nM for 72 h before validation of knockdown. EGFR-mCitrine transfection was performed 48 h after siRNA transfection as described above (see Transient Transfection).

ErbB2/3/4 and non-targeting control siRNA were used at a final concentration of 100 nM for 48 h before validation of knockdown. Transfection was performed using Dharmafect1 according to the manufacturer's instructions.

3.4.4 CRISPR/Cas9

pSpCas9(BB)-2A-GFP (PX458) was a gift from Feng Zhang (Addgene plasmid #481138). The CRISPR guide sequences were designed using the Broad Institute sgRNA design website (https://portals.broadinstitute.org/gpp/public/analysis-tools/sgrna-design):

- KSR1 exon 14: 5'-GGATGCCTACCGGGTACCGT-3'
- KSR2 exon 2: 5'-AATCGTCGATGTGCGCAAGG-3'

The sgRNAs were cloned into the BbsI site of the pX458 expression vector as described previously by Ran et al.[115]. MCF7 cells were plated into 6 well dishes and transfected with 2 µg of each pX458 construct using Fugene® 6, cells were FACS sorted 24 h post-transfection using GFP expression and seeded into 96 well dishes by serial dilutions. Single clones were expanded and evaluated for knockout status by western blot analysis for KSR1 and KSR2.

3.5 Immunohistochemistry

3.5.1 In-cell western assay

Cells were seeded on black, transparent bottomed 96-well plates coated with poly-L-lysine. Following growth factor administration cells were fixed with 4 % Histofix in PBS (v/v) for 5 min at 37 °C and permeabilized with 0.1 % Triton X-100 (v/v) for 5 min at room temperature. Samples were incubated in Odyssey TBS blocking buffer (LI-COR Biosciences) for 30 min at room temperature. Primary antibodies were incubated overnight at 4 °C and secondary antibodies (IRDyes, LI-COR Biosciences) were incubated for 30 min at room temperature. All wash steps were performed with TBS (pH 7.4). Intensity measurements were performed using the Odyssey Infrared Imaging System (LI-COR Biosciences). Quantification of the mean intensity in each well was performed in FIJI using the MicroArray Profile plugin.

3.5.2 Immunofluorescence

Cells grown in 4- or 8-well Labteks were rinsed once with PBS (pH 7.4) and fixed using 4 % Histofix or paraformaldehyde in PBS (v/v) for 10 min at room temperature. Cells were permeabilized with 0.1 % Triton X-100 (v/v) for 5 min. Background staining was blocked by incubation with Odyssey Blocking Buffer for 1 h at room temperature. Primary antibodies were applied in an antibody dependent ratio (1:200 - 1:400) for 1 h 30 min at room temperature or at 4 °C overnight. Secondary antibodies were diluted 1:200 and incubated for 1 h at room temperature. Primary and secondary antibodies were diluted in Odyssey Blocking Buffer. Fixed cells were imaged in PBS. All wash steps following fixation, permeabilization, primary or secondary antibody incubation were performed with TBS.

3.6 Microscopy

3.6.1 Leica SP5

The Leica TCS SP5 DMI6000 confocal microscope was equipped with an environment-controlled chamber maintained at 37˚C and a HCX PL APO 63x/1.4 NA oil objective. Fluorescent proteins were excited using, a 405 nm Cube laser (1162002/AF, Coherent, Santa Clara, CA) and 514 nm Argon laser line (LGK 7872 ML05, Lasos, Jena, Germany), a 561 nm DPSS laser (YLK 6120 T02, Lasos, Jena, Germany. Detection of fluorescence emission was restricted with an Acousto-Optical

Beam Splitter (AOBS) as follows - BFP (415–458 nm), mCitrine (524–551 nm), mCherry (571–623 nm. The pinhole was set to 250 µm and 16-bit images of 512x512 pixels were acquired.

3.6.2 Leica SP8

The Leica TCS SP8 confocal microscope was equipped with an environment-controlled chamber (LIFE IMAGING SERVICES, Switzerland) maintained at 37 ˚C and a HC PL APO CS2 1.4 NA oil objective (Leica Microsystems). Fluorescent fusion proteins with mCitrine, mCherry and Alexa647 labeled secondary antibodies were excited with a 470–670 nm white light laser (white light laser Kit WLL2, NKT Photonics) at 514 nm, 561 nm and 633 nm, respectively. mTagBFP was excited with a 405 nm diode laser and mCerulean with a 458 nm Argon laser line. Detection of fluorescence emission was restricted with an Acousto-Optical Beam Splitter (AOBS): mCitrine (498-551 nm), mCherry (575-675 nm), mCerulean (468-505 nm), mTagBFP (425-448 nm), Alexa647 (643–755 nm). The pinhole was set between 1.5 and 2.5 airy units and 12-bit images of 512x512 pixels were acquired in sequential mode.

3.6.3 OlympusFV1000

The Olympus Fluoview FV1000 confocal microscope was equipped with a environment-controlled CO_2 incubation chamber at 37 ˚C and a 60x/1.35 NA Oil UPLSApo objective. Fluorescent fusion proteins with BFP, mCitrine and mCherry or Alexa647-, Alexa555-, Alexa488-labeled secondary antibodies were excited using the 405 nm Diode-UV laser (FV5-LD05, Hatagaya), 488 nm Argon-laser (GLG 3135, Showa Optronics, Tokyo, Japan), 561 nm DPSS laser (85-YCA-020-230, Melles Griot) and 633 nm HeNe laser (05LHP-991, Melles Griot), respectively. Detection of fluorescence emission was restricted as follows: mTagBFP (425-478 nm), mCitrine/Alexa488 (498-551 nm), mCherry/Alexa555 (575-675 nm), Alexa647 (655-755 nm). Scanning was performed in frame-by-frame sequential mode with 2x frame averaging. The pinhole was set between 1.5 and 2.5 airy units.

3.6.4 Cell migration

MCF7 cells were seeded onto fibronectin-coated (F0895, Sigma) 24-well culture dishes containing 2-well silicone culture-inserts to create a cell-free area. After the culture-insert was removed, cells were stimulated and imaged immediately. Wide field images were acquired using an Olympus IX81 inverted microscope equipped

with a MT20 illumination system, a 10x/0.16 NA air objective and an Orca CCD camera. Transmission images were acquired every 10 min for 12 h. During each experiment up to three fields were imaged for each condition. Segmentation of the cell-free area was performed using the MRI Wound Healing plugin in FIJI. The average distance (D) between the two edges was calculated using the assumption, that the length (L) of the cell-free area (A) is constant, since cells did not migrate into the field of view from the sites. Also, the width closes in at twice the speed the cell migration, resulting in $D = \frac{A}{L*2}$. The edge migration distance in µm (EMD) was calculated by relating the obtained distance for a given time point ($D_{t=i}$) to the initial distance of the cell-free area ($D_{t=0}$): $EMD = D_{t=0} - D_{t=i}$. This metric is independent of the initial distance and thus enables robust quantitative comparison between different wells.

3.6.5 Single cell migration

MCF7 cells were seeded at low densities on fibronection-coated (F0895, Sigma) 24-well dishes and nuclei were stained using SiiR-Hoechst (0.5 nM). Transmission and fluorescence images were acquired every 10 min for 24 h using an Olympus IX81 inverted microscope equipped with a MT20 illumination system, a 10x/0.16 NA air objective and an Orca CCD camera. Following stimulation individual cells were detected and tracked by their nuclear staining in FIJI using the TrackMate plugin (https://imagej.net/TrackMate) to extract migration parameters. A minimum track length of 40 frames was applied.

3.7 Analysis of confocal fluorescence imaging data

All analysis of fluorescence imaging data required an initial background subtraction for all images obtained. A cell segmentor tool was developed in-house in Anaconda Python (Python Software Foundation, version 2.7, https://www.python.org/) to obtain radial profiles.

3.7.1 Quantification of the EGFR fraction at the RE

Binary masks of the RE were generated from thresholded BFP-Rab11a images and endosomal EGFR from thresholded EGFR-mCitrine images. The integrated fluorescence intensity of EGFR-mCitrine was determined from the corresponding

endosomal masks. The fraction of endosomal EGFR at the RE was determined by dividing EGFR intensities at the RE by total intensities of endosomal EGFR.

3.7.2 Quantification of the spatial distribution of pY845

Plasma membrane EGFR-mCitrine and pY845 intensities were quantified as mean fluorescence intensities in a 5-pixel ring of the cell periphery. Mean fluorescence intensities at the RE were obtained by using binary masks of the RE, generated from thresholded BFP-Rab11a images. The difference in the relative phosphorylation level (pY845/EGFR-mCitrine) at the PM and RE ($(pY845/EGFR)_{PM}$ - $(pY845/EGFR)_{RE}$) was plotted as a function of the overall EGFR phosphorylation level in individual cells.

3.7.3 Quantification of PH-Akt translocation

To quantify the plasma membrane recruitment of PH-Akt-mCerulean cells were divided into 6 equally spaced radial bins emanating from the nuclear membrane and the normalized ratio of the mean intensities between the most inner (cytosol) and outer (plasma membrane) segments was measured for individual cells.

3.7.4 Quantification of ErbB-mCitrine internalization

To quantify the PM loss of EGFR-, ErbB2- and ErbB3-mCitrine cells were divided into 11 equally spaced radial bins emanating from the center off mass and the normalized ratio of the outer (plasma membrane) segment over the total intensity was measured for individual cells.

3.7.5 Quantification of pRb and CyclinD1 expression

Mean fluorescence intensities of nuclear pRb and CyclinD1 obtained were obtained following segmentation of Hoechst stained nuclei using CellProfiler.

3.7.6 Quantification of EGFR phosphorylation

Masks for single cells were generated and mean fluorescence intensities for EGFR-mCitrine and phospho-specific antibodies were measured in FIJI. The obtained values were used to calculate the relative EGFR phosphorylation level (pY/EGFR) for individual cells.

4 Results

4.1 Spatial regulation of EGFR activity by vesicular trafficking

Autocatalytic amplification of ligand-induced EGFR activation ensures robust receptor activation to extracellular signals, but on the other hand creates the potential to amplify spontaneous phosphorylation events in the absence of growth factors. Since the propagation of EGFR activity depends on its the expression level, regulation of EGFR plasma membrane abundance and phosphorylation form important parameters to suppress spontaneous EGFR activity[41,45]. Endocytosis of ligand-activated EGFR has been shown to promote its interaction with spatially distributed protein tyrosine phosphatases, however the role of vesicular trafficking in the regulation of autonomous receptor activity has not been addressed yet[78]. In the first part of this thesis we examined the role of EGFR vesicular dynamics in the regulation of autonomous receptor activity.

4.1.1 The dependence of spontaneous EGFR phosphorylation on its expression level

To study the dependency of EGFR activity on its plasma membrane density, the relative phosphorylation of three tyrosine residues with different regulatory functions (autocatalysis, Y845; trafficking, Y1045; and signaling, Y1068) was quantified as a function of EGFR expression level in single cells (**Fig.7A**). Cell-by-cell variation in receptor expression following transient transfection of COS-7 cells with EGFR-mCitrine was exploited to obtain various levels of receptor expression. EGFR expression was determined relative to the expression of endogenous EGFR within a separate experiment using the abscissa-intercept of a linear fit to an EGFR-mCitrine intensity versus anti-EGFR antibody intensity plot (see Baumdick et al. 2015[116]). The expression of EGFR-mCitrine was comparable to the expression level of endogenous receptors and varied by a factor of 6 (from ~ 0.5 – 3)[116]. Single cell immunofluorescence analysis revealed that the fraction of phosphorylated receptors in unstimulated cells increased for each of the individual residues as function of EGFR-mCitrine expression (**Fig.7B**). The relative phosphorylation between the different tyrosine residues showed a higher increase for Y845 (~ sixfold increase) and Y1068 (~ eightfold increase) compared to the c-Cbl docking site Y1045 (~ twofold increase). In order to quantitatively compare the levels of autonomous

phosphorylation between the three residues, the ratio of relative phosphorylation (pY/EGFR) before and after stimulation with EGF was calculated (pre/2'EGF). This 'ratio of fractions' (pre/EGF) gives a comparable measure, despite potential differences in the inherent immunoreactivity of the employed antibodies. This analysis showed that the Y1045 site was significantly less phosphorylated as compared to tyrosine Y845 and Y1068 (**Fig.7C**).

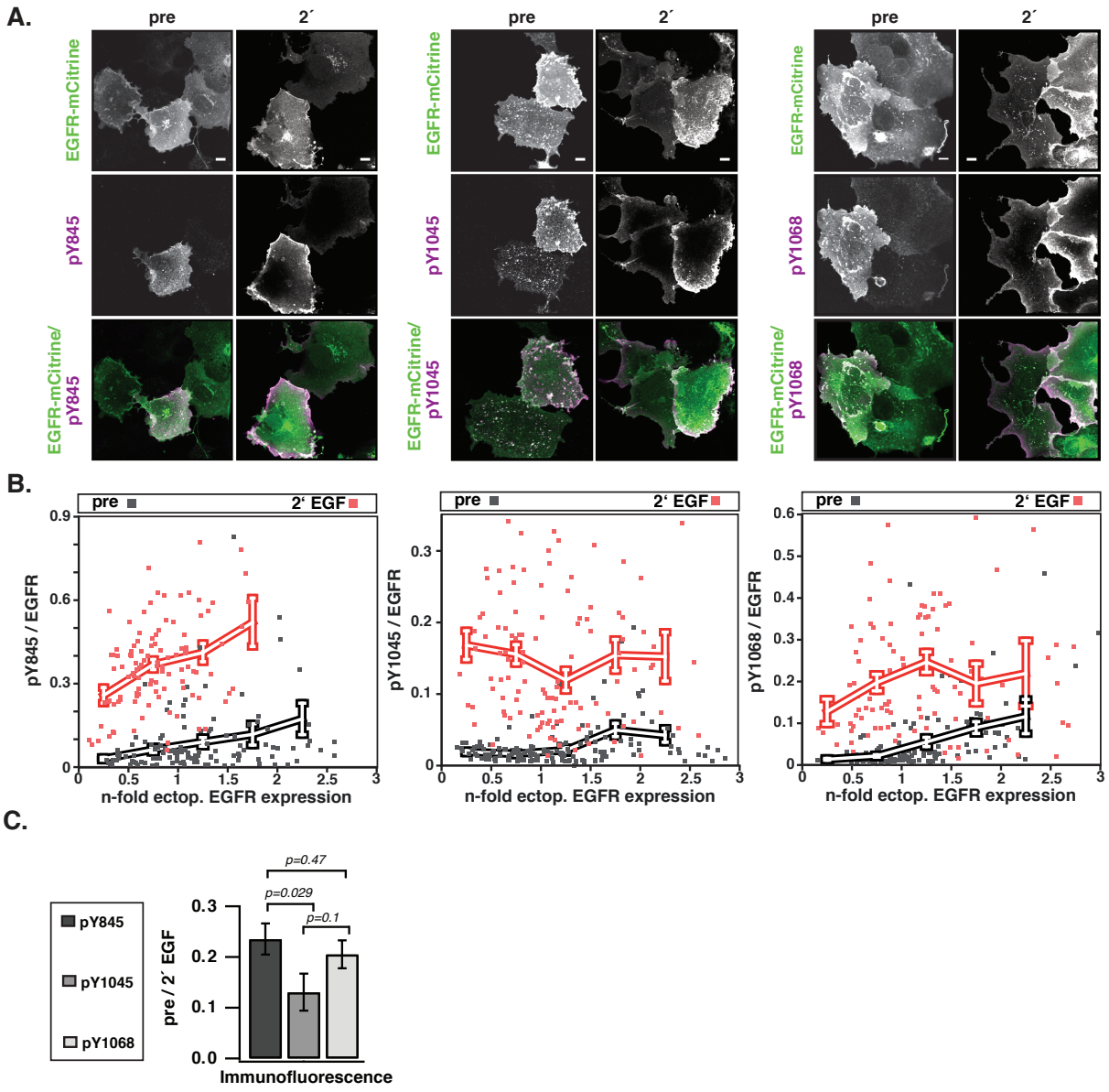

Figure 7: Expression level dependency of EGFR phosphorylation. (A) Immunofluorescence images of COS-7 cells ectopically expressing EGFR-mCitrine (first column) stained with specific pYN-antibodies (second column) and corresponding green/magenta overlay (third column) before or after 2 min stimulation with 100 ng/ml EGF. Scale bars = 10 µm. **(B)** Relative phosphorylation (pYN-antibody/EGFR-mCitrine) of the three tyrosine residues (Y845, Y1045, or Y1068) versus EGFR-mCitrine expression displayed as n-fold ectopic EGFR expression (see Baumdick et al. 2015 for details[116]). Data points (black: pre-; red: 2 min post-stimulation with EGF) represent single cells (87 - 145 cells/condition) and thick lines show mean values of binned data ± s.e.m..

(C) Ratio of relative phosphorylation (pY/EGFR) of Y845, Y1045 and Y1068 before (pre) and after 2 min stimulation with EGF (means ± s.e.m.). (Data obtained together with Dr. G.Xouri, Dr. M.Baumdick and Dr. M.Schmick).

To further assess autonomous EGFR phosphorylation among these distinct phosphosites, we performed quantitative Western blot analysis. COS-7 cells were transfected with different amounts of EGFR-mCitrine (0.5 µg, 1.5 µg, 3 µg, **Fig.8A**). The level of EGFR expression was determined relative to the maximally applied amount of cDNA (3 µg) and the ratio of relative phosphorylation (pre/EGF) before and after EGF stimulation was calculated to compare the level of autonomous phosphorylation among the three sites (**Fig.8B**). Similar to the immunofluorescence analysis, Y845 and Y1068 phosphorylation were more sensitive to increases in EGFR expression than Y0145, indicating higher levels of autonomous phosphorylation (**Fig.8C**).

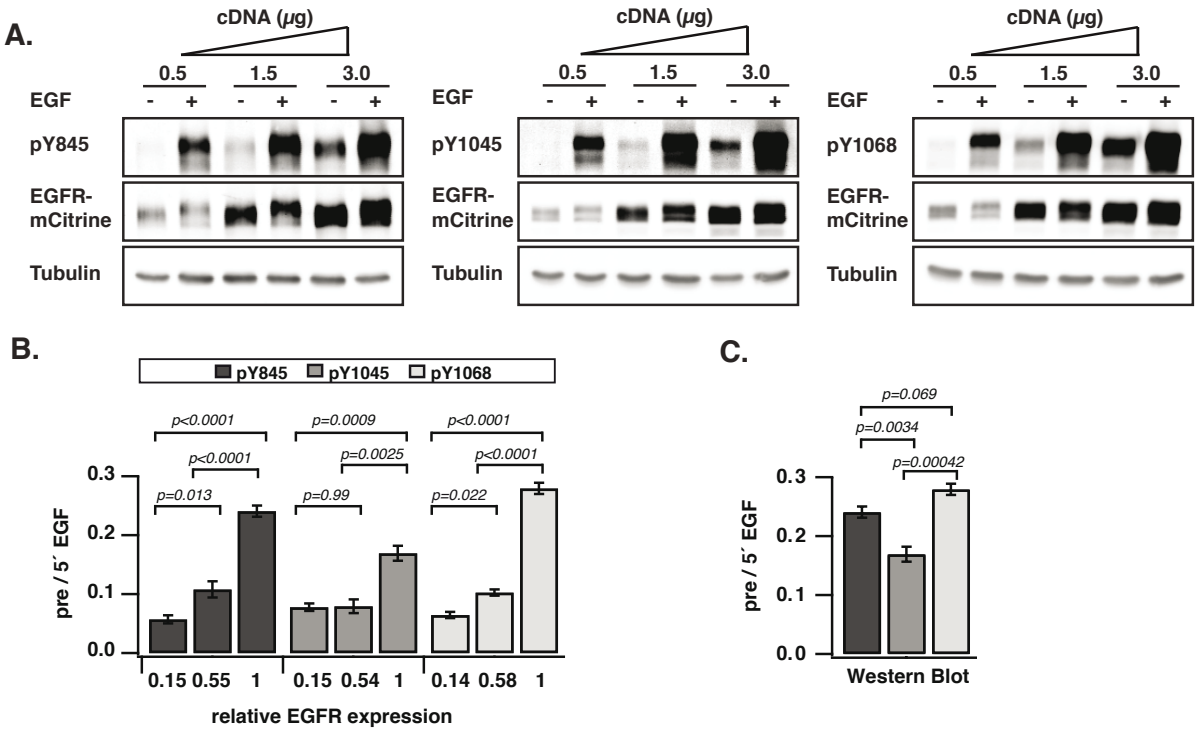

Figure 8: Expression level dependency of EGFR phosphorylation. (A) Cell lysates of COS-7 ectopically expressing increasing amounts of EGFR-mCitrine cDNA were collected before or 5 min post-stimulation with 100 ng/ml EGF. Lysates were immunoblotted for either anti-pY845 (left), anti-pY1045 (middle) or anti-pY1068 (right) and anti-tubulin, anti-GFP (EGFR-mCitrine). **(B)** Ratio of the relative phosphorylation (pY/EGFR) of Y845 (n = 5 blots), Y1045 (n = 3), or Y1068 (n = 3) before (pre) and after 5 min stimulation with EGF (5' EGF) from data shown in **(A)**. EGFR-expression levels are displayed as fraction of EGFR over the respective tubulin band in each lane relative to 3 µg cDNA (means ± s.e.m.). **(C)** Ratio of the relative phosphorylation (pY/EGFR) of Y845, Y1045, or Y1068 before (pre) and after 5 min stimulation with EGF (5' EGF). Data correspond to the highest levels of expressed EGFR-mCitrine (3 µg cDNA, means ± s.e.m.). Statistical significance in **(B)** and **(C)** was determined using an ordinary one-way ANOVA followed

by Tukey's multiple comparison test. (Data were acquired and analyzed together with Dr. M.Baumdick).

The overall level of EGFR phosphorylation results from a continuous and rapid cycle of phosphorylation and de-phosphorylation events. In order to distinguish the contributions of EGFR kinase activity from the counterbalancing PTP activity in generating the autonomous phosphorylation profile, the thiol reactive compound pervanadate was employed to globally inhibit PTP activity[54]. By this means, the obtained phosphorylation profile reflects only the catalytic efficiency of EGFR kinase for the three tyrosine residues and negates the potential influence of different dephosphorylation rates for each residue. Relative phosphorylation levels (pY/EGFR) were determined by Western blot analysis of COS-7 cells expressing EGFR-mCitrine upon treatment with EGF or PV (**Fig.9A**). Phosphorylation of Y845 was approximately 2.5 times higher upon PV treatment as compared to EGF stimulation, while Y1045 and Y1068 displayed similar phosphorylation levels upon either treatment (**Fig.9B**). Comparison of the ratio between autonomous and PV-induced phosphorylation allowed an estimation of the relative PTP activity in suppressing phosphorylation of the three tyrosine residues. The highest increase was observed for Y845 (~ twelve-fold increase), as compared to Y1045 (~ five-fold increase) and Y1068 (~ six-fold increase) (**Fig.9C**). Together these findings show that the autocatalytic phosphorylation site Y845 requires higher levels of PTP activity to suppress its autonomous phosphorylation as compared to the other two residues. The similar PTP activity acting on Y1045 and Y1068 further implies that differences in the catalytic efficiency of the EGFR kinase towards specific phospho-sites account for the differences observed in their autonomous phosphorylation.

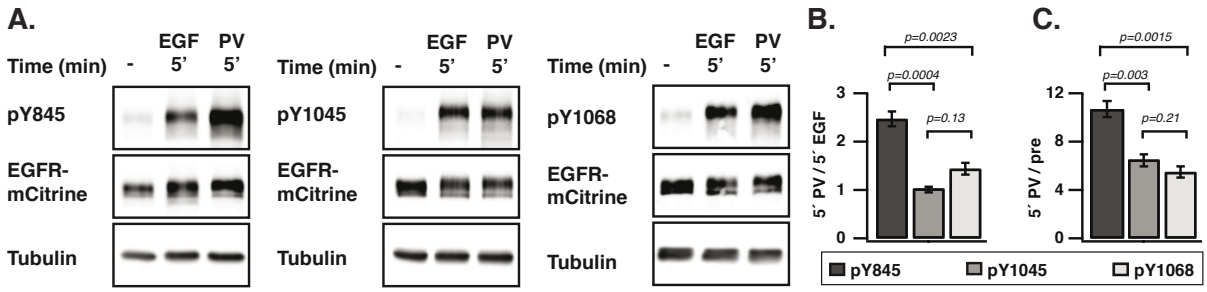

Figure 9: EGFR phosphorylation induced by PV-mediated PTP inhibition and EGF stimulation. (A) Lysates of COS-7 ectopically expressing EGFR-mCitrine were collected before or 5 min post-stimulation with 100 ng/ml EGF or 10 mM pervanadate (PV). Lysates were immunoblotted for either anti-pY845 (left), anti-pY1045 (middle) or anti-pY1068 (right), anti-tubulin and anti-GFP (EGFR-mCitrine). **(B)** Ratio of the relative phosphorylation (pY/EGFR) of Y845 (n = 3), Y1045 (n = 3), or Y1068 (n = 3) after 5 min treatment with pervanadate (5' PV) or stimulation

with EGF (5' EGF). **(C)** Ratio of the relative phosphorylation (pY/EGFR) of Y845, Y1045 or Y1068 before (pre) and after 5 min treatment with pervanadate (5' PV). Means ± s.e.m. in **(B)** and **(C)**. Statistical significance in **(B)** and **(C)** was determined using an ordinary one-way ANOVA followed by Tukey's multiple comparison test. (Data were acquired and analyzed together with Dr. M.Baumdick).

In order to examine whether autonomously activated EGFR promotes the activation of downstream signaling molecules, the phosphorylation of Erk and Akt was examined by Western blot analysis (**Fig.10A**). Interestingly, increasing levels of EGFR-mCitrine expression promoted the phosphorylation of Akt, while the phosphorylation of Erk was not affected (**Fig.10B, C**). Similar results were obtained upon ectopic expression of an EGFR mutant often found in lung cancer (EGFR-L834R-mCitrine), which showed elevated phosphorylation levels in the absence of ligand, but not upon stimulation with EGF as compared to wild type EGFR (EGFR-mCitrine)[34] (**Fig.10D, E**). The expression of EGFR-L834R-mCitrine resulted in a significant increase of Akt phosphorylation, while the phosphorylation of Erk was not significantly affected (**Fig.10E**). In addition to dimer formation, ligand-induced self-association of EGFR has also been reported to generate higher-order multimers, whose function is poorly understood[39,40]. We therefore examined whether the distinct phosphorylation pattern and signaling behavior of autonomously activated receptors and ligand-activated receptors correlates with differences in the self-association state of the receptor. Therefore fluorescence anisotropy microscopy measurements were performed to detect EGFR self-association via homo-FRET[117,118]. To this end an EGFR construct with mCitrine inserted via a linker between amino acids Q958 and G959 (EGFR-QG-mCitrine) was employed, which exhibited a similar phosphorylation response as EGFR-mCitrine (see Baumdick et al. 2015[116]). In the absence of ligand, EGFR-QG-mCitrine displayed similar anisotropy values independent of its expression level, implying a low self-association state of autonomously activated receptors even at high expression levels (**Fig.10F**). Consistent with this finding, increasing EGFR phosphorylation by PV treatment did not induce a change in anisotropy compared to unstimulated cells (**Fig.10G**). In contrast, EGF stimulation resulted in a decrease in anisotropy values, demonstrating that ligand binding promotes an increase in receptor self-association (**Fig.10F**). Collectively, these findings suggest that autonomously activated and ligand-activated receptors represent different signaling entities with distinct states of self-association.

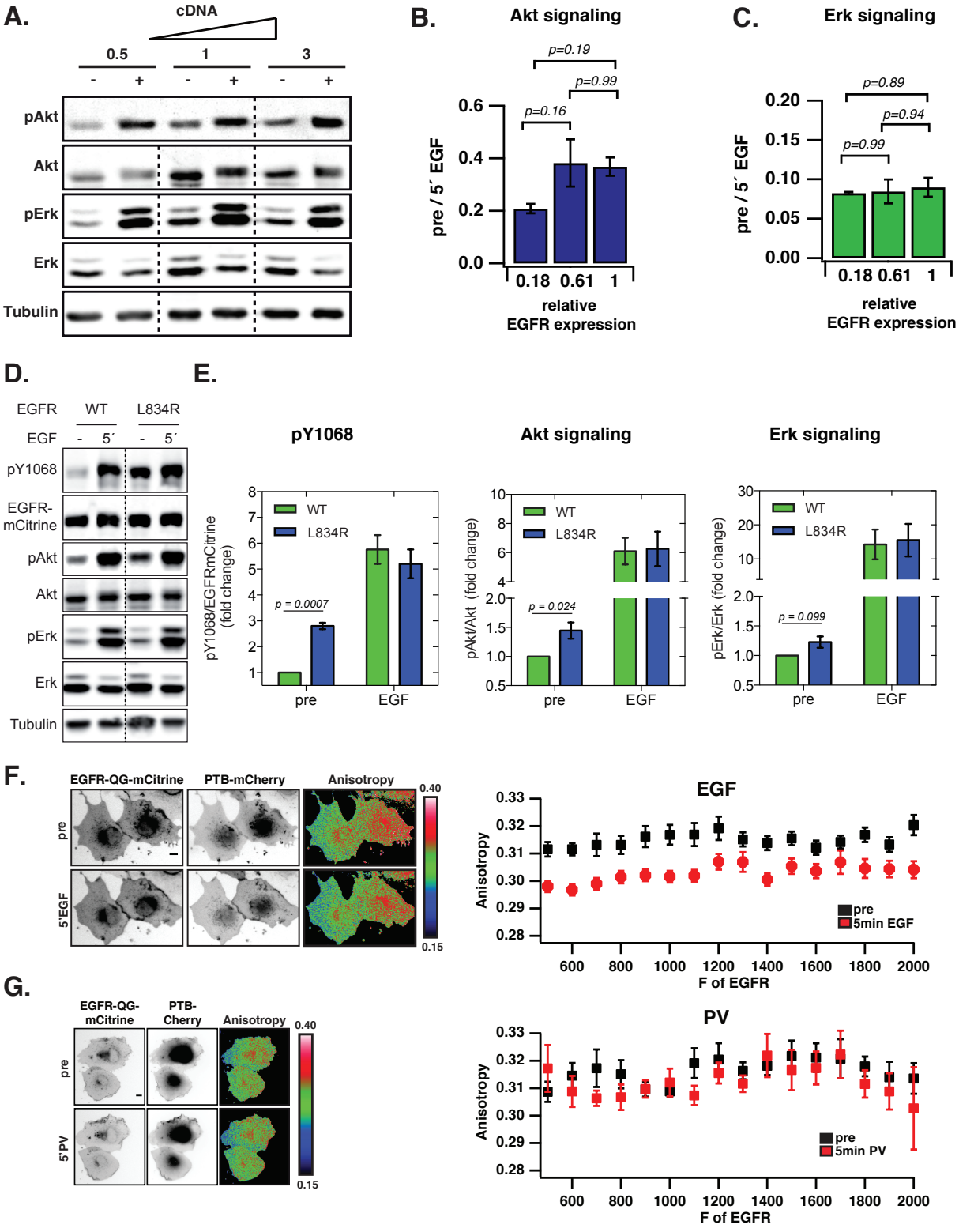

Figure 10: Autonomously and ligand-activated receptors represent different signaling entities. (A) Lysates of COS-7 ectopically expressing increasing amounts of EGFR-mCitrine cDNA were collected before or 5 min post-stimulation with 100 ng/ml EGF. Lysates were immunoblotted for anti-pAkt (S473), anti-Akt, anti-pErk, anti-Erk and anti-tubulin. **(B)** Ratio of the relative phosphorylation (pAkt/Akt) of Akt S473 before (pre) and after 5 min stimulation with EGF (5' EGF). EGFR-expression levels are displayed as fraction of EGFR over tubulin band in each lane relative to 3 µg cDNA. (n = 3, means ± s.e.m.). **(C)** Ratio of the relative phosphorylation (pErk/Erk) of Erk before (pre) and after 5 min stimulation with EGF (5' EGF). EGFR-expression

levels are displayed as fraction of EGFR over the respective tubulin band in each lane relative to 3 µg cDNA (n = 3, means ± s.e.m.). Statistical significance in **(B)** and **(C)** was determined using an ordinary one-way ANOVA followed by Tukey's multiple comparison test. **(D)** Lysates of COS-7 ectopically expressing EGFR-mCitrine or EGFR-L834R-mCitrine cDNA were collected before or 5 min post-stimulation with 100 ng/ml EGF. Lysates were immunoblotted for anti-GFP (EGFR-mCitrine), anti-pY1068, anti-pAkt (S473), anti-Akt, anti-pErk, anti-Erk and anti-tubulin. **(E)** Quantification of the relative phosphorylation of EGFR (left), Akt (middle) and Erk (right) (n = 4, means ± s.e.m.). Statistical significance was determined using a one sample t test. **(F)** and **(G)** Left panel: COS-7 cells ectopically expression EGFR-QG-mCitrine and PTB-mCherry to assess EGFR phosphorylation and corresponding mCitrine anisotropy before and 5 min post-stimulation with 100 ng/ml EGF or 10 mM pervanadate (PV)[22,55]. Scale bars = 10 µm. Right panel: Anisotropy of EGFR-QG-mCitrine versus binned mean fluorescence intensities of EGFR (F of EGFR) before and after EGF or PV stimulation (means ± s.e.m.). (Data in **(F)** and **(G)** were acquired together with Dr. G.Xouri and Dr. M.Baumdick, see Baumdick et al. 2015[116]).

4.1.2 EGFR continuously recycles through the pericentriolar recycling endosome

The balance between receptor internalization and recycling determines the density of EGFR at the plasma membrane. To assess whether, in the absence of ligand, EGFR is maintained at the plasma membrane via vesicular recycling, it was investigated whether EGFR partitions in the Rab11-positive pericentriolar recycling endosome (RE)[119]. Both immunofluorescent staining of endogenous Rab11 and EGFR and ectopic expression of EGFR-mCitrine and BFP-Rab11a in unstimulated COS-7 cells showed co-localization within the perinuclear area (**Fig.11A**). Ectopic expression of BFP-Rab11a resulted in enhanced biogenesis of the RE and thereby shifted the distribution of EGFR towards this compartment (**Fig.11B**). Blocking protein synthesis did not affect the localization of either EGFR-mCitrine or BFP-Rab11a, demonstrating that co-localization did not originate from newly synthesized EGFR transiting through the Golgi via the secretory pathway (**Fig.11C**).

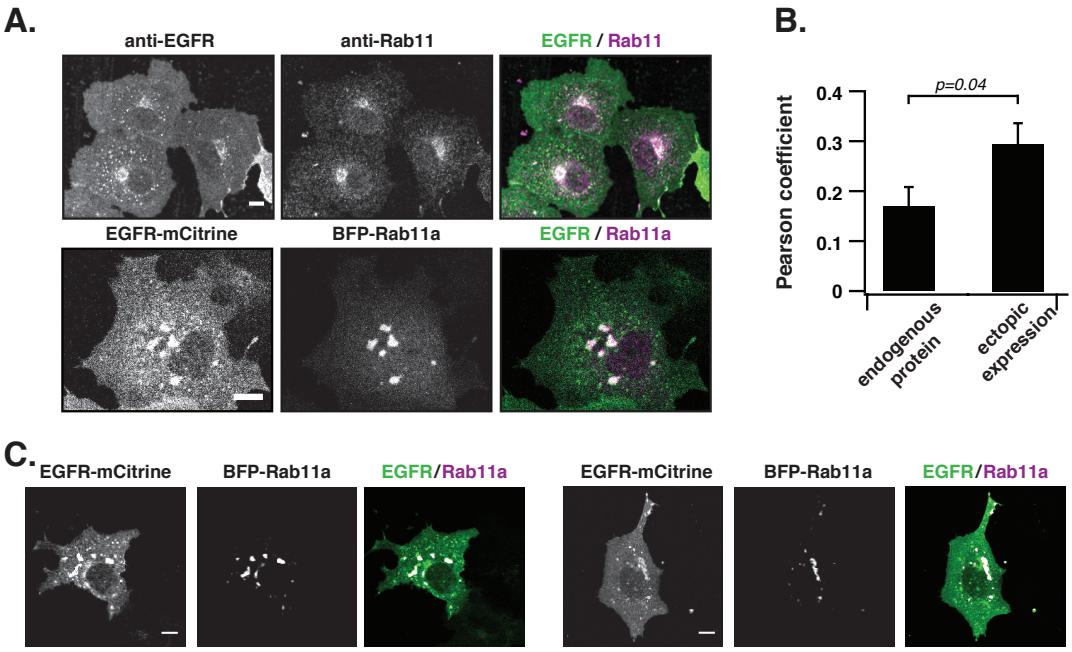

Figure 11: Co-localization of EGFR and Rab11. (A) Upper row: Immunofluorescence images of COS-7 cells stained for endogenous EGFR (first column) and Rab11a (second column) with corresponding green/magenta overlay (third column). Lower row: Fluorescence images of COS-7 cells ectopically expressing EGFR-mCitrine and BFP-Rab11a with corresponding green/magenta overlay (third column). **(B)** Quantification of co-localization between EGFR and Rab11 (n = 12-15 cells/condition) by Pearson's correlation coefficient (means ± s.e.m.). (Data for ectopic expression kindly provided by Dr. G.Xouri). **(C)** Fluorescence images of two individual COS-7 cells co-expressing of EGFR-mCitrine, BFP-Rab11a and corresponding green/magenta overlay after treatment with cyclohexamide (10 µg/ml) for approximately 20 h. All scale bars = 10 µm.

In order to assess the kinetics of EGFR recycling, fluorescence loss after photoactivation (FLAP) and fluorescence recovery after photobleaching (FRAP) measurements were performed (**Fig.12A, C**). FLAP of EGFR fused to photoactivatable GFP (EGFR-paGFP) on Rab11 positive endosomes demonstrated that EGFR is exported from the RE (t = 273 ± 15 s) and is concurrently transported to the plasma membrane (t = 167 ± 33 s, **Fig.12B**). The differences in tau can be explained due to the differences in the surface area of the PM with respect to the RE, which determines the rate PM-association and the RE-dissociation. Fitting the FLAP data based on a two-compartment model estimated a residence time of ~7.6 min of EGFR at the RE (see Baumdick et al. 2015[116]). FRAP measurements further confirmed that EGFR enters the RE (t = 540 ± 47 s, **Fig.12C**). Together these findings confirm that continuous vesicular recycling of EGFR maintains a steady state spatial distribution of the receptors residing at the plasma membrane. In a set of complementary experiments, it was further shown that EGFR traffics from the PM to the RE through Rab5-positive endosomes. EGF stimulation redirects vesicular

trafficking from Rab5-positive endosomes to LAMP1-positive endosomes (see Baumdick et al. 2015[116]).

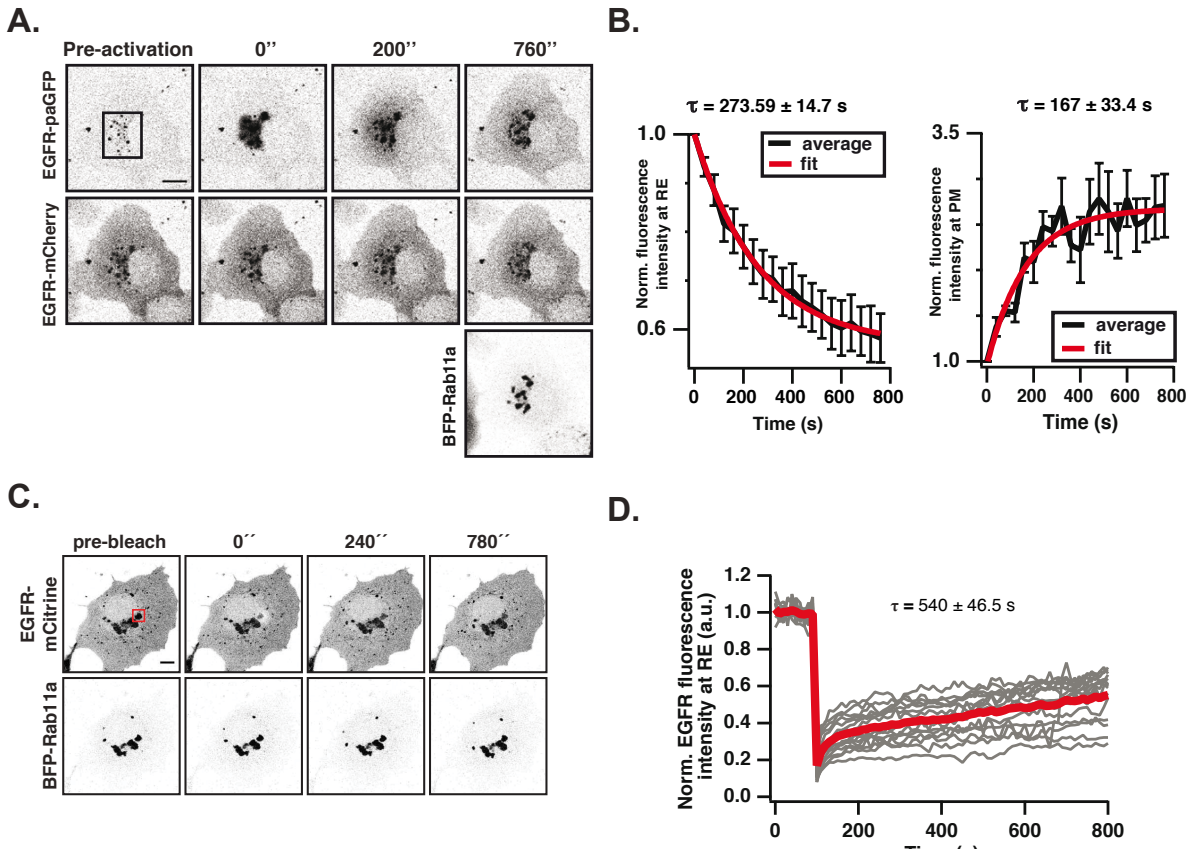

Figure 12: Continuous recycling of EGFR through the RE. (A) Fluorescence redistribution of EGFR-paGFP upon photoactivation on the RE in COS-7 cells. First row EGFR-paGFP before (black rectangle) and after photoactivation for the indicated times in seconds, second row: corresponding fluorescence images of EGFR-mCherry, third row: fluorescence image of BFP-Rab11a. **(B)** Loss of EGFR-paGFP/EGFR-mCherry fluorescence at the RE (left) and concomitant gain of at the PM (right). Normalized average traces (mean ± s.e.m., n = 6 cells) were fitted to an exponential function (red) to retrieve time constants (t). **(C)** Fluorescence recovery after photobleaching of EGFR-mCitrine in COS-7 cells co-expressing BFP-Rab11a before and after photobleaching (black rectangle) for the indicated times in seconds. **(D)** Normalized mean fluorescence intensity of the bleached area (red line: mean values, grey lines: individual recovery curves, n = 16 cells). All scale bars = 10 µm. (Data kindly provided by Dr. G.Xouri, Dr. M.Baumdick and Dr. M.Schmick).

4.1.3 Vesicular recycling suppresses autonomous EGFR activation

Next, to examine the contribution of vesicular recycling to the regulation of autonomous EGFR phosphorylation, the biogenesis of the RE was decreased by siRNA mediated knockdown of Rab11 or enlarged upon ectopic expression of BFP-Rab11a (**Fig.13A, E, G**) and EGFR phosphorylation was measured via immunofluorescence in COS-7 cells ectopically expressing EGFR-mCitrine (**Fig.13C, G**). Knockdown of Rab11 with two different pools of siRNAs resulted in a significant

increase in phosphorylation of the autocatalytic site Y845 (~ threefold) and to a lesser extend of Y1045 (~ 1.5-fold), without affecting the expression levels of EGFR-mCitrine (**Fig.13B, D, F**). In contrast, Rab11 knockdown did not affect the phosphorylation of Y1068. In agreement with these findings, ectopic expression of BFP-Rab11a lowered the phosphorylation levels of Y845 and Y1045, while the phosphorylation of Y1068 was not affected (**Fig.13H**). Comparison of the phosphorylation levels of Y845 at the PM and RE revealed higher phosphorylation at the PM compared to the RE (**Fig.13I**). Together these findings imply that vesicular recycling EGFR through perinuclear recycling endosomes reduces autonomous receptor activation.

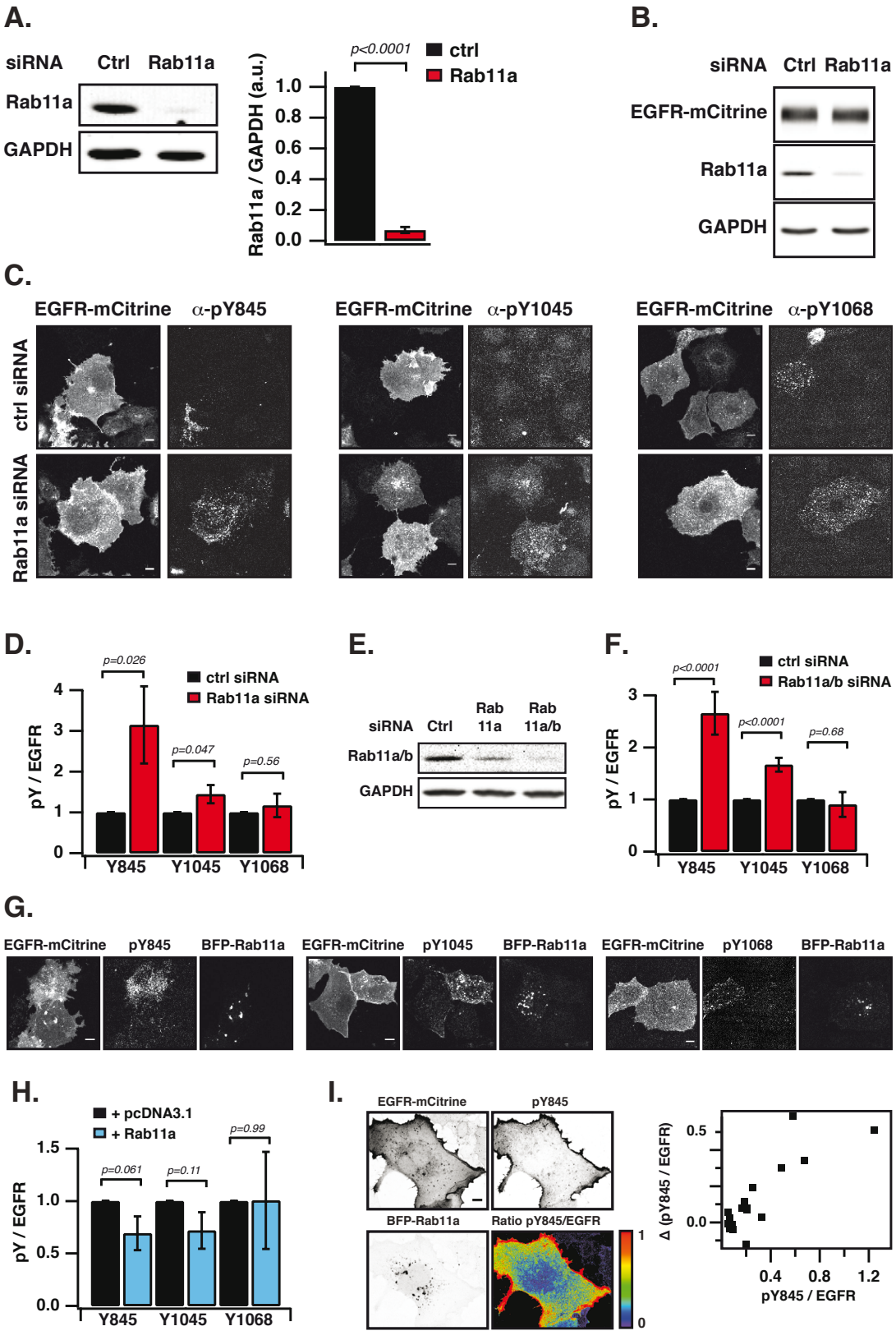

Figure 13: Suppression of autonomous EGFR activation by vesicular recycling. (A) Left panel: Lysates of COS-7 cells 72 h post-transfection with non-targeting siRNA (Ctrl) or Rab11a siRNA (siRab11a) were immunoblotted and probed for anti-Rab11a and anti-GAPDH. Right panel: Normalized ratio of Rab11a to GAPDH (means ± s.e.m., n = 5). **(B)** EGFR-mCitrine expression upon Rab11a knockdown. Lysates of COS-7 cells EGFR-mCitrine after transfection with non-targeting siRNA (Ctrl) or Rab11a siRNA (siRab11a) were immunoblotted and probed for

anti-Rab11a, anti-GAPDH and anti-GFP (EGFR-mCitrine). **(C)** COS-7 cells expressing EGFR-mCitrine were immunostained with specific pYN-antibodies to detect phosphorylation of Y845, Y1045, and Y1068 upon transfection with non-targeting siRNA (Ctrl, upper columns) or upon siRNA-mediated Rab11a knockdown (Rab11a, lower columns). **(D)** and **(F)** Relative phosphorylation (pY/EGFR) of EGFR-mCitrine on Y845, Y1045, and Y1068 upon siRNA-mediated Rab11a **(D)** or Rab11a/b **(F)** knockdown normalized to pY/EGFR for cells transfected with non-targeting siRNA (means ± s.e.m., n=69-147 cells/condition). **(E)** Lysates of COS-7 cells 72 h post-transfection with non-targeting siRNA (Ctrl), Rab11a siRNA (siRab11a) or Rab11a/b were immunoblotted and probed for anti-Rab11a/b and anti-GAPDH. **(G)** COS-7 cells expressing EGFR-mCitrine were immunostained with specific pYN-antibodies to detect phosphorylation of Y845, Y1045, and Y1068 in the presence of empty pcDNA 3.1 or BFP-Rab11a. **(H)** Relative phosphorylation (pY/EGFR) of EGFR-mCitrine on Y845, Y1045, and Y1068 upon ectopic expression of BFP-Rab11a normalized to pY/EGFR for cells transfected with empty pcDNA 3.1 (means ± s.e.m., n = 34-138 cells/condition). Data were acquired together with Dr. M.Baumdick. **(I)** Spatial distribution of autonomously phosphorylated Y845 in COS-7 cells. Left panel: Fluorescence images of EGFR-mCitrine, immunostaining of pY845, BFP-Rab11a, and a ratio image of pY845/EGFR-mCitrine. Right panel: Difference in Y845 auto-phosphorylation between the PM and RE (D pY845 over EGFR) as a function of overall EGFR phosphorylation level in individual cells (pY845/EGFR). All scale bars = 10 µm. Statistical significance was determined using a one sample t test. Data in **(D)** and **(F)** kindly provided by Dr. M.Baumdick.

4.1.4 PTP1B dephosphorylates autonomously activated EGFR in the perinuclear area

Previous studies showed that upon ligand-induced internalization, EGFR is dephosphorylated within perinuclear area by the ER-associated phosphatase PTP1B[59,77,78]. To assess whether PTP1B is also implicated in the regulation of autonomously activated EGFR, phosphorylation of EGFR-mCitrine in COS-7 cells co-expressing BFP-PTP1B was assessed via immunofluorescence and Western blotting (**Fig.14A, C**). The overall phosphorylation on the three tyrosine residues (Y845, Y1045, Y1068) was significantly lowered upon ectopic expression of BFP-PTP1B as compared to control cells (**Fig.14B, D**). In order to spatially resolve where autonomously activated EGFR is dephosphorylated by PTP1B, the interaction between EGFR-mCitrine and a substrate trapping mutant of PTP1B (mCherry-PTP1B-D181A) was examined by FLIM-FRET[78]. The catalytically impaired substrate trapping mutant retains its ability to bind substrate proteins and therefore can be employed to identify substrate complexes within the cell[120]. The spatially distributed interacting fraction (α) of EGFR-mCitrine with mCherry-PTP1B-D1881A obtained by global analysis, revealed an interaction between both proteins in the perinuclear area[121] (**Fig.14E**). The mean spatial coincidence of this interaction and BFP-Rab11a (63 ± 29 %; n = 20 cells) implied that receptor dephosphorylation mainly occurs within the perinuclear area in close proximity to the RE. Ectopic expression of BFP-

Rab11a shifted the distribution of EGFR towards this compartment, leading to an elevated interacting fraction between mCherry-PTP1B-D1881A and EGFR-mCitrine. Targeting PTP1B to the plasma membrane using the C-terminal membrane anchoring residues of KRas (PTP1B-RFP-tKRas) rendered EGFR unresponsive to ligand stimulation (**Fig.14F, H**), demonstrating that the spatial segregation of catalytically superior PTPs from EGFR is a prerequisite to permit growth factor induced receptor activation[56–58]. Collectively these findings show that vesicular recycling of EGFR through perinuclear areas promotes its interaction with the ER-associated PTP1B, thereby reducing autonomous activation of the receptor in the absence of ligand, while maintaining responsiveness to EGF stimulation.

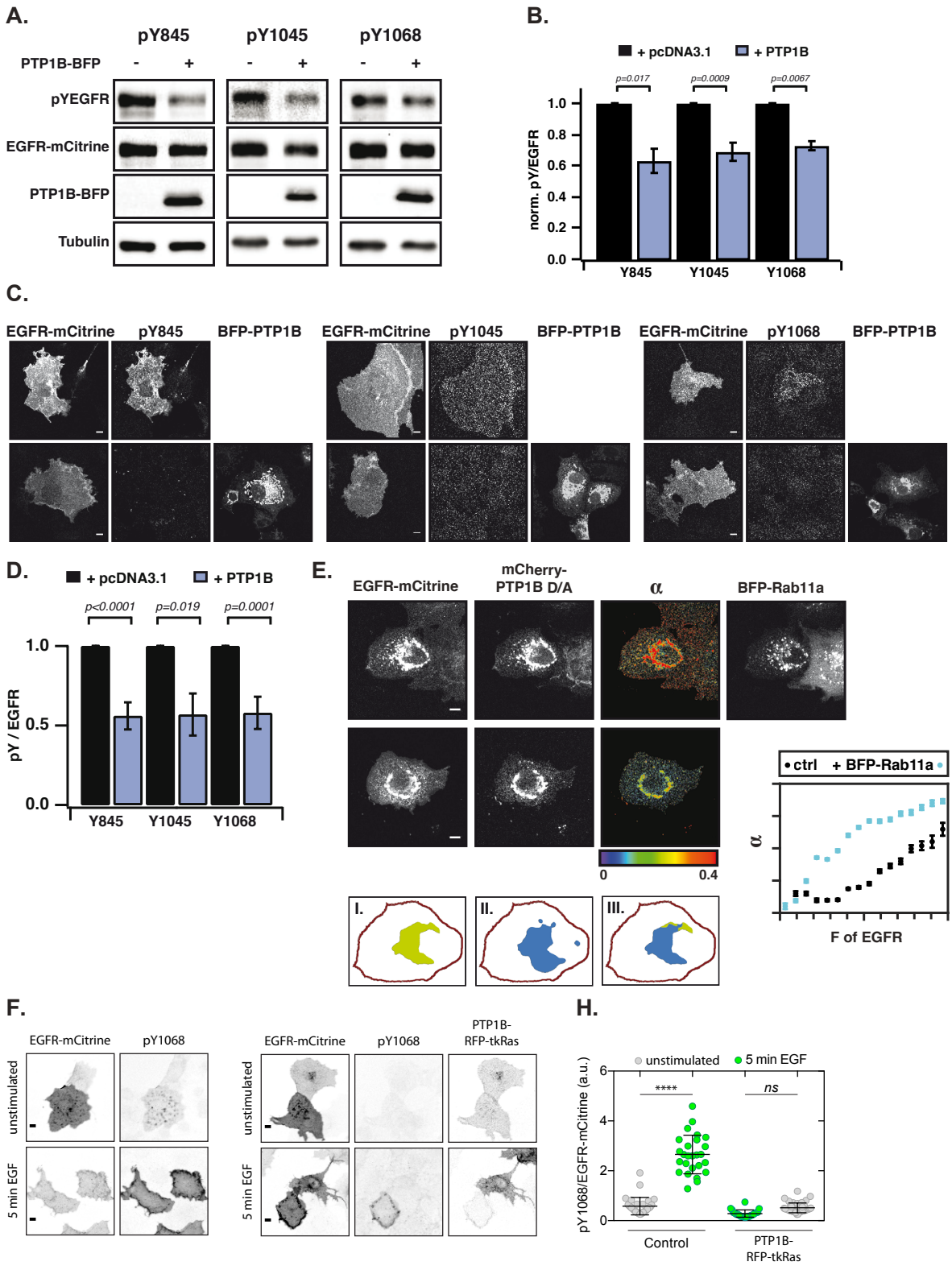

Figure 14: PTP1B dephosphorylates autonomously activated EGFR in the perinuclear area. **(A)** Lysates of COS-7 cells ectopically expressing EGFR-mCitrine in the presence of empty pcDNA 3.1 or BFP-PTP1B were immunoblotted and probed for either anti-pY845 (left), anti-pY1045 (middle) or anti-pY1068 (right), anti-tubulin, anti-GFP (EGFR-mCitrine) and anti-tRFP (BFP-PTP1B). **(B)** Relative phosphorylation (pY/EGFR) of EGFR-mCitrine on Y845, Y1045, and Y1068 upon ectopic expression of BFP-PTP1B normalized to pY/EGFR for cells transfected with empty pcDNA 3.1 (means ± s.e.m., n = 4 - 5). **(C)** COS-7 cells expressing EGFR-mCitrine were immunostained with specific pYN-antibodies to detect phosphorylation of Y845, Y1045, and

Y1068 in the presence of empty pcDNA 3.1 or BFP-PTP1B. **(D)** Relative phosphorylation (pY/EGFR) of EGFR-mCitrine on Y845, Y1045, and Y1068 upon ectopic expression of BFP-PTP1B normalized to pY/EGFR for cells transfected with empty pcDNA 3.1 (means ± s.e.m., n = 51 - 61 cells/condition). Data acquired together with Dr. Martin Baumdick. **(E)** Interacting fraction (α) of EGFR-mCitrine with mCherry-PTP1B D/A in COS-7 cells detected by FLIM-FRET, with (upper row) or without (lower row) ectopic expression of BFP-Rab11a. Graph shows average α in regions of high EGFR-mCitrine intensity as function of the EGFR mean fluorescence (F of EGFR) with (blue, n = 28 cells) or without ectopic expression of BFP- Rab11a (black, n = 20 cells). Lower row: Percentage of EGFR/PTP1B D/A interactions in the vicinity of the RE was retrieved from the overlap (III) between areas with high α values (I) and areas with high intensity of BFP-Rab11a fluorescence (II). Data in kindly provided by Dr. Martin Baumdick and Angel Stanoev (see Baumdick et al. 2015[116]). **(F)** COS-7 cells expressing EGFR-mCitrine were immunostained to detect phosphorylation of Y1068 and upon co-expressiong of PTP1B-tk before (upper rows) and after 5 min stimulation with 100 ng/ml EGF (lower rows). **(H)** Quantification of the relative EGFR-mCitrine phosphorylation (pY1068/EGFR-mCitrine) before (pre) and after stimulation with 100 ng/ml EGF in COS-7 cells ectopically expressing PTP1B-RFP-tkRas and control cells (means ± s.d., n = 22 - 40 cells/condition). Statistical significance was determined using an ordinary one-way ANOVA followed by Tukeys multiple comparison test (****, p > 0.0001). All scale bars = 10 µm. Statistical significance in **(B)** and **(D)** was determined using a one sample t test.

4.1.5 EGF triggers a ubiquitin-mediated switch in vesicular trafficking of EGFR

Constitutive vesicular recycling in the absence of ligand reduces autonomous receptor activation, while maintaining a steady state population of EGFR at the plasma membrane. In contrast, EGF stimulation results in enhanced receptor internalization, trafficking towards the perinuclear area and subsequent lysosomal degradation (**Fig.15A**). EGF stimulation triggers ubiquitination of the receptor by the E3-ligase c-Cbl, resulting in lysosomal degradation of the receptor[71]. In order to assess whether ubiquitination functions as the decisive signal to switch vesicular trafficking of ligand-activated EGFR towards lysosomal degradation, the amount of receptor ubiquitination was assessed upon EGF and PV treatment (**Fig.15B**). EGF stimulation induced higher levels of receptor ubiquitination and degradation as compared to autonomously activated EGFR upon PV treatment (**Fig.15C**). In line with these observations autonomously activated receptors did not recruit c-Cbl and continued to traffic via the Rab11-positive RE (**Fig.15D, E**). In contrast, EGF stimulation recruited c-Cbl to EGFR positive endosomes and reduced the fraction of EGFR at the RE. Together these findings imply that c-Cbl mediated ubiquitination redirects EGFR from continuous vesicular recycling towards lysosomal degradation.

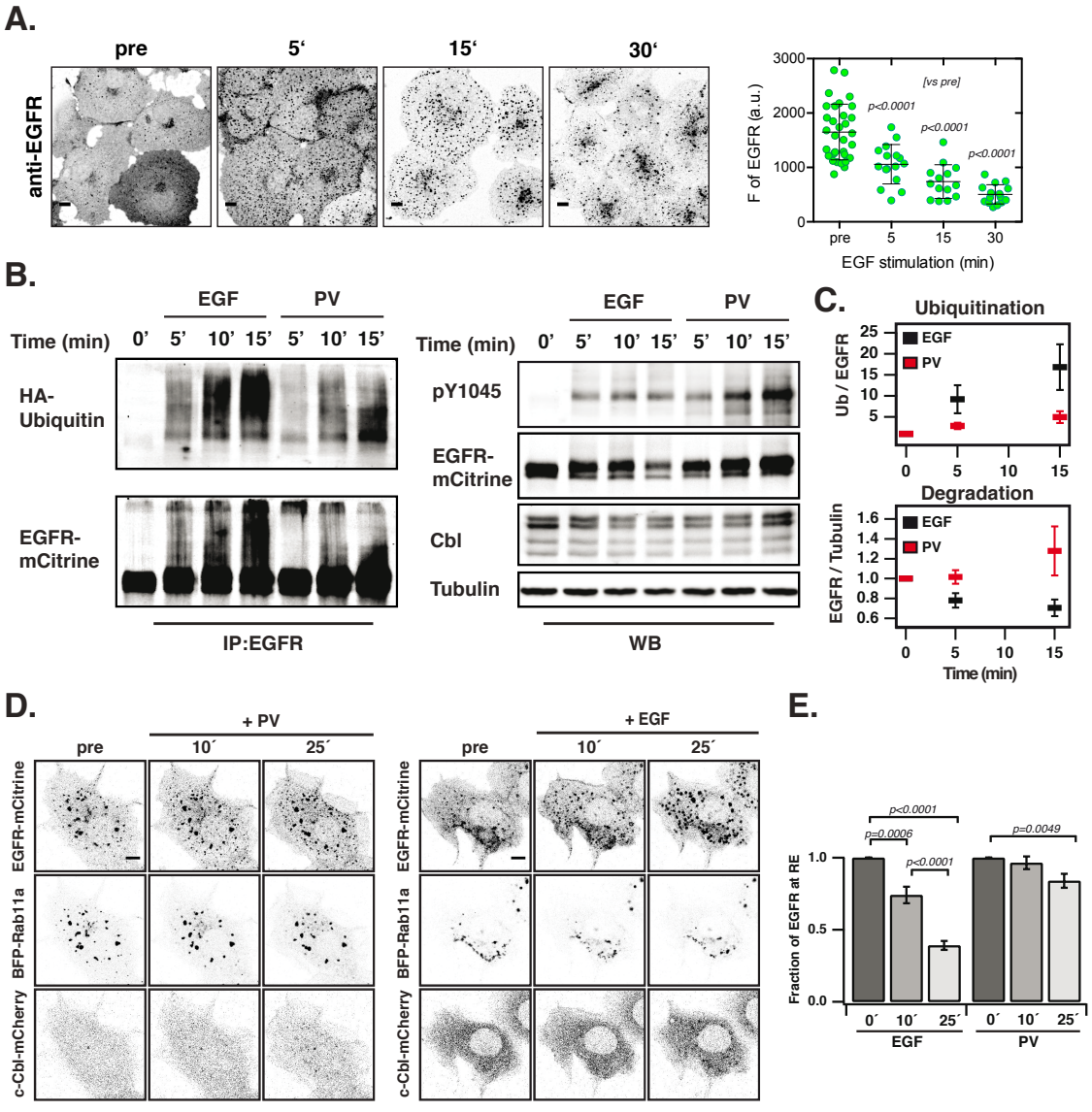

Figure 15: EGF triggers a ubiquitin-mediated switch in vesicular trafficking of EGFR (A) Immunofluorescence images of COS-7 cells stained for endogenous EGFR (left panel) and quantification of mean EGFR fluorescence intensities (right panel) following stimulation with 100 ng/ml EGF for the indicated time points (means ± s.d., n = 14 - 32 cells/condition). Statistical significance in was determined using an ordinary one-way ANOVA followed by Sidak's post-hoc test. **(B)** COS-7 cells expressing EGFR-mCitrine, HA-c-Cbl-mCherry and HA-Ubiquitin were treated with 100 ng/ml EGF or 0.33 mM PV for the indicated times in min. Lysates were immunoprecipitated with anti-EGFR (left panel) or blotted for total proteins (right panel). IP was probed with anti-HA (HA-ubiquitin) and anti-GFP (EGFR-mCitrine) and total lysates were probed with anti-GFP (EGFR-mCitrine), anti-Cbl (c-Cbl-mCherry), anti-tubulin, and anti-pY1045. **(C)** Relative EGFR ubiquitination (Ub/EGFR, upper panel) and EGFR-mCitrine degradation (EGFR/Tubulin, lower panel). Means ± s.e.m. (n = 3). **(D)** Fluorescence images of COS-7 cells expressing EGFR-mCitrine, BFP-Rab11a and HA-c-Cbl-mCherry upon stimulation with 100 ng/ml EGF (left panel) or 0.33 mM PV (right panel) for the indicated times in min. **(E)** Fraction of EGFR-mCitrine fluorescence at the RE upon treatment with 100 ng/ml EGF (n = 12 cells) or 0.33 mM PV (n = 14 cells). Statistical significance in was determined using an ordinary one-way ANOVA followed by Tukey's multiple comparison test. All scale bars = 10µm.

Mutation of the c-Cbl binding site within the C-tail of EGFR (EGFR-Y1045F-Citrine), also impaired c-Cbl recruitment, resulting in constitutive recycling of the receptor upon EGF stimulation (**Fig.16A**). Perturbing the EGFR-c-Cbl interaction via mutagenesis of the direct (Y1045) and indirect Grb2-mediated binding sites (Y1068 and 1086) further resulted in equally sustained receptor phosphorylation as compared to the remaining fraction of wild type EGFR, lower levels of c-Cbl phosphorylation and ultimately impaired receptor degradation (**Fig.16B, C**). Interestingly, phosphorylation of Y1045 was not is not sufficient for the recruitment of c-Cbl as PV and EGF treated cells displayed comparable levels of Y1045 phosphorylation, indicating the necessity of EGF induced self-association of the receptor to promote efficient receptor ubiquitination (**Fig.15B**). EGF promoted receptor ubiquitination thereby functions as a secondary signal, which redirects EGFR towards lysosomal degradation to avoid reactivation at the PM, imposing a finite response of receptor activity.

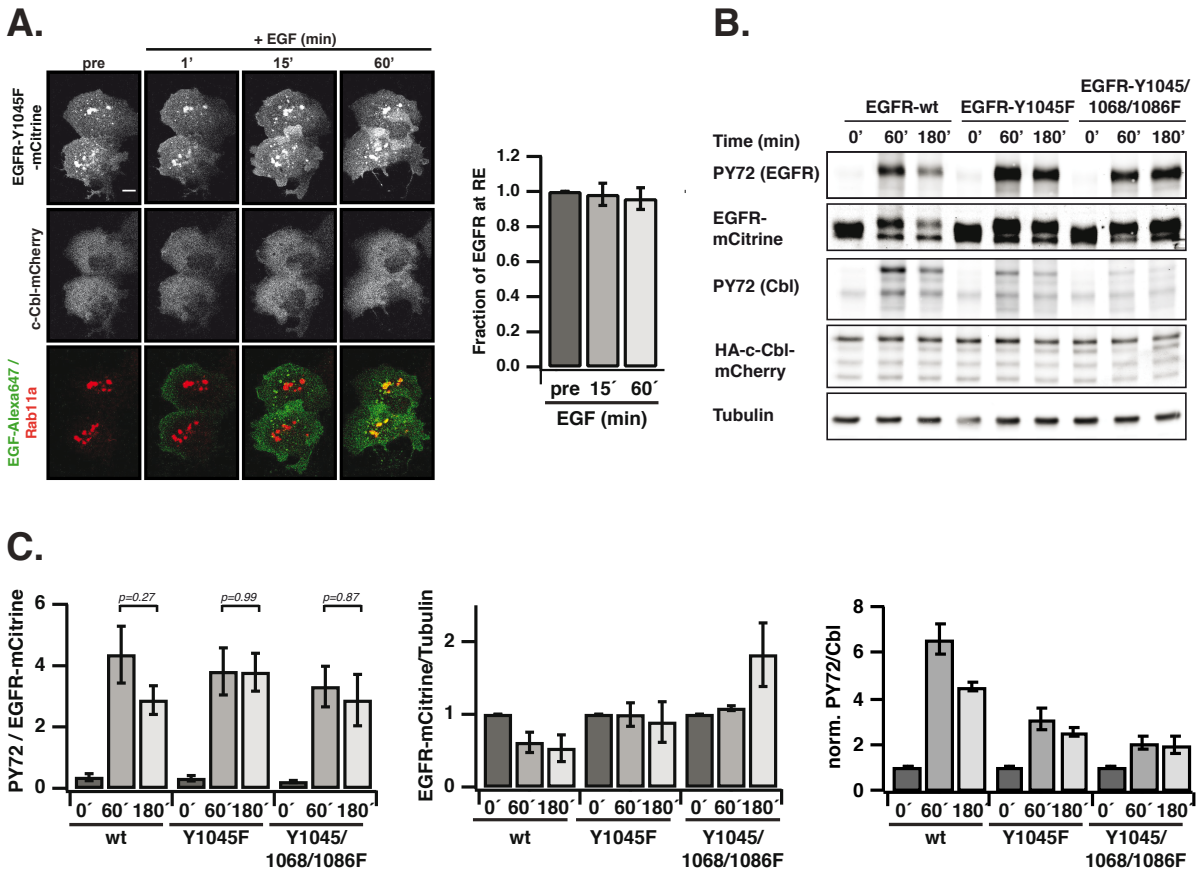

Figure 16: Continuous recycling of ubiquitination-deficient EGFR. (A) Left panel: Fluorescence images of COS-7 cells expressing EGFR-Y1045F-mCitrine, BFP-Rab11a and HA-c-Cbl-mCherry upon stimulation with 100 ng/ml EGF (for the indicated times in min. Right panel: Fraction of EGFR-Y1045F-mCitrine fluorescence at the RE upon treatment with 100 ng/ml EGF (means ± s.e.m., n = 9 cells) for the indicated times in min (Data kindly provided by Dr. M.

Baumdick). Scale bar = 10 µm. **(B)** Lysates of COS-7 cells expressing EGFR-mCitrine or EGFR-Y1045F-mCitrine or EGFR-Y1045/1068/1086F-mCitrine and HA-c-Cbl-mCherry were collected before or after stimulation with 100 ng/ml for the indicated times in min. Lysates were immunoblotted and probed with the generic phospho tyrosine antibody PY72, anti-GFP (EGFR-mCitrine), anti-tubulin and anti-c-Cbl. **(C)** Quantification of EGFR degradation (EGFR/Tubulin, left), relative EGFR phosphorylation (PY72/EGFR) and relative c-Cbl phosphorylation (PY72/Cbl) for wild type EGFR and ubiquitination-deficient EGFR mutants (means ± s.e.m. n = 3). Statistical significance in **(C)** was determined using an ordinary one-way ANOVA followed by Tukey's multiple comparison test.

4.2 Ligand-specific ErbB receptor trafficking determines Erk signaling specificity

The ErbB signaling network mediates fundamental, often opposing cellular responses including proliferation, differentiation, migration, survival and/or apoptosis. Intriguingly, despite the promiscuous activation of shared signal transducing proteins, such as the Ras/Erk cascade, different ErbB ligands can induce distinct cellular responses. Vesicular membrane dynamics allow the cell to regulate the spatial distribution of cell surface receptors between the plasma membrane and different endosomal compartments. In the second part of this thesis we examined how ligand-specific differences in the spatial organization of active ErbB receptors determines Erk signaling dynamics and localization to generate different cellular responses.

4.2.1 HRG and EGF induce distinct spatial distributions of active ErbB receptors

The human breast cancer cell line MCF7 endogenously expresses all ErbB family members (EGFR, ErbB2/3/4), activation of ErbB receptors by EGF or HRG promotes transient and sustained activation of Erk, respectively **(Fig.17A)**. Administration of the ErbB inhibitor Lapatinib 10 min after HRG treatment resulted in a loss of Erk phosphorylation, demonstrating the necessity of prolonged ErbB signaling for persistent Erk activation **(Fig.17B)**. EGF is a specific ligand for EGFR, while HRG binds to ErbB3 and ErbB4 and further promotes transactivation ErbB2 via receptor hetereodimerization[52]. To elucidate which receptors, mediate the sustained Erk response upon HRG stimulation, we performed siRNA knockdown experiments for ErbB2, ErbB3 and ErbB4. Knockdown of either ErbB2 or ErbB3 reduced HRG-induced Erk activation, while ErbB4 knockdown had no effect, implying that ErbB2/3 heterodimers form the major HRG responsive receptor complex with regard to Erk activation **(Fig.17C, D)**.

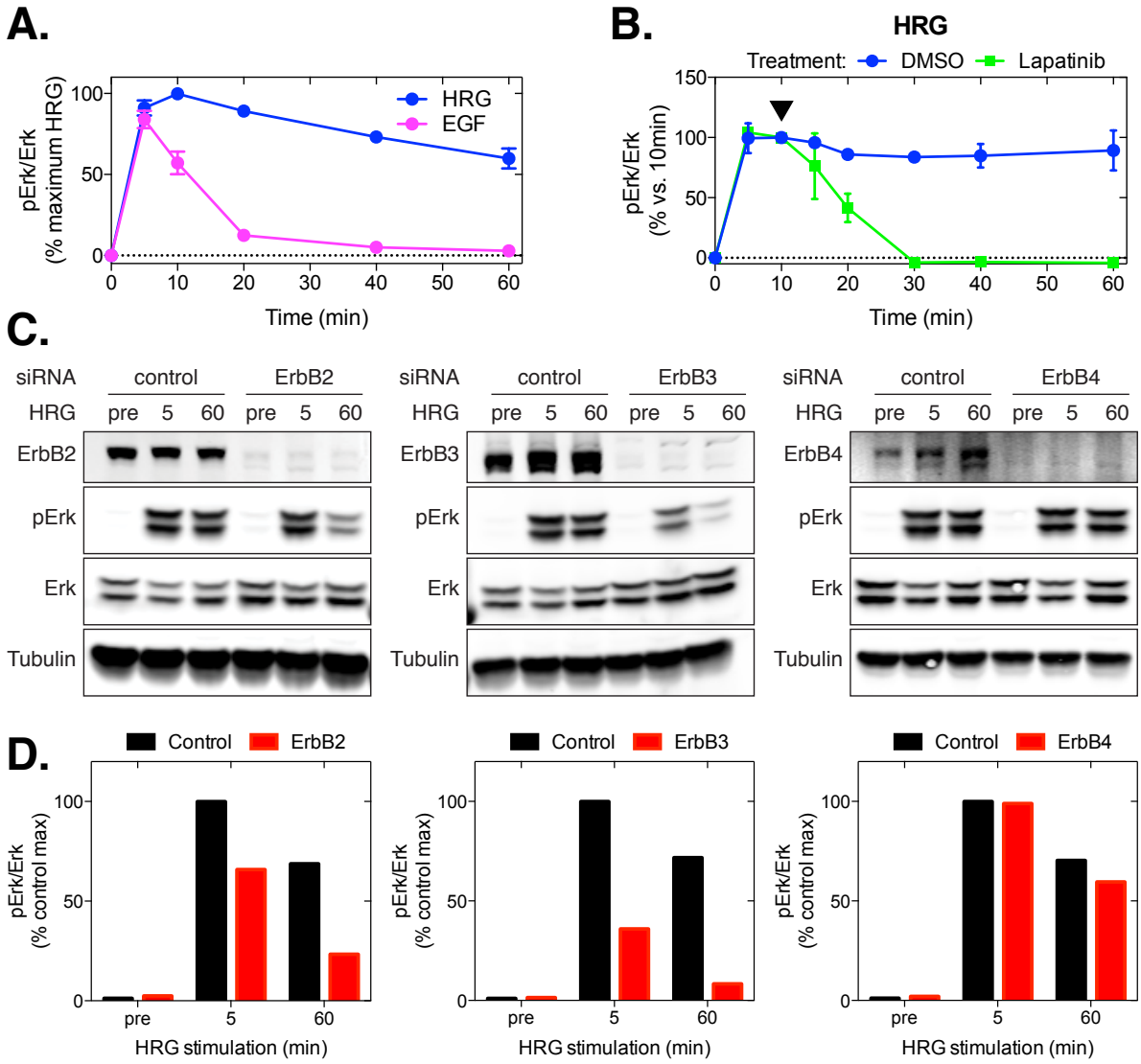

Figure 17: EGF and HRG induce different temporal responses of Erk. (A) Time-dependent Erk activation profiles were measured by ICW in MCF7 cells stimulated with 100 ng/ml EGF or HRG for the indicated times (means ± s.e.m., n = 3). **(B)** Erk phosphorylation upon ErbB inhibition were measured by ICW in MCF7 cells stimulated with 100 ng/ml HRG for 10 min and subsequently treated with DMSO or 2 uM Lapatinib (means ± s.e.m., n = 3). **(C)** Lysates of MCF7 cells transfected with non-targeting siRNA (control) or siRNA targeting ErbB receptors were collected following stimulation with 100 ng/ml HRG for the indicated times. Lysates were immunoblotted and probed for ErbB receptors, anti-pErk, anti-Erk and anti-tubulin. **(D)** Quantification of Erk activation upon ErbB receptor knockdown for ErbB2 (left), ErbB3 (middle), ErbB4 (right).

To address the impact of EGF and HRG on the localization of the respective ErbB receptors, immunofluorescence measurements of endogenous receptors and live cell confocal imaging of fluorescently tagged receptors were performed (**Fig.18.A-C**). EGF-stimulation resulted in rapid EGFR internalization, while upon HRG stimulation ErbB2 and ErbB3 were not internalized and remained at the plasma membrane **(Fig.18A-C)**. In agreement with this, HRG-induced activation of ErbB2 and ErbB3 did

not promote receptor degradation, while EGFR was rapidly degraded upon EGF stimulation **(Fig.18D)**.

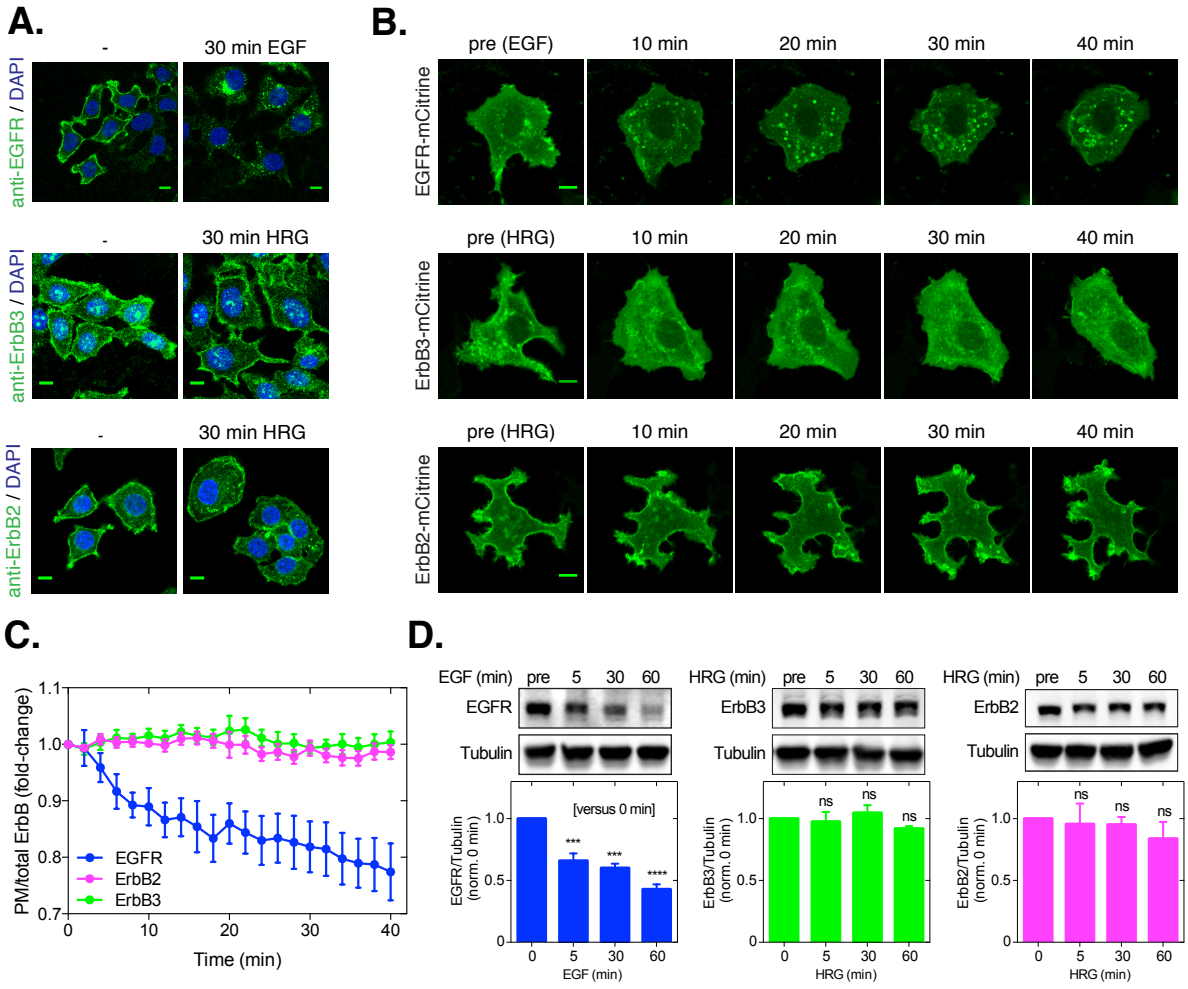

Figure 18: ErbB localization and degradation upon EGF and HRG stimulation. (A) Representative immunofluorescence images of MCF7 cells stained for endogenous EGFR (top), ErbB3 (middle) and ErbB2 (bottom) before and after 30 min with 100 ng/ml EGF or HRG, respectively. Nuclei were stained with Hoechst. **(B)** Fluorescence images of MCF7 cells expressing EGFR-mCitrine (top), ErbB2-mCitrine (middle) and ErbB3-mCitrine (bottom) before and after with 100 ng/ml EGF or HRG for the indicated times, respectively. **(C)** Quantification of the normalized relative plasma membrane fractions of EGFR-mCitrine upon EGF stimulation and ErbB2/3-mCitrine upon HRG stimulation (means ± s.e.m., n = 11 cells/condition). **(D)** Upper panel: Lysates of MCF7 cells following stimulation with 100 ng/ml EGF or HRG for the indicated times were immunoblotted and probed for EGFR upon EGF stimulation and ErbB2/3 upon HRG stimulation. Anti-tubulin was used as loading control. Lower panel: Quantification of total ErbB abundance normalized to unstimulated conditions (means ± s.e.m, n = 3). Statistical significance was determined using a one-way ANOVA with Dunnett's post-hoc test (****, p > 0.0001; ***, p > 0.001). All scale bars = 10µm.

The differences in receptor internalization and degradation were further reflected in the temporal ErbB activity, as EGF stimulation resulted in transient phosphorylation of EGFR and HRG induced sustained activity of ErbB2 and ErbB3 **(Fig.19A)**. To

further test whether HRG stimulation also induced sustained downstream ErbB signaling from the plasma membrane, we used an PH-Akt based translocation sensor for phosphatidylinositol 3,4,5-triphosphate (PtdIns(3,4,5)P3)[122]. Since PtdIns(3,4,5)P3-production is spatially restrained to the plasma membrane this sensor can be employed to selectively probe for plasma membrane receptor activity. EGF induced a weak, transient recruitment of the sensor to the PM, while HRG promoted stronger and more sustained PM recruitment **(Fig.19B)**. The HRG-promoted translocation of PH-Akt was reversed following treatment with the tyrosine kinase inhibitor Erlotinib, indicating that PH-Akt translocation directly reflects PM ErbB receptor activity **(Fig.19C)**. Interestingly, the duration of the PH-Akt translocation response upon EGF stimulation was markedly shorter (~10 min, **Fig.19B**) than the respective Erk response (~30 min, **Fig.17A**). Previous studies showed that endosomal EGFR can continue to activate Erk following internalization[123]. To assess whether EGFR continues to activate Erk from endosomal membranes we pulsed cells for 10 min with EGF to allow internalization of active receptors and then removed extracellular EGF to prevent further EGFR activation at the PM (**Fig.19D**). EGF-induced Erk activation following pulsed stimulation was identical to sustained stimulation, suggesting that EGFR continues to activate Erk from endosomal membranes following internalization. On the other hand, pulsed stimulation with HRG generated a transient Erk response, indicating the necessity of persistent PM receptor activity to sustain Erk activation during HRG stimulation (**Fig.19D**). HRG and EGF thus induce distinct spatiotemporal patterns of active ErbB receptors during stimulation, leading to the activation of Erk from different subcellular compartments (PM and endosomes, respectively). Finite EGFR activation due to rapid internalization and lysosomal degradation further limited its capacity to efficiently engage Akt activation at the plasma membrane, as compared to HRG activated ErbB2/3 **(Fig.19E)**.

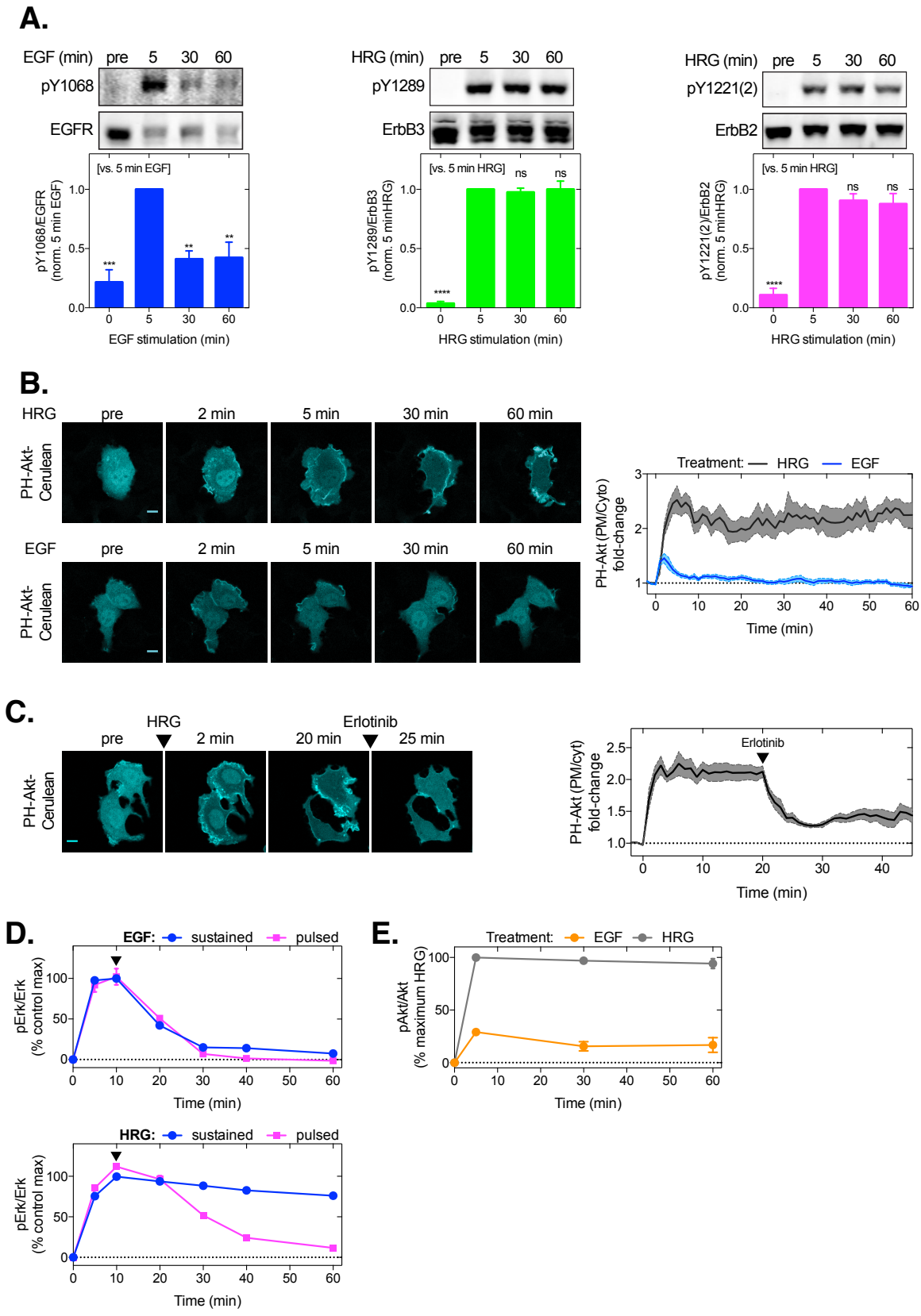

Figure 19: HRG and EGF promote different spatial and temporal localizations of active ErbB receptors. (A) Upper panel: Lysates of MCF7 cells following stimulation with 100 ng/ml EGF or HRG for the indicated times were immunoblotted and probed for anti-EGFR and anti-pY1068 upon EGF stimulation and anti-ErbB2/3 and anti-pY1289 (ErbB3) or anti-pY1221/2 (ErbB2) upon HRG stimulation. Lower panel: Quantification of ErbB phosphorylation normalized

to 5 min stimulation (means ± s.e.m., n = 3). Statistical significance was determined using a one-way ANOVA with Dunnett's post-hoc test (****, p > 0.0001; ***, p > 0.001; **, p > 0.001). **(B)** Left: Fluorescence images of MCF7 cells expressing PH-Akt-mCerulean before and after stimulation with 100 ng/ml EGF (top) or HRG (bottom) for the indicated times. Right: Quantification of normalized PH-Akt recruitment (means ± s.e.m., n = 8-10 cells/condition). **(C)** Left: Fluorescence images of MCF7 cells expressing PH-Akt-mCerulean were stimulated with 100 ng/ml HRG and after 20 min treated with 10 µM Erlotinib. Right: Quantification of normalized pH-Akt recruitment (means ± s.e.m., n = 6 cells). **(D)** Time-dependent Erk activation profiles were measured by ICW in MCF7 cells following sustained stimulation with 100 ng/ml EGF or HRG or a 10 min pulsed stimulation and subsequent washout. (means ± s.e.m., n = 3). **(E)** Time-dependent Akt activation profiles were measured by ICW in MCF7 cells following sustained stimulation with 100 ng/ml EGF or HRG for the indicated times (means ± s.e.m., n = 4). All scale bars = 10 µm.

4.2.2 KSR enhances HRG-induced Erk activation at the PM

Scaffolding proteins play a critical role in the assembly of many multiprotein complexes that drive signal transduction and have been shown to promote Erk activation from various subcellular localizations (e.g. PM, endosomes, golgi, nucleus)[124]. As such, KSR proteins have been shown to be translocate to the plasma membrane and facilitate the activation of Mek and thus Erk from the plasma membrane upon growth factor stimulation[125]. Given that HRG stimulation promotes Erk activation specifically from the plasma membrane, we examined whether KSR is implicated in the HRG-induced Erk response. We employed CRISPR-Cas9 genome editing to knock out both KSR1 and KSR2 proteins and examined two single cell derived clones, to account for potential clonal effects **(Fig.20A)**. Knockout of KSR1/2 attenuated HRG-induced Erk phosphorylation, while EGF-induced Erk phosphorylation was not affected **(Fig.20B)**. Different temporal Erk activities can be decoded at the level of immediate early genes (IEG) like cFos, which selectively respond to sustained Erk signals. Consistent with the reduction of HRG-induced Erk activation, knockdown of KSR1/2, specifically reduced cFos accumulation in response to HRG, while the smaller EGF-induced cFos accumulation was not affected **(Fig.20C)**. The contrasting effects of KSR knockout on the EGF- versus or HRG-induced Erk activation and downstream signaling further reflect the differences in the spatiotemporal patterns of ErbB activity generated by these ligands.

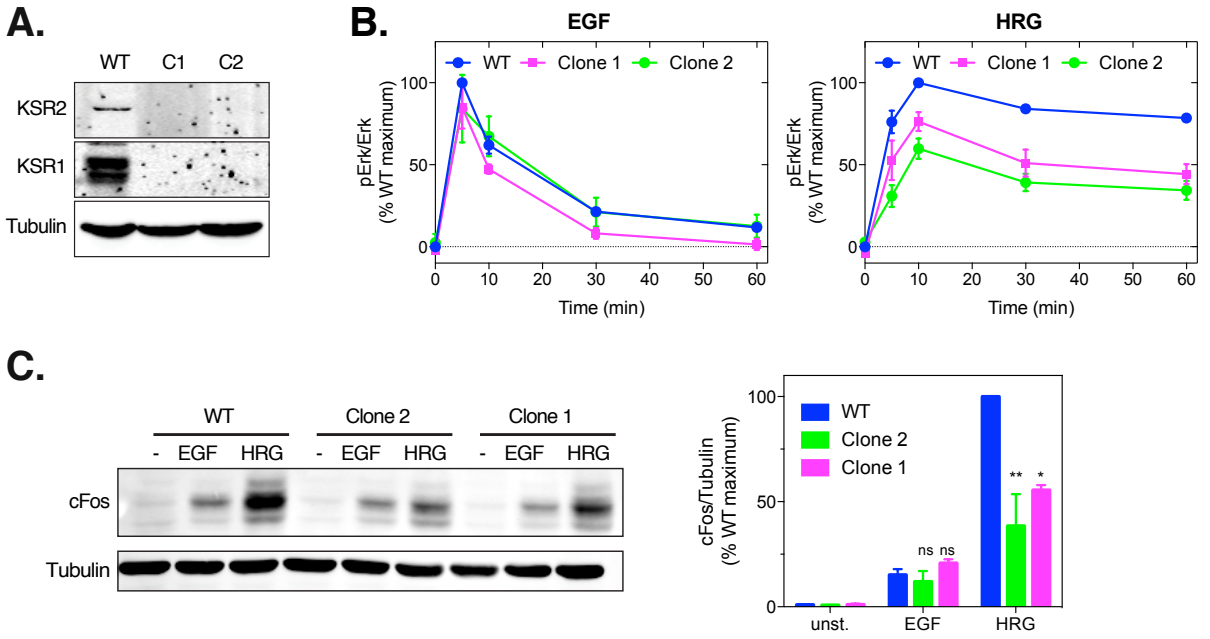

Figure 20: KSR enhances HRG-induced Erk activation at the PM. (A) Cell lysates of wild type MCF7 (WT) or MCF7 KSR knockout cells (Clone1/2) were immunoblotted for anti-KSR1, anti-KSR2 and anti-tubulin. **(B)** Time-dependent Erk activation profiles were measured by ICW in MCF7 wild type or MCF7 KSR knockout cells (Clone1/2) stimulated with 100 ng/ml EGF or HRG for the indicated times (means ± s.e.m, n = 4). **(C)** Left: Cell lysates of wild type MCF7 (WT) or MCF7 KSR knockout cells (Clone1/2) following 1 h stimulation with 100 ng/ml EGF or HRG were immunoblotted for anti-c-Fos and anti-tubulin. Right: Quantification of cFos expression for wild type MCF7 or MCF7 KSR knockout cells (means ± s.e.m, n = 3). Statistical significance was determined in using a repeated measures one-way ANOVA with a Dunnett's post-hoc test (**,p > 0.01; *, p > 0.05).

4.2.3 EGF and HRG promote Erk-dependent cell proliferation

To determine if the differences in the spatial distribution of EGF-activated EGFR and HRG-activated ErbB2/3 and the resultant spatial and temporal dynamics of Erk activity generate distinct cellular outcomes, we next investigated the effects of EGF and HRG stimulation on cell proliferation. Erk signaling plays a pivotal role regulating cellular proliferation in response to growth factors via nuclear translocation and activation of multiple transcription factors. Phosphorylated retinoblastoma protein (pRb) and CyclinD1 were employed as indicators of cell proliferation and assessed by immunofluorescence in individual cells (**Fig.21A, C**). Both ligands induced a similar increase in the fraction pRb-positive positive cells and CyclinD1 expression as compared to control cells treated with DMEM **(Fig.21B, D)**. We confirmed the role of Erk activation on cell proliferation using the noncompetitive Mek inhibitor PD0325901 (PD03), which efficiently suppressed Erk phosphorylation in MCF7 cells upon EGF and HRG stimulation **(Fig.21E)**. Treatment with PD03 significantly reduced the

fraction of pRb-positive cells for both EGF and HRG, directly demonstrating the requirement of Erk activity for EGF- and HRG-induced cell proliferation **(Fig.21F)**. Together these findings show that differences in the spatiotemporal activation of Erk (PM/sustained versus endosomes/transient), do not influence its capability to transmit growth factor signals to the nucleus to initiate a proliferative cellular response.

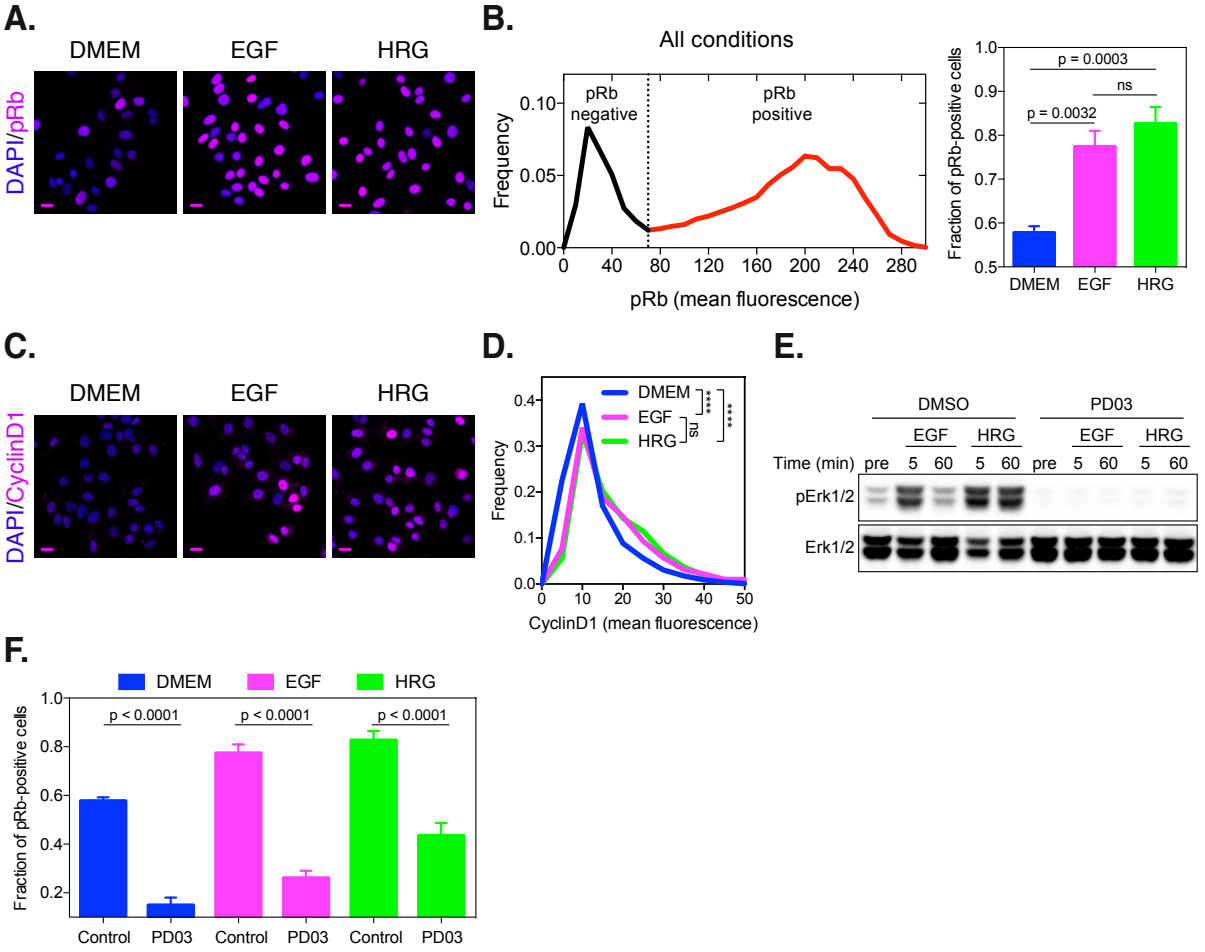

Figure 21: EGF and HRG induce Erk-dependent cell proliferation. (A) Immunofluorescence images of MCF7 cells stained for phospho-Rb (Ser807/811) following 24 h stimulation with 100 ng/ml EGF or HRG and control cells treated with DMEM. Nuclei were stained with Hoechst. **(B)** Left: Distribution of pRb fluorescence intensities for all measured cells. A minimum mean fluorescence intensity of 70 was used as a threshold to distinguish between pRb-negative and -positive cells (n = 12643 cells). Right: Quantification of pRb-positive cells (means ± s.e.m., n = 5) following 24 h stimulation with 100 ng/ml EGF or HRG and control cells treated with DMEM. **(C)** Immunofluorescence images of MCF7 cells stained for CyclinD1 following 24 h stimulation with 100 ng/ml EGF or HRG and control cells treated with DMEM. Nuclei were stained with Hoechst. **(D)** Quantification of CyclinD1 expression in MCF7 cells (n = 3075 - 3482 cells/condition) **(E)** Lysates of MCF7 cells following stimulation with 100 ng/ml EGF or HRG for the indicated times upon pretreatment with DMSO or PD03 (1 uM, 1h) were immunoblotted and probed with anti-Erk and anti-pErk. **(F)** Quantification of pRb-positive cells (means ± s.e.m., n = 3 - 5) following 24 h stimulation with 100 ng/ml EGF or HRG in control cells and cells treated with PD03 (1 uM). Control data previously shown in **(B)**. Statistical significance in **(B)**, **(D)** and **(F)** was determined

using an ordinary one-way ANOVA followed by Tukey's multiple comparison test (****, p > 0.0001; ***, p > 0.001; **, p > 0.01). All scale bars = 10 µm.

4.2.4 HRG stimulation promotes cellular motility

Erk signaling has also been previously described to play an essential role controlling cellular motility[126]. To assess the contribution of EGF and HRG to cellular motility, MCF7 cells were grown to a confluent monolayer in a 2-well culture-insert to create a defined cell-free area, while causing minimal cell damage (**Fig.22A**). Following removal of the confinement, cells were uniformly stimulated with EGF or HRG and the relative migration distance of the edges was quantified. Stimulation with HRG induced in a significant increase in migration, while EGF stimulation had no effect on cellular motility relative to non-treated control cells (**Fig.22B**). Treatment with the Mek inhibitor PD0325901 strongly attenuated the HRG-induced increase in cellular migration, demonstrating a pro-migratory role of HRG-induced Erk signaling (**Fig.22C**). The pro-migratory effect of HRG was further examined during a single cell motility assay. In this assay, MCF7 cells were seeded at low density on fibronection-coated surfaces, followed by live-cell time-lapse imaging to track individual cells upon EGF or HRG treatment (**Fig.22D, E**). In agreement with our previous observations, HRG stimulation promoted a strong increase in cellular motility, leading to a significant increase in average cell migration distance, velocity and displacement, as compared to EGF or non-treated control cells (**Fig.22F**). Comparison of the directionality (displacement/distance) did not reveal any significant differences throughout the different conditions, indicating HRG does not affect the intrinsic persistence of migration.

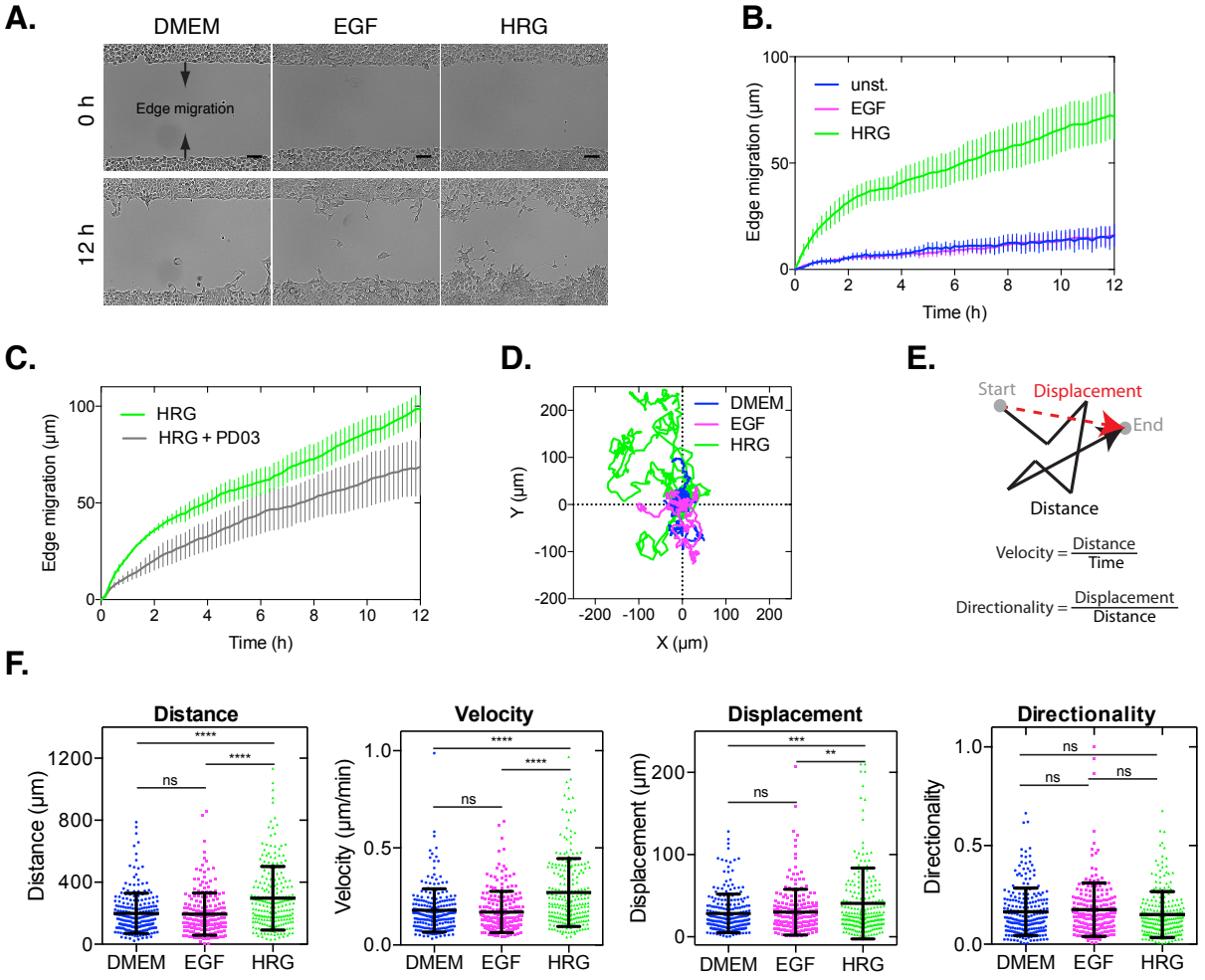

Figure 22. HRG stimulation promotes cellular motility in an Erk dependent-manner. (A) Phase contrast images of MCF7 cells following removal of the 2-well culture-insert for the indicated times upon stimulation with 100 ng/ml EGF or HRG and non-treated control cells (DMEM). Scale bars = 50 µm. **(B)** Quantification of the edge migration of MCF7 cells upon stimulation with EGF or HRG and non-treated control cells (DMEM) (means ± s.e.m. n = 5). **(C)** Quantification of the edge migration of PD03 (10 uM, 1 h) pretreated and non-treated MCF7 cells following stimulation with 100 ng/ml HRG (means ± s.e.m. n = 3). **(D)** Trajectories of single MCF7 cells following stimulation with 100 ng/ml EGF or HRG and non-treated control cells (DMEM) plotted with a common origin (10 cells/condition). **(E)** Schematic representation of quantified migration properties. **(F)** Quantifications of migration distance, velocity, displacement and directionality of single MCF7 cells following stimulation with 100 ng/ml EGF or HRG and non-treated control cells (means ± s.d., n = 210 - 233 cells/condition from three independent experiments). Statistical significance was determined using an ordinary one-way ANOVA followed by Tukey's multiple comparison test (****, p > 0.0001; ***, p > 0.001; **, p > 0.01).

Phosphorylation of the cell guidance receptor EphA2 on serine 897 (S897) enhances cell migration/invasion, whereas ligand-dependent EphA2 activation suppresses cell migration[127,128]. Modulating the balance between ligand-dependent and ligand-independent EphA2 signaling thereby can have profound effects on cellular motility. In agreement with the positive effect of HRG on cellular motility, we observed a

strong increase of S897 phosphorylation in response HRG as compared to EGF stimulation (**Fig.23A, B**). HRG-induced phosphorylation of S897 was strongly attenuated upon Mek inhibition, demonstrating the requirement of Erk activity for S897 phosphorylation. Erk can further promote cellular movement through phosphorylation of various effector molecules involved in the regulation of the cytoskeletal machinery, such as the WAVE Regulatory Complex (WAVE2) or the focal adhesion adaptor protein Paxillin[129]. We observed a strong mobility shift of the WAVE2 and Paxillin protein bands upon HRG stimulation, indicative of their respective active states, as compared to EGF stimulation, which was reduced upon Mek inhibition (**Fig.23C**). Collectively, these findings imply, that HRG-induced Erk activity promotes migration via phosphorylation of different effector molecules, necessary for cellular motility. This direct role of Erk signaling in cell motility is strongly supported by previous studies, which reported that activated Erk localizes to cell protrusions and cell-matrix adhesion sites[129,130]. The spatial confinement of active Erk to membrane-proximal regions might provide a mechanism to affect the local state of the cytoskeleton, via the targeted phosphorylation of migratory effectors at the PM such as S897 of EphA2. To control the subcellular localization of Erk activity, we constructed membrane-targeted (GFP-Erk2-CA-tKRas) or “soluble” (GFP-Erk2-CA) Erk proteins containing L73P and S151A substitutions, which promote enhanced Erk2 autophosphorylation as compared to wild type Erk2 (**Fig.23D, E**). Despite similar phosphorylation levels, localization of active Erk to the cytosol did not affect the phosphorylation of S897 of EphA2, while membrane-targeted Erk significantly enhanced S897 phosphorylation (**Fig.23E**). Phosphorylation of S897 therefore depends on Erk activity in membrane-proximal regions. Collectively, our findings imply that HRG-induced, membrane-proximal Erk activity promotes the phosphorylation different effector molecules involved in the regulation of the cytoskeletal machinery, to confer a motile phenotype.

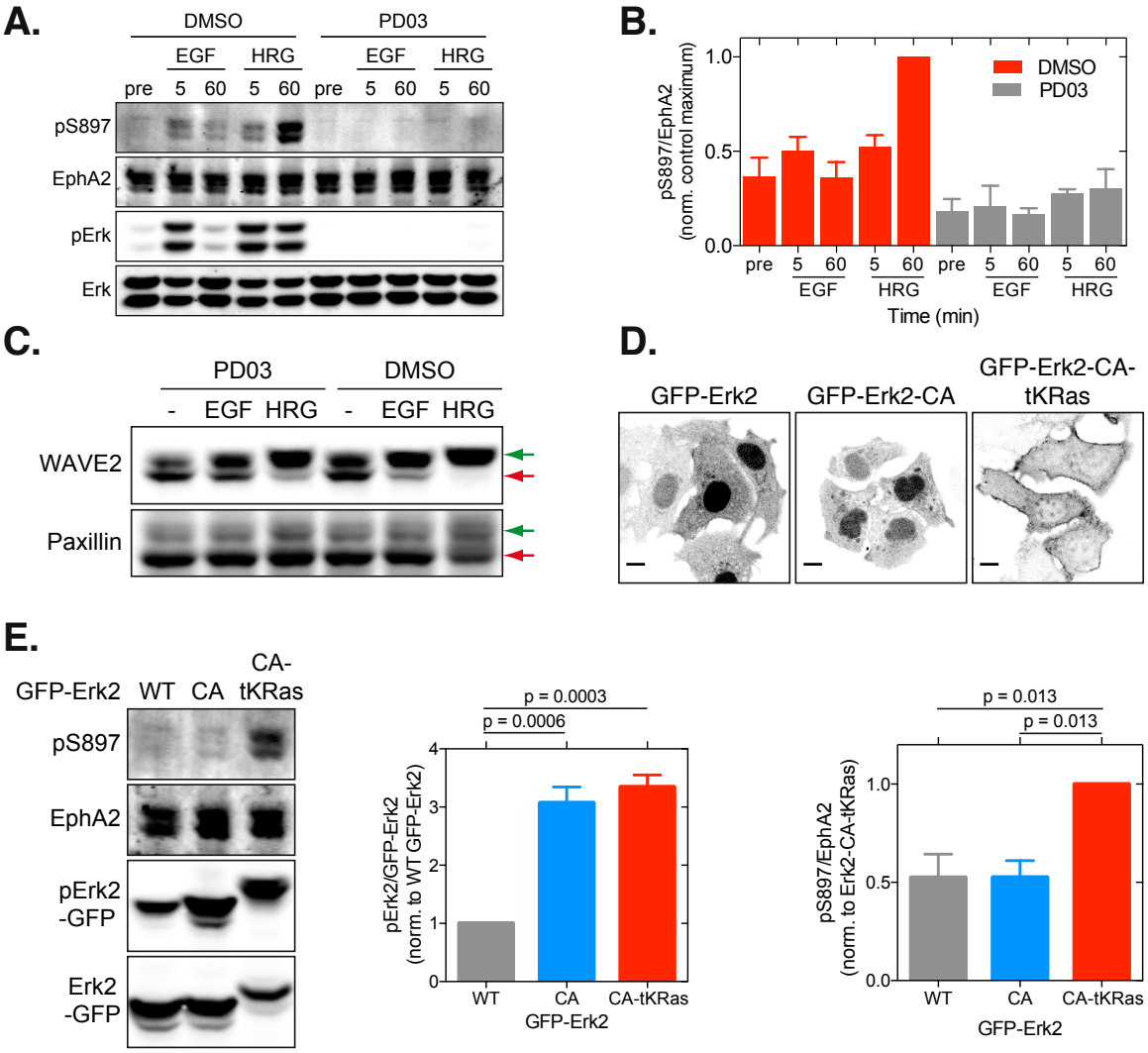

Figure 23. **Membrane proximal Erk signaling promotes phosphorylation of S897 of EphA2.** **(A)** Lysates of MCF7 cells following stimulation with 100 ng/ml EGF or HRG for the indicated times upon pretreatment with DMSO or PD03 (1 uM, 1h) were immunoblotted and probed for anti-pS897, anti-EphA2, anti-pErk and anti-Erk. **(B)** Quantification of S897 phosphorylation normalized to 60 min HRG stimulation (means ± s.e.m., n = 2). **(C)** Lysates of MCF7 cells following stimulation with 100 ng/ml EGF or HRG for 60 min upon pretreatment with DMSO or PD03 (1 uM, 1h) were immunoblotted and probed for anti-WAVE2, anti-Paxillin. Green arrows indicate gel shift of the phosphorylated fractions. **(D)** Fluorescence images of MCF7 cells expressing eGFP-Erk2 (left), eGFP-Erk2-L73P/S151D (middle, GFP-Erk2-CA), eGFP-Erk2-L73P/S151D-tKRas (right, GFP-Erk2-CA-tKRas). Scale bars = 10 µm. **(E)** Lysates of MCF7 cells expressing eGFP-Erk2 (WT), eGFP-Erk2-L73P/S151D (CA) or eGFP-Erk2-L73P/S151D-tKRas (CA-tKRas) were immunoblotted and probed for anti-pS897, anti-EphA2, anti-pErk and anti-Erk (left) and the phosphorylation of eGFP-Erk2 variants (middle) and S897 of EphA2 (right) was quantified (means ± s.e.m., n = 3). Statistical significance was determined using a one-way ANOVA with Dunnett's post-hoc test.

Since KSR proteins facilitate Erk activation at the plasma membrane, we hypothesized, that active Erk in association with KSR might form a membrane-associated signaling complex, which facilities cellular motility. We therefore assessed the effects of KSR knockout on cellular motility as described above using a 2-well

culture-insert to create a defined cell-free area (**Fig.22A**). Unstimulated control cells showed slightly elevated levels of cell migration upon KSR knockout, as compared to wild type MCF7 cells (**Fig.24A**). Unexpectedly, KSR knockout clones further showed a clear migratory response upon EGF stimulation, as compared to wild type MCF7 cells. In, contrast, upon HRG stimulation both clones showed reduced levels of cell migration, during the first six hours of migration and similar levels of migration at later time points (**Fig.24A**). Cell migration can broadly be grouped into two modes: single cell migration and collective cell migration, with cells moving individually or as an assembly of multiple cells, respectively[131]. During our experiments we noticed, that KSR knockout cells showed less collective cell migration, but enhanced cell-cell dissociation, scattering and migration of individual cells (**Fig.24B**). In agreement with this notion we observed enhanced migration distances of individual MCF7 cells throughout all conditions upon KSR knockout, as compared to wild type MCF7 cells (**Fig.24C**). However, KSR knockout cells displayed significantly less intrinsic directed migration (**Fig.24D**). Together these findings imply, that KSR is involved in the regulation of coordinated and directed movement of collectively migrating cells, but lowers the migratory behavior of single cells.

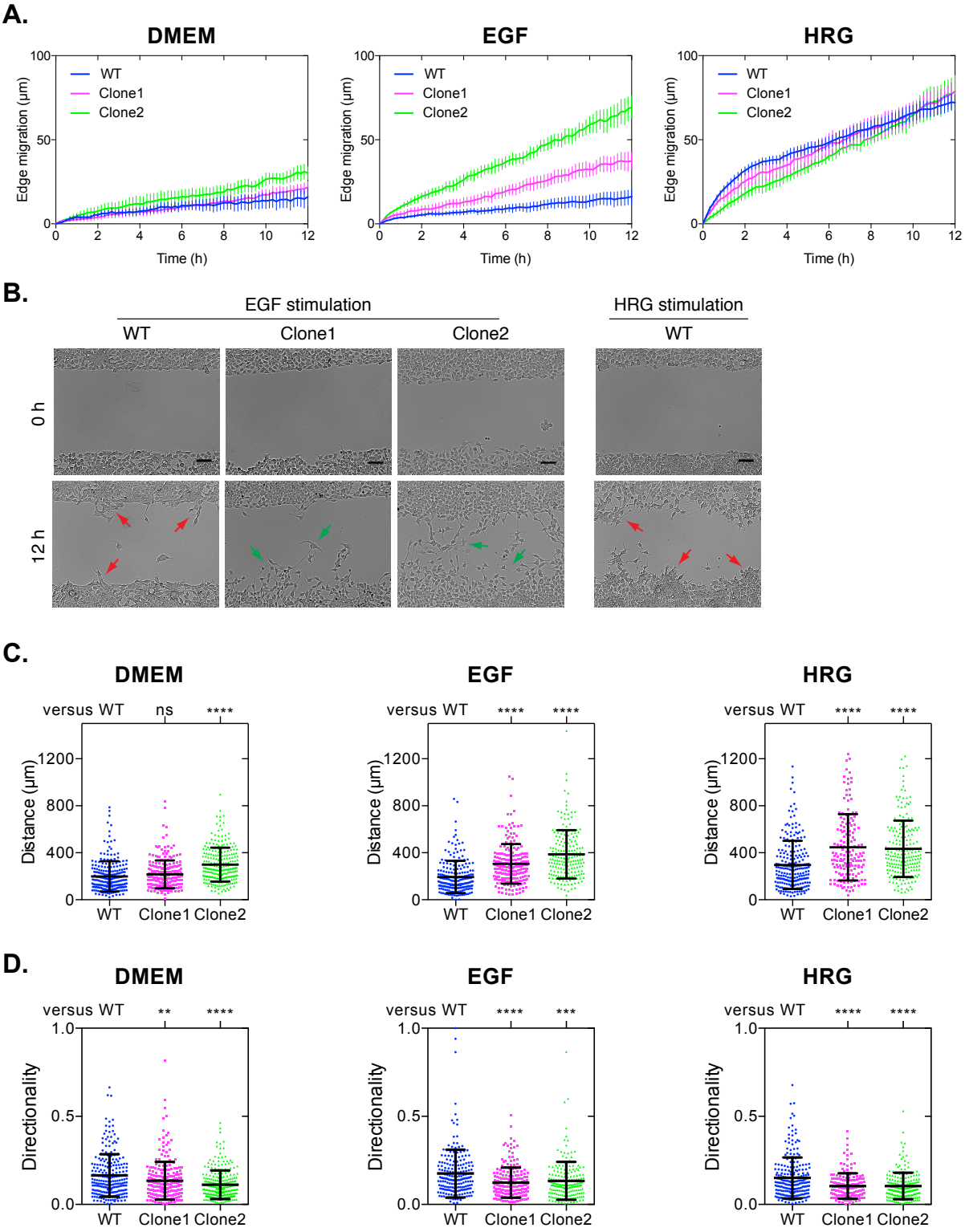

Figure 24: Effect of KSR knockout on cell migration. (A) Quantification of the edge migration of wild type MCF7 (WT) or MCF7 KSR knockout cells (Clone1/2) in the absence of growth factors (DMEM, left) and upon stimulation with 100 ng/ml EGF (middle) or HRG (right). Means ± s.e.m. from three independent experiments for MCF7 KSR knockout cells. Data of wild type MCF7 cells were previously shown in (**Fig.22A**). **(B)** Phase contrast images of wild type MCF7 (WT) or MCF7 KSR knockout cells (Clone1/2) following removal of the 2-well culture-insert for the indicated times upon stimulation with 100 ng/ml EGF for the indicated times. Arrows indicate areas of collectively migrating cells (red arrows) and single cells (green arrows). Scale bars = 50 µm. **(C)**

and **(D)** Quantifications of migration distances **(C)** and directionality **(D)** from single cell trajectories of wild type MCF7 (WT) or MCF7 KSR knockout cells (Clone1/2) in the absence of growth factors (DMEM, left) and upon stimulation with 100 ng/ml EGF (middle) or HRG (right). Means ± s.d., n = 163 - 252 cells/condition from three independent experiments. Data of wild type MCF7 cells were previously shown in (**Fig.22F**). Statistical significance was determined using an ordinary one-way ANOVA followed by Tukey's multiple comparison test (****, p > 0.0001).

5 Discussion

In this thesis, we examined how vesicular trafficking dynamics regulate the distribution of ErbB receptors between the plasma membrane and different endosomal compartments to enable contextual regulation of receptor activity and signaling.

5.1 Spatial regulation of EGFR activity by vesicular trafficking

In the first part we examined the role of EGFR vesicular dynamics in the regulation of autonomous receptor activity and how endosomal trafficking differentially controls the activity of autonomously and ligand-activated EGFR. The canonical scheme of EGFR activation describes ligand-induced dimerization, followed by allosteric activation of its intrinsic kinase activity and trans-autophosphorylation[19]. However, the collective response properties of EGFR emerge from its autocatalytic activation, coupled to local PTP inhibition at the plasma membrane, establishing a bistable reaction network with switch like response properties[41,46]. Analogous to a toggle switch, this reaction network converts growth factor stimuli into threshold-activated, but on the other hand creates the potential to amplify spontaneous phosphorylation events even in the absence of growth factors responses[41,50]. Therefore, regulatory mechanisms are required to control autonomous autocatalytic EGFR activity. We identified how the coupling of EGFR self-association state, ubiquitination and vesicular dynamics allows for the coexistence of a continuous safeguard cycle, to maintain low EGFR phosphorylation at the PM, while preserving sensitivity to growth factor stimulation.

5.1.1 Autonomous activation of EGFR in the absence of ligand

Recent studies reported that EGFR can also be activated in the absence of ligand at high surface densities[36,132]. Despite steric auto-inhibitory features, a subpopulation of EGFR can adopt an active conformation in the absence of ligand, due to thermal conformational fluctuations[43,133]. We investigated the extent of autonomous phosphorylation of three tyrosine residues that possess different regulatory functions, of autocatalysis (Y845), trafficking (Y1045), and signaling (Y1068) as a function of EGFR expression (**Fig.7A, Fig.8A**). The extent of ligand independent activation for all three sites increased with the expression of the receptor (**Fig.7B, Fig.8B**). Y845 and Y1068 showed significantly higher levels of autonomous phosphorylation as compared to Y1045 (**Fig.7C, Fig.8C**). Phosphorylation of Y1045 creates a docking

site for the E3-ubiquitin ligase c-Cbl, thereby functioning as an important determinant regulating the trafficking of the receptor. The low efficiency of autonomous Y1045 phosphorylation potentially avoids receptor ubiquitination and degradation in the absence of ligand. A recent study revealed that trans-phosphorylation of Y845 can stabilize monomeric EGFR in an active conformation, promoting autocatalytic amplification of its activity[43]. Tight regulation of the Y845 phosphorylation status is therefore essential to avoid its spontaneous phosphorylation and autocatalytic amplification of EGFR activation, which otherwise would result in uncontrolled receptor phosphorylation in the absence of ligand. Consistent with this notion, Y845 phosphorylation was most efficiently suppressed by phosphatases in the absence of ligand as compared to Y1045 and Y1068 (**Fig.9C**).

Autonomously activated and ligand-activated receptors differed with regard to their self-association state and their capability to engage downstream signaling molecules (**Fig.10**). High levels of autonomous EGFR phosphorylation were found to promote the phosphorylation of Akt (**Fig.10B, E**). The activation of Akt promotes vesicular recycling of EGFR to increase its abundance at the plasma membrane, effectively generating a positive feedback due to the autocatalytic nature of EGFR phosphorylation[66], which might further increase the propensity for autonomous activation. Interestingly, the phosphorylation of Erk remained unresponsive to autonomous receptor activation (**Fig.10B, E**), implying negative feedbacks within the Erk circuity conferring robustness to EGFR expression levels or inefficient coupling between autonomously activated EGFR to Erk at the plasma membrane, as compared to internalized endosomal EGFR[132,134,135].

5.1.2 Continuous vesicular recycling suppresses autonomous EGFR activation

Autocatalytic amplification of EGFR activity can result in uncontrolled receptor activation and signaling, even in the absence of ligand, necessitating regulatory mechanisms to counteract autonomous receptor activation at the plasma membrane. We addressed whether the endocytic machinery contributes to the regulation of autonomous phosphorylation of unliganded receptors. Vesicular membrane dynamics allow the cell to regulate the spatial distribution of cell surface receptors between the plasma membrane and different endosomal compartments that are rich in suppressive phosphatase activity. It was observed that, in the absence of ligand,

EGFR continuously cycles between the plasma membrane (PM) and Rab11-positive perinuclear recycling endosomes (RE) (**Fig.11, Fig.12**). Alterations in the vesicular recycling of EGFR using genetic perturbations of Rab11, influenced the magnitude of EGFR activation in the absence of EGF (enhanced and decreased receptor phosphorylation upon Rab11 knockdown and overexpression, respectively (**Fig.13D, F, H**). These findings suggest that a continuous vesicular recycling of EGFR through this compartment regulates the autonomous phosphorylation of unliganded receptors. Previous work established that the activity of the endoplasmic reticulum-anchored phosphatase PTP1B is highest on perinuclear membranes and PTP1B-catalyzed dephosphorylation of EGF-bound EGFR requires receptor endocytosis of the receptor[59,78]. In agreement with these findings, the spatially distributed interacting fraction displayed an interaction between EGFR and PTP1B in the perinuclear area (**Fig.14E**). Considering that the catalytic activity of fully active PTPs (e.g. PTP1B or TCPTP) exceeds the catalytic activity of EGFR by up to two orders of magnitude, the spatial segregation of catalytically superior PTPs from EGFR is a prerequisite to permit growth factor induced receptor activation at the plasma membrane (**Fig.14F, H**)[56–58]. Our results show that continuous vesicular recycling of EGFR in the absence of ligand between the PM and RE promotes the interaction with the ER-localized PTP1B and thereby counteracts autonomous receptor activation to maintain low levels of EGFR phosphorylation at the PM. The spatial separation of EGFR activity at the plasma membrane and PTP activity at the perinuclear area provides a system which safeguards against autonomous receptor activation at the PM and maintains cellular responsiveness to both new and sustained stimuli by regulating PM EGFR abundance.

5.1.3 A ubiquitin mediated switch in vesicular trafficking

Constitutive vesicular recycling of EGFR suppresses autonomous receptor activation, while maintaining a growth factor responsive receptor population at the plasma membrane (**Fig.25**). EGF stimulation results in enhanced receptor internalization, promoting receptor inactivation via ER-associated PTPs, followed by either endosomal-plasma membrane recycling or lysosomal degradation[67,77,78]. In order to identify the decisive factor that determines the fate of the receptor between these distinct trafficking routes, we compared the vesicular trafficking of PV-mediated, autonomously activated and EGF-activated receptors (**Fig.15D**). Autonomously

activated receptors continued to cyclically traffic via the Rab11-positive RE, while EGF stimulation recruited c-Cbl to EGFR positive endosomes, redirecting the receptor towards lysosomal degradation (**Fig.15E**). Despite high levels of Y1045 phosphorylation, autonomously activated EGFR was inefficiently ubiquitinated and degraded (**Fig.15B, C**). These findings imply that Y1045 is not sufficient to trigger c-Cbl mediated receptor ubiquitination and thereby switch receptor trafficking from vesicular recycling to lysosomal degradation. Since EGF stimulation also promotes enhanced receptor self-association (**Fig.10F**), EGFR ubiquitination forms a secondary signal that relies on both the phosphorylation of Y1045 and the formation of EGFR oligomers. A ubiquitin-deficient EGFR mutant continued to recycle via the RE after ligand stimulation, resulting in a sustained phosphorylation response (**Fig16A, C**). These findings demonstrate that redirecting vesicular trafficking towards lysosomal degradation to is necessary impose a finite signaling response, since recycling of EGF-EGFR complexes would consequently result in sustained receptor reactivation at the plasma membrane. Recent studies showed that receptor ubiquitination upon EGF-stimulation follows a threshold-controlled mechanism, due to the cooperative recruitment of c- Cbl, in complex with Grb2, resulting inefficient receptor ubiquitination at low EGF concentrations[73]. Hence vesicular recycling of the receptor is the preferential trafficking route in response to subsaturating EGF concentrations, which maintains the sensitivity of the cell to persistent stimulation, whereas at saturating EGF doses ubiquitin-dependent lysosomal degradation of EGFR generates a finite signaling response[66,71,72]. Inefficient receptor degradation due to mutation or overexpression of EGFR and c-Cbl mutations, resulting in prolonged receptor activation, has further been implicated in human disease[136–138]. Our findings show that autonomously activated and EGF activated receptors are processed differently by the endocytic machinery (**Fig.25**). Receptor ubiquitination functions as a decisive factor promoting different trafficking fates of EGFR (endosomal-plasma membrane recycling versus lysosomal degradation). Similar features have been observed for the cell guidance ephrin receptor type-A2 (EphA2), implying a common cellular mechanism for the regulation of RTK activity[139].

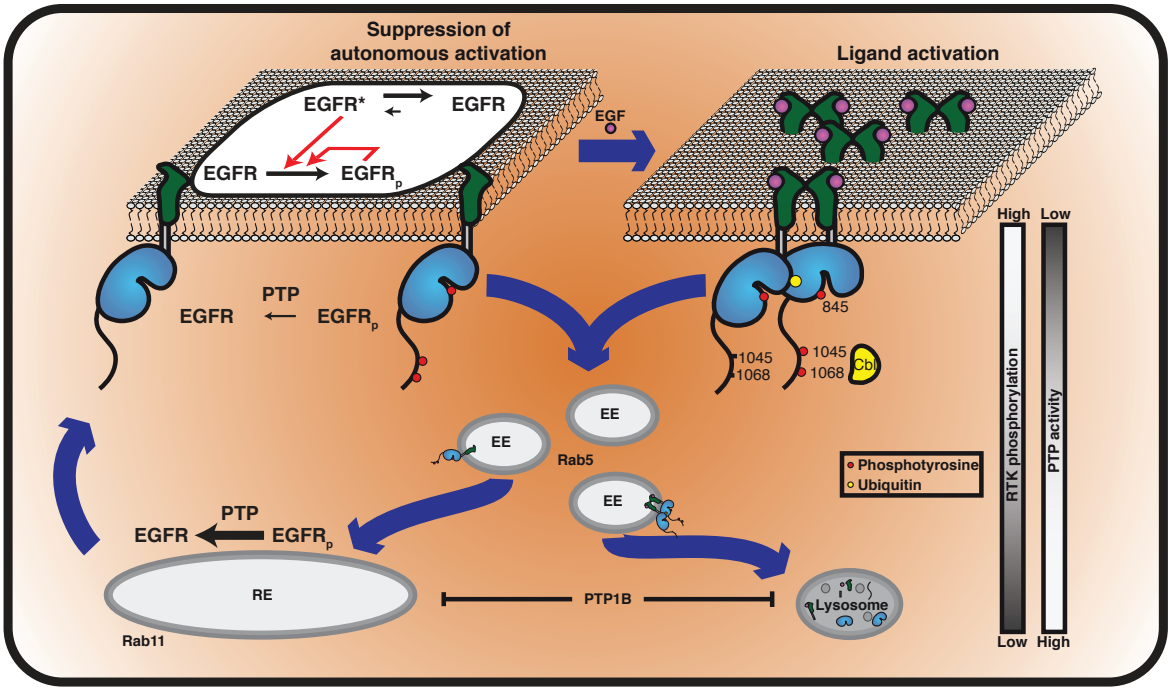

Figure 25: Differential vesicular dynamics of autonomously activated and ligand-activated EGFR. Constitutive vesicular recycling of EGFR through perinuclear areas with high PTP activity suppresses autonomous receptor activation in the absence of ligand, while maintaining a growth factor responsive receptor population at the plasma membrane (left). EGF-induced ubiquitination of EGFR clusters switches vesicular trafficking from continuous recycling towards lysosomal degradation, thereby imposing a finite signaling response (right).

5.2 Ligand-specific ErbB receptor trafficking determines Erk signaling specificity

In the second part of this thesis we examined how the spatial and temporal distribution of active ErbB receptors within the endosomal system determines the spatiotemporal organization of Erk signaling. Different ErbB ligands have been shown to induce distinct temporal patterns of Erk activation, which were linked to different cellular fates[105]. However, if different growth factors modulate Erk signaling in a spatially dependent fashion, to control cellular responses remains unclear. We show that EGF or heregulin (HRG) differentially modulate ErbB receptor trafficking to generate distinct spatiotemporal patterns of receptor activities, leading to the activation of Erk from different subcellular compartments (plasma membrane and endosomes). The subcellular localization of Erk activation influences its interaction with different effector proteins and thereby generates different cellular responses.

5.2.1 EGF and HRG promote Erk activation from different subcellular locations

Stimulation of the human breast cancer cell line MCF7 with EGF or HRG promotes transient or sustained activation of Erk, respectively (**Fig.17A**). Furthermore, we find that these growth factors further promote the activation of Erk from distinct subcellular localizations (endosomes and PM, respectively) (**Fig.19**). These differences in the spatial dynamics of Erk activation are the result of differences in vesicular trafficking, and, consequently, the localization of active ErbB receptors following EGF or HRG stimulation. As described previously, EGF stimulation promotes the internalization and ubiquitination of EGFR, leading to lysosomal degradation and transient, receptor activity (**Fig.18, 19A**). In contrast, following HRG stimulation, active ErbB2/3 receptors remain predominantly at the plasma membrane, generating a persistent Erk response from this compartment (**Fig.18, 19A**). This differential receptor trafficking has important implications on cellular behavior, as the signaling repertoire of endosomal and plasma membrane localized receptors can differ if biochemical components of the signal transduction machinery are not equally accessible in these distinct subcellular compartments. Rapid internalization of EGFR following EGF stimulation limits its capacity to efficiently induce the production of PIP_3 at the plasma membrane and engage Akt signaling (**Fig.19B, D**). However, internalized EGFR can continue to activate signaling effectors such as Erk from endosomal membranes, resulting in comparable amplitudes of Erk phosphorylation between both growth factors (**Fig.17A, Fig.19D**). Modulating EGFR trafficking by different types of context, such as ligand concentration, ligand identity or cell-cell contacts can generate considerable plasticity in EGFR function to alter cellular behavior. The dichotomy between lysosomal degradation and recycling, for example, determines signaling duration[72,140]. Furthermore, a recent study revealed that cell-cell interactions can alter the spatial distribution of EGFR activity, thereby selectively suppressing pro-migratory receptor signaling from the plasma membrane, while preserving proliferative endosomal signaling[66]. Similar relationships, have also been reported for other RTKs, such as PDGFR or Met[141,142]. In contrast, the spatial confinement of the active ErbB2/3 heterodimer to the plasma membrane could potentially limit its functional plasticity, as compared to receptor systems, that possess tunable vesicular dynamics. As various different receptor molecules can elicit similar cellular behaviors within a given cellular system, it seems plausible, that cellular responses to ErbB receptor activation are governed by the context-

dependent spatiotemporal distribution of active receptors rather than relying solely on their molecular identity.

5.2.2 KSR enhances Erk activation at the PM

Scaffold proteins can assemble multiprotein complexes to coordinate Erk activation from various subcellular localizations (e.g. PM, endosomes, golgi, nucleus)[124]. Using CRISPR-Cas9 genome editing, to knockout the plasma membrane scaffolds KSR1/2, we find that KSR knockout specifically attenuated HRG-induced Erk phosphorylation and signaling, while EGF-induced Erk phosphorylation was not affected. The contrasting effects of KSR knockout on the EGF- versus or HRG-induced Erk signaling are the result of the different spatiotemporal patterns of ErbB activity generated by these ligands (PM versus endosomes). On the other hand, EGF-induced endosomal Erk signaling might be facilitated by an endosomal scaffold protein, such as MP1[143]. The local confinement of Erk activity towards subcellular structures and the cytosolic localization of inactivating phosphatases have further been suggested to generate spatial gradients of Erk activity[5,144]. The signal-dependent localization of Erk activity to distinct subcellular localizations via scaffold proteins could thereby provide a mechanism to direct Erk activity towards specific local pools of substrates[104]. Aside from the localization and the physical assembly of molecular components, scaffold proteins can further generate diverse functions by insulating signaling modules or the direction of feedback regulation[145]. A recent study revealed that the input sensitivity of the Erk module is determined by its subcellular location[146]. At the plasma membrane, the Erk module is sensitive to low-level input, whereas the threshold for activation is high in the cytosol. At the plasma membrane KSR might thereby not only influence the amplitude of Erk activity, but also determine the sensitivity of the module towards different ligand concentrations.

5.2.3 EGF and HRG promote Erk-dependent cell proliferation

Differences in the spatial and temporal organization of signaling molecules plays a key role modulating their context-dependent function, thereby ultimately controlling cellular responses. The different spatial organization of ErbB receptor kinase activity in response to EGF and HRG stimulation were found to promote the activation of Erk from different subcellular compartments (endosomes and plasma membrane, respectively). We assessed whether these differences in the spatial dynamics of Erk correlate with different cellular outcomes. EGF and HRG induced a similar, Erk-

dependent increase in cellular proliferation (**Fig.21**). In agreement with this notion, it was previously reported, that both ligands induce transient nuclear Erk activity, while HRG additionally promotes sustained cytoplasmic Erk activity[107]. The transient nuclear Erk activity upon HRG stimulation was explained due to an elevated expression of nuclear localized dual specific phosphatases (DUSPs), inactivating Erk in the nucleus over time[107]. Comparable nuclear activity of Erk in response to HRG and EGF, might therefore account for the similar increase in cellular proliferation. Furthermore, previous studies identified, distinct periods of competency for cell-cycle induction by Erk[147,148]. Such a process might further restrain the ability of different Erk kinetics (transient versus sustained) to prime different populations of cells for cell-cycle progression, resulting in comparable levels of proliferation within the observed time frame (24 h). Furthermore, our findings imply that proliferative Erk signals are transmitted to the nucleus, irrespective of their spatial origin (endosomes and plasma membrane, respectively).

5.2.4 Membrane proximal Erk signaling promotes cellular motility

Directional cellular movement requires cells to remain responsive to the chemoattractant for prolonged periods of times. Accumulating evidence suggests that HRG ligands promote tumorigenesis of breast cancer cells by increasing both, cellular proliferation and invasion[149,150,151]. In agreement with this, we observe that persistent plasma membrane receptor activity upon HRG stimulation, correlates with enhanced cellular motility, as compared to finite EGFR signaling upon EGF stimulation (**Fig.22B, F**). Single cell measurements further indicated, that HRG increases the overall cellular motility rather than affecting the intrinsic persistence of migration **(Fig.22F)**. This HRG-induced increase in cellular motility was dependent on Erk activity, as Mek inhibition, strongly attenuated cellular migration (**Fig.22C**). Consistent with this notion, we observed the Erk-dependent phosphorylation of various effector molecules involved in the regulation of cellular motility in response to HRG stimulation, but not upon EGF stimulation (**Fig.23A, E**). In addition to the temporal regulation of Erk activity, the spatial organization of ErbB kinase activity may further enable the cell to generate different pools of active Erk with distinct functionality (transcriptional activity in the nucleus and local morphogenetic function at the plasma membrane). Such a dual functionality has been suggested for the mating-pheromone MAPK cascade in yeast, in which membrane proximal activity of

the MAPK Fus3 locally affects cytoskeletal structures, whereas in the nucleus it affects gene expression[46,152]. In agreement with this, we found that pro-migratory phosphorylation of EphA2 on serine 897 (S897), relies on membrane proximal Erk activity (**Fig.23A, C**). In previous studies, phospho-S897-EphA2 was found to localize to the leading edge of migrating cells, promoting the assembly of actin cytoskeleton and extension of lamellipodia[127]. Localized phosphorylation of S897 might thereby provide a mechanism to promote cell motility in a spatially controlled manner. In addition to membrane proximal Erk signaling, the HRG-induced pro-migratory behavior is most likely further facilitated by the activation plasma membrane signaling events, such as PIP_3 production and Akt activation (**Fig.19B, E**).

To test whether the plasma membrane scaffold KSR contributes to cellular migration, the migratory behavior of KSR1/2 knockout cells was examined. Knockout of KSR1/2 enhanced the motility of individual cells but reduced their intrinsic directionality and further the coordinated movement of cell groups during collective migration (**Fig.24**). KSR proteins might therefore exert a dual role regarding cellular migration, by reducing the overall motility of single cells to allow for the maintenance of cell-cell contacts and thereby enhance the efficiency of collective cellular movement. Furthermore, KSR1/2 knockout cells displayed a strong migratory response upon EGF stimulation, as compared to wild type cells. In this regard, it could be speculated, that the knockout of KSR causes the loss of an Erk-mediated negative feedback, such as phosphorylation of Thr669 in the juxtamembrane segment of EGFR and thereby enhances the overall activity of EGFR[153]. However, in addition to their interactions with components of the MAPK cascade, KSR proteins have been shown to interact with a multitude of other signaling molecules[154]. In this regard, pleiotropic effects on a complex cellular phenotype such as migration, due to chronic genetic perturbations could not be excluded.

Collectively our findings suggest that the confinement of active Erk to membrane proximal regions is a possible means to promote cellular motility, as pro-migratory phosphorylation of the EphA2 S897 was dependent on the presence of membrane proximal Erk activity (**Fig.23E**). In contrast, proliferative Erk signals are transmitted to the nucleus, irrespective of their spatial origin (**Fig.26**). Differences in the spatial distribution of active ErbB receptors due to different vesicular trafficking determine

the spatial distribution of Erk activity and thereby modulate its interaction with different pools of substrates to generate different cellular responses.

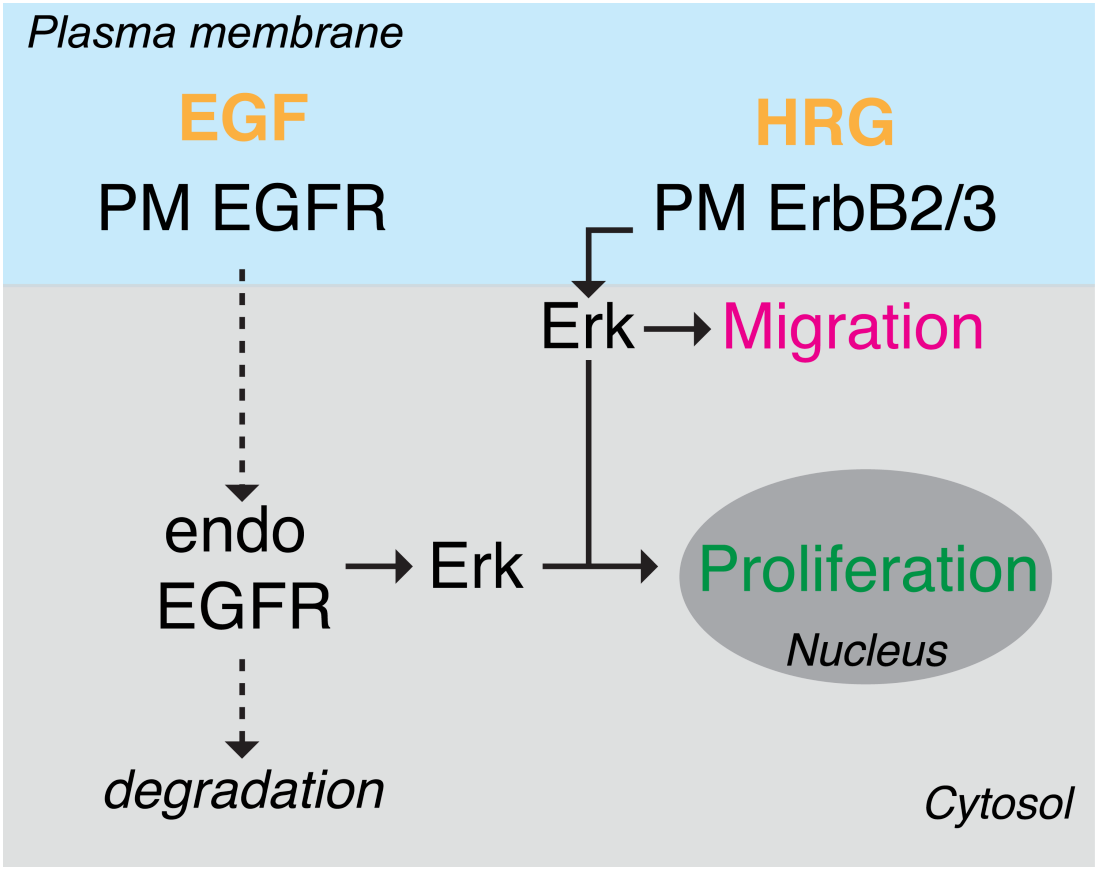

Figure 26: EGF-and HRG-induced ErbB/Erk dynamics. EGF and HRG promote the activation of Erk from distinct subcellular localizations (endosomes and PM, respectively). Proliferative Erk signals are transmitted to the nucleus, irrespective of their spatial origin, while HRG-induced membrane proximal Erk signaling promotes the phosphorylation of migratory effectors such as S897 of EphA2.

6 References

1. Rue, P. & Martinez Arias, A. Cell dynamics and gene expression control in tissue homeostasis and development. *Mol. Syst. Biol.* **11,** 792–792 (2015).

2. Biteau, B., Hochmuth, C. E. & Jasper, H. Maintaining tissue homeostasis: Dynamic control of somatic stem cell activity. *Cell Stem Cell* **9,** 402–411 (2011).

3. Koseska, A. & Bastiaens, P. I. Cell signaling as a cognitive process. *EMBO J.* **36,** 568–582 (2017).

4. Santos, S. D. M., Verveer, P. J. & Bastiaens, P. I. H. Growth factor-induced MAPK network topology shapes Erk response determining PC-12 cell fate. *Nat. Cell Biol.* **9,** 324–30 (2007).

5. Kholodenko, B. N. Cell-signalling dynamics in time and space. *Nat. Rev. Mol. Cell Biol.* **7,** 165–76 (2006).

6. Duncan, J. S. *et al.* Dynamic reprogramming of the kinome in response to targeted MEK inhibition in triple-negative breast cancer. *Cell* **149,** 307–21 (2012).

7. Kholodenko, B. N., Hancock, J. F. & Kolch, W. Signalling ballet in space and time. *Nat. Rev. Mol. Cell Biol.* **11,** 414–26 (2010).

8. Dehmelt, L. & Bastiaens, P. I. H. Spatial organization of intracellular communication: insights from imaging. *Nat. Rev. Mol. Cell Biol.* **11,** 440–52 (2010).

9. Purvis, J. E. & Lahav, G. Encoding and decoding cellular information through signaling dynamics. *Cell* **152,** 945–56 (2013).

10. Scott, J. D. & Pawson, T. *Cell signaling in space and time: Where proteins come together and when they're apart*. *Science* **326,** 1220–4 (American Association for the Advancement of Science, 2009).

11. Lee, M. J. *et al.* Sequential application of anticancer drugs enhances cell death by rewiring apoptotic signaling networks. *Cell* **149,** 780–94 (2012).

12. Zhao, S. & Iyengar, R. Systems pharmacology: network analysis to identify

multiscale mechanisms of drug action. *Annu. Rev. Pharmacol. Toxicol.* **52,** 505–21 (2012).

13. Uings, I. J. & Farrow, S. N. Cell receptors and cell signalling. *J Clin Pathol Mol Pathol* **53,** 295–299 (2000).

14. Lemmon, M. a & Schlessinger, J. Cell signaling by receptor tyrosine kinases. *Cell* **141,** 1117–1134 (2010).

15. Yarden, Y. & Sliwkowski, M. X. Untangling the ErbB signalling network. *Nat. Rev. Mol. Cell Biol.* **2,** 127–37 (2001).

16. Roskoski, R. The ErbB/HER family of protein-tyrosine kinases and cancer. *Pharmacol. Res.* **79,** 34–74 (2014).

17. Lemmon, M. a, Schlessinger, J. & Ferguson, K. M. The EGFR Family: Not So Prototypical Receptor Tyrosine Kinases. *Cold Spring Harb. Perspect. Biol.* **6,** (2014).

18. Ushiro, H., Cohen, S. & Cohens, S. Identification of Phosphotyrosine as a Product of Epidermal Growth Factor-activated Protein Kinase in A-431 Cell Membranes. *J. Biol. Chem.* **255,** 8363–8365 (1980).

19. Zhang, X., Gureasko, J., Shen, K., Cole, P. a & Kuriyan, J. An allosteric mechanism for activation of the kinase domain of epidermal growth factor receptor. *Cell* **125,** 1137–49 (2006).

20. Schlessinger, J. Receptor tyrosine kinases: legacy of the first two decades. *Cold Spring Harb. Perspect. Biol.* **6,** (2014).

21. Moran, M. F. *et al.* Src homology region 2 domains direct protein-protein interactions in signal transduction. **87,** 8622–8626 (1990).

22. Batzer, a G., Blaikie, P., Nelson, K., Schlessinger, J. & Margolis, B. The phosphotyrosine interaction domain of Shc binds an LXNPXY motif on the epidermal growth factor receptor. *Mol. Cell. Biol.* **15,** 4403–4409 (1995).

23. Pinkas-Kramarski, R. *et al.* Diversification of Neu differentiation factor and epidermal growth factor signaling by combinatorial receptor interactions. *EMBO J.* **15,** 2452–2467 (1996).

24. Freed, D. M. *et al.* EGFR Ligands Differentially Stabilize Receptor Dimers to Specify Signaling Kinetics. *Cell* **171,** 683–695 (2017).

25. Sibilia, M. *et al.* The epidermal growth factor receptor: from development to tumorigenesis. *Differentiation.* **75,** 770–87 (2007).

26. Yu, F.-S. X., Yin, J., Xu, K. & Huang, J. Growth factors and corneal epithelial wound healing. *Brain Res. Bull.* **81,** 229–35 (2010).

27. Normanno, N. *et al.* Epidermal growth factor receptor (EGFR) signaling in cancer. *Gene* **366,** 2–16 (2006).

28. Arteaga, C. L. & Engelman, J. a. ERBB Receptors: From Oncogene Discovery to Basic Science to Mechanism-Based Cancer Therapeutics. *Cancer Cell* **25,** 282–303 (2014).

29. Rowinsky, E. K. The erbB family: targets for therapeutic development against cancer and therapeutic strategies using monoclonal antibodies and tyrosine kinase inhibitors. *Annu. Rev. Med.* **55,** 433–57 (2004).

30. Han, W. & Lo, H.-W. Landscape of EGFR signaling network in human cancers: Biology and therapeutic response in relation to receptor subcellular locations. *Cancer Lett.* **318,** 124–134 (2012).

31. Kovacs, E., Zorn, J. A., Huang, Y., Barros, T. & Kuriyan, J. A Structural Perspective on the Regulation of the Epidermal Growth Factor Receptor. *Annu. Rev. Biochem.* **84,** 739–764 (2015).

32. Ferguson, K. M. *et al.* EGF Activates Its Receptor by Removing Interactions that Autoinhibit Ectodomain Dimerization. *Mol. Cell* **11,** 507–517 (2003).

33. Jura, N. *et al.* Catalytic control in the EGF receptor and its connection to general kinase regulatory mechanisms. *Mol. Cell* **42,** 9–22 (2011).

34. Shan, Y. *et al.* Oncogenic mutations counteract intrinsic disorder in the EGFR kinase and promote receptor dimerization. *Cell* **149,** 860–70 (2012).

35. Huse, M. & Kuriyan, J. The conformational plasticity of protein kinases. *Cell* **109,** 275–82 (2002).

36. Endres, N. F. *et al.* Conformational coupling across the plasma membrane in

activation of the EGF receptor. *Cell* **152,** 543–56 (2013).

37. Arkhipov, A. *et al.* Architecture and membrane interactions of the EGF receptor. *Cell* **152,** 557–69 (2013).

38. Jura, N. *et al.* Mechanism for activation of the EGF receptor catalytic domain by the juxtamembrane segment. *Cell* **137,** 1293–307 (2009).

39. Huang, Y. *et al.* Molecular basis for multimerization in the activation of the epidermal growth factor receptor. *Elife* **5,** e14107 (2016).

40. Needham, S. R. *et al.* EGFR oligomerization organizes kinase-active dimers into competent signalling platforms. *Nat. Publ. Gr.* **7,** (2016).

41. Reynolds, A. R., Tischer, C., Verveer, P. J., Rocks, O. & Bastiaens, P. I. H. EGFR activation coupled to inhibition of tyrosine phosphatases causes lateral signal propagation. *Nat. Cell Biol.* **5,** 447–53 (2003).

42. Low-Nam, S. T. *et al.* ErbB1 dimerization is promoted by domain co-confinement and stabilized by ligand binding. *Nat. Publ. Gr.* **18,** (2011).

43. Baumdick, M. *et al.* A conformational sensor based on genetic code expansion reveals an 1 autocatalytic component in EGFR activation 2 3. *Biorxiv* (2018). doi:10.1101/314682

44. Peter J. Verveer, Fred S. Wouters, Andrew R. Reynolds, P. I. H. B. Quantitative Imaging of Lateral ErbB1 Receptor Signal Propagation in the Plasma Membrane. *Science (80-.).* **290,** 1567–1570 (2000).

45. Sawano, A., Takayama, S., Matsuda, M. & Miyawaki, A. Lateral propagation of EGF signaling after local stimulation is dependent on receptor density. *Dev. Cell* **3,** 245–57 (2002).

46. Grecco, H. E., Schmick, M. & Bastiaens, P. I. H. Signaling from the living plasma membrane. *Cell* **144,** 897–909 (2011).

47. Rhee, S. G. H2O2, a necessary evil for cell signaling. *Science* (2006). doi:10.1126/science.1130481

48. Rhee, S. G. *et al.* Epidermal Growth Factor (EGF)-induced Generation of Hydrogen Peroxide. *J. Biol. Chem.* **272,** 217–221 (1997).

49. Salmeen, A. *et al.* Redox regulation of protein tyrosine phosphatase 1B involves a sulphenyl-amide intermediate. *Nature* **423,** 769–773 (2003).

50. Tischer, C. & Bastiaens, P. I. H. Lateral phosphorylation propagation: An aspect of feedback signalling? *Nature Reviews Molecular Cell Biology* (2003). doi:10.1038/nrm1258

51. Kaplan, M. *et al.* EGFR Dynamics Change during Activation in Native Membranes as Revealed by NMR. *Cell* **167,** 1241–1251 (2016).

52. Sorkin, A. & Goh, L. Endocytosis and intracellular trafficking of ErbBs. *Exp. Cell Res.* **314,** 3093–3106 (2009).

53. Kleiman, L. B., Maiwald, T., Conzelmann, H., Lauffenburger, D. A. & Sorger, P. K. Rapid phospho-turnover by receptor tyrosine kinases impacts downstream signaling and drug binding. *Mol. Cell* **43,** 723–37 (2011).

54. Huyer, G. *et al.* Mechanism of Inhibition of Protein-tyrosine Phosphatases by Vanadate and Pervanadate *. **272,** 843–851 (1997).

55. Offterdinger, M., Georget, V., Girod, A. & Bastiaens, P. I. H. Imaging phosphorylation dynamics of the epidermal growth factor receptor. *J. Biol. Chem.* **279,** 36972–81 (2004).

56. Fan, Y. X., Wong, L., Deb, T. B. & Johnson, G. R. Ligand regulates epidermal growth factor receptor kinase specificity: Activation increases preference for Gab1 and Shc versus autophosphorylation sites. *J. Biol. Chem.* **279,** 38143–38150 (2004).

57. Zhang, Z. Y., Maclean, D., Thiemesefler, A. M., Roeske, R. W. & Dixon, J. E. A Continuous Spectrophotometric and Fluorometric Assay for Protein Tyrosine Phosphatase Using Phosphotyrosine-Containing Peptides. *Anal. Biochem.* **211,** 7–15 (1993).

58. Phosphatases, P. *et al.* Diverse Levels of Sequence Selectivity and Catalytic Efficiency of Protein-Tyrosine Phosphatases. *Biochemistry* **53,** 397–412 (2014).

59. Yudushkin, I. a *et al.* Live-cell imaging of enzyme-substrate interaction reveals spatial regulation of PTP1B. *Science* **315,** 115–9 (2007).

60. Hutagalung, A. & Novick, P. Role of Rab GTPases in membrane traffic and cell physiology. *Physiol. Rev.* **91,** 119–149 (2011).

61. Stenmark, H. Rab GTPases as coordinators of vesicle traffic. *Nat. Rev. Mol. Cell Biol.* **10,** 513–25 (2009).

62. Zerial, M. & McBride, H. Rab proteins as membrane organisers. *Nat. Rev. Mol. Cell Biol.* **2,** 107–117 (2001).

63. Rink, J., Ghigo, E., Kalaidzidis, Y. & Zerial, M. Rab conversion as a mechanism of progression from early to late endosomes. *Cell* **122,** 735–49 (2005).

64. Maxfield, F. R. & McGraw, T. E. Endocytic recycling. *Nat. Rev. Mol. Cell Biol.* **5,** 121–32 (2004).

65. Hutagalung, A. H. & Novick, P. J. Role of Rab GTPases in Membrane Traffic and Cell Physiology.

66. Stallaert, W., Sabet, O., Brüggemann, Y., Baak, L. & Philippe, I. H. Contact inhibitory Eph signaling suppresses EGF-promoted cell migration by decoupling EGFR activity from vesicular recycling. (2017).

67. Ceresa, B. P. Regulation of EGFR endocytic trafficking by rab proteins. *Histol. Histopathol.* **21,** 987–93 (2006).

68. Wiley, H. Trafficking of the ErbB receptors and its influence on signaling. *Exp. Cell Res.* **284,** 78–88 (2003).

69. Herbst, J. J., Opresko, L. K., Walsh, B. J., Lauffenburger, D. a & Wiley, H. S. Regulation of postendocytic trafficking of the epidermal growth factor receptor through endosomal retention. *J. Biol. Chem.* **269,** 12865–73 (1994).

70. Di Guglielmo, G. M., Baass, P. C., Ou, W. J., Posner, B. I. & Bergeron, J. J. Compartmentalization of SHC, GRB2 and mSOS, and hyperphosphorylation of Raf-1 by EGF but not insulin in liver parenchyma. *EMBO J.* **13,** 4269–77 (1994).

71. Polo, S., Di Fiore, P. P. & Sigismund, S. Keeping EGFR signaling in check: ubiquitin is the guardian. *Cell Cycle* **13,** 681–2 (2014).

72. Sigismund, S. *et al.* Clathrin-mediated internalization is essential for sustained

EGFR signaling but dispensable for degradation. *Dev. Cell* **15,** 209–19 (2008).

73. Sigismund, S. *et al.* Threshold-controlled ubiquitination of the EGFR directs receptor fate. *EMBO J.* **32,** 2140–57 (2013).

74. Grøvdal, L. M., Stang, E., Sorkin, A. & Madshus, I. H. Direct interaction of Cbl with pTyr 1045 of the EGF receptor (EGFR) is required to sort the EGFR to lysosomes for degradation. *Exp. Cell Res.* **300,** 388–395 (2004).

75. Levkowitz, G. *et al.* c-Cbl/Sli-1 regulates endocytic sorting and ubiquitination of the epidermal growth factor receptor. *Genes Dev.* **12,** 3663–3674 (1998).

76. Xuejun Jiang, Fangtian Huang, Andriy Marusyk, and A. S. Grb2 Regulates Internalization of EGF Receptors through Clathrin-coated Pits Xuejun. *Mol. Biol. Cell* **14,** 2372–2384 (2003).

77. Eden, E., White, I., Tsapara, A. & Futter, C. Membrane contacts between endosomes and ER provide sites for PTP1B–epidermal growth factor receptor interaction. *Nat. Cell Biol.* **12,** 267–272 (2010).

78. Haj, F. G., Verveer, P. J., Squire, A., Neel, B. G. & Bastiaens, P. I. H. Imaging sites of receptor dephosphorylation by PTP1B on the surface of the endoplasmic reticulum. *Science* **295,** 1708–11 (2002).

79. Rozakis-Adcock, M., Fernley, R., Wade, J., Pawson, T. & Bowtell, D. The SH2 and SH3 domains of mammalian Grb2 couple the EGF receptor to the Ras activator mSos1. *Nature* **363,** 83–85 (1993).

80. Li, N. *et al.* Guanine-nucleotide-releasing factor hSos1 binds to Grb2 and links receptor tyrosine kinases to Ras signalling. *Nature* **363,** 85–88 (1993).

81. Egan, S. E. *et al.* Association of Sos Ras exchange protein with Grb2 is implicated in tyrosine kinase signal transduction and transformation. *Nature* (1993). doi:10.1038/363045a0

82. Chang, L. & Karin, M. Mammalian MAP kinase signalling cascades. *Nature* **410,** 37–40 (2001).

83. Widmann, C., Gibson, S., Jarpe, M. B. & Johnson, G. L. Mitogen-activated protein kinase: conservation of a three-kinase module from yeast to human.

Physiol. Rev. **79,** 143–80 (1999).

84. Li, M., Liu, J. & Zhang, C. Evolutionary history of the vertebrate mitogen activated protein kinases family. *PLoS One* **6,** e26999 (2011).

85. Cargnello, M. & Roux, P. P. Activation and Function of the MAPKs and Their Substrates, the MAPK-Activated Protein Kinases. *Microbiol. Mol. Biol. Rev.* **75,** 50–83 (2011).

86. Davis, R. J. The mitogen-activated protein kinase signal transduction. *J. Biol. Chem.* **268,** 14553–14556 (1993).

87. Tanoue, T. & Nishida, E. Docking interactions in the mitogen-activated protein kinase cascades. *Pharmacol. Ther.* **93,** 193–202 (2002).

88. Tidyman, W. E. & Rauen, K. A. The RASopathies: Developmental syndromes of Ras/MAPK pathway dysregulation. doi:10.1016/j.gde.2009.04.001

89. Dhillon, A., Hagan, S., Rath, O. & Kolch, W. MAP kinase signalling pathways in cancer. *Oncogene* **26,** 3279–3290 (2007).

90. Kim, E. K. & Choi, E.-J. Pathological roles of MAPK signaling pathways in human diseases. *BBA - Mol. Basis Dis.* **1802,** 396–405 (2010).

91. Plotnikov, A., Zehorai, E., Procaccia, S. & Seger, R. The MAPK cascades: signaling components, nuclear roles and mechanisms of nuclear translocation. *Biochim. Biophys. Acta* **1813,** 1619–33 (2011).

92. Downward, J. Targeting RAS signalling pathways in cancer therapy. *Nat. Rev. Cancer* **3,** 11–22 (2003).

93. Schmick, M. & Bastiaens, P. I. H. The Interdependence of Membrane Shape and Cellular Signal Processing. *Cell* **156,** 1132–1138 (2014).

94. Lavoie, H. & Therrien, M. Regulation of RAF protein kinases in ERK signalling. *Nat. Rev. Mol. Cell Biol.* **16,** 281–298 (2015).

95. Roskoski, R. MEK1/2 dual-specificity protein kinases: structure and regulation. *Biochem. Biophys. Res. Commun.* **417,** 5–10 (2012).

96. Roskoski, R. ERK1/2 MAP kinases: structure, function, and regulation.

Pharmacol. Res. **66,** 105–43 (2012).

97. Caunt, C. J. & Keyse, S. M. Dual-specificity MAP kinase phosphatases (MKPs): Shaping the outcome of MAP kinase signalling. *FEBS Journal* **280,** 489–504 (2013).

98. Yoon, S. & Seger, R. The extracellular signal-regulated kinase: multiple substrates regulate diverse cellular functions. *Growth Factors* **24,** 21–44 (2006).

99. Chen, R. H., Sarnecki, C. & Blenis, J. Nuclear localization and regulation of erk- and rsk-encoded protein kinases. *Mol. Cell. Biol.* **12,** 915–927 (1992).

100. von Kriegsheim, A. *et al.* Cell fate decisions are specified by the dynamic ERK interactome. *Nat. Cell Biol.* **11,** 1458–64 (2009).

101. Shaul, Y. D. & Seger, R. *The MEK/ERK cascade: From signaling specificity to diverse functions*. *Biochimica et Biophysica Acta - Molecular Cell Research* **1773,** 1213–1226 (Elsevier, 2007).

102. Roberts, P. J. & Der, C. J. Targeting the Raf-MEK-ERK mitogen-activated protein kinase cascade for the treatment of cancer. *Oncogene* **26,** 3291–310 (2007).

103. Herrero, A. & Casar, B. Defined spatiotemporal features of RAS-ERK signals dictate cell fate in MCF-7 mammary epithelial cells. *Mol. Biol. …* 1–35 (2016).

104. Casar, B. & Crespo, P. ERK Signals: Scaffolding Scaffolds? *Front. cell Dev. Biol.* **4,** 49 (2016).

105. Marshall, C. J. & Laboratories, C. B. Specificity of Receptor Tyrosine Kinase Signaling : Transient versus Sustained Extracellular Signal-Regulated Kinase Activation. **2,** 179–185 (1995).

106. Murphy, L. O., Smith, S., Chen, R.-H., Fingar, D. C. & Blenis, J. Molecular interpretation of ERK signal duration by immediate early gene products. *Nat. Cell Biol.* **4,** (2002).

107. Nakakuki, T. *et al.* Ligand-specific c-Fos expression emerges from the spatiotemporal control of ErbB network dynamics. *Cell* **141,** 884–96 (2010).

108. Uhlitz, F. *et al.* An immediate–late gene expression module decodes ERK signal duration. *Mol. Syst. Biol.* **13,** 928 (2017).

109. Casar, B., Pinto, A. & Crespo, P. Essential role of ERK dimers in the activation of cytoplasmic but not nuclear substrates by ERK-scaffold complexes. *Mol. Cell* **31,** 708–21 (2008).

110. Casar, B. *et al.* Ras Subcellular Localization Defines Extracellular Signal-Regulated Kinase 1 and 2 Substrate Specificity through Distinct Utilization of Scaffold Proteins. *Mol. Cell. Biol.* **29,** 1338–1353 (2009).

111. Michailovici, I. *et al.* Nuclear to cytoplasmic shuttling of ERK promotes differentiation of muscle stem/progenitor cells. *Development* **141,** 2611–20 (2014).

112. Zeke, A., Lukács, M., Lim, W. a & Reményi, A. Scaffolds: interaction platforms for cellular signalling circuits. *Trends Cell Biol.* **19,** 364–74 (2009).

113. Schindelin, J. *et al.* Fiji: an open-source platform for biological-image analysis. *Nat. Methods* **9,** 676–682 (2012).

114. Kamentsky, L. *et al.* Improved structure, function and compatibility for CellProfiler: modular high-throughput image analysis software. *Bioinformatics* **27,** 1179–1180 (2011).

115. Ran, F. A. *et al.* Genome engineering using the CRISPR-Cas9 system. **8,** 2281–2308 (2013).

116. Baumdick, M. *et al.* EGF-dependent re-routing of vesicular recycling switches spontaneous phosphorylation suppression to EGFR signaling. *Elife* (2015).

117. Squire, A., Verveer, P. J., Rocks, O. & Bastiaens, P. I. H. Red-edge anisotropy microscopy enables dynamic imaging of homo-FRET between green fluorescent proteins in cells. *J. Struct. Biol.* **147,** 62–9 (2004).

118. Mayor, S. & Varma, R. GPI-anchored proteins are organized in submicron domains at the cell surface. *Nature* **394,** 798–801 (1998).

119. Ullrich, O., Reinsch, S., Urbé, S., Zerial, M. & Parton, R. G. Rab11 regulates recycling through the pericentriolar recycling endosome. *J. Cell Biol.* **135,** 913–

924 (1996).

120. Flint, A. J., Tiganis, T., Barford, D. & Tonks, N. K. Development of '"substrate-trapping"' mutants to identify physiological substrates of protein tyrosine phosphatases. *Biochemistry* **94,** 1680–1685 (1997).

121. Grecco, H. E., Roda-Navarro, P. & Verveer, P. J. Global analysis of time correlated single photon counting FRET-FLIM data. *Opt. Express* **17,** 6493 (2009).

122. Toettcher, J. E., Gong, D., Lim, W. A. & Weiner, O. D. Light-based feedback for controlling intracellular signaling dynamics. doi:10.1038/nmeth.1700

123. Villaseñor, R., Kalaidzidis, Y., Zerial, M. & Villasen, R. Signal processing by the endosomal system. *Curr. Opin. Cell Biol.* **39,** 53–60 (2016).

124. Kolch, W. Coordinating ERK/MAPK signalling through scaffolds and inhibitors. *Nat. Rev. Mol. Cell Biol.* **6,** 827–37 (2005).

125. McKay, M. M., Ritt, D. a & Morrison, D. K. Signaling dynamics of the KSR1 scaffold complex. *Proc. Natl. Acad. Sci. U. S. A.* **106,** 11022–7 (2009).

126. Tanimura, S. & Takeda, K. ERK signalling as a regulator of cell motility. *Journal of biochemistry* (2017). doi:10.1093/jb/mvx048

127. Miao, H. *et al.* EphA2 Mediates Ligand-Dependent Inhibition and Ligand-Independent Promotion of Cell Migration and Invasion via a Reciprocal Regulatory Loop with Akt. *Cancer Cell* **16,** 9–20 (2009).

128. Zhou, Y. *et al.* Crucial roles of RSK in cell motility by catalysing serine phosphorylation of EphA2. *Nat. Commun.* **6,** 7679 (2015).

129. Tanimura, S. & Takeda, K. Erk as a regulator of cell motility. **162,** 145–154 (2017).

130. Mendoza, M. C. *et al.* ERK-MAPK Drives Lamellipodia Protrusion by Activating the WAVE2 Regulatory Complex. *Mol. Cell* **41,** 661–671 (2011).

131. Friedl, P. & Gilmour, D. Collective cell migration in morphogenesis, regeneration and cancer. *Nat. Rev. Mol. Cell Biol.* **10,** 445–457 (2009).

132. Chakraborty, S. *et al.* Constitutive and ligand-induced EGFR signalling triggers distinct and mutually exclusive downstream signalling networks. *Nat. Commun.* **5,** 5811 (2014).

133. Schlessinger, J. Cell Signaling by Receptor Tyrosine Kinases A large group of genes in all eukaryotes encode for. *Cell* **103,** 211–225 (2000).

134. Sturm, O. E. *et al.* The Mammalian MAPK / ERK Pathway Exhibits Properties of a Negative Feedback Amplifier. **3,** 1–8 (2010).

135. Lake, D., Corrêa, S. a L. & Müller, J. Negative feedback regulation of the ERK1/2 MAPK pathway. *Cell. Mol. Life Sci.* (2016). doi:10.1007/s00018-016-2297-8

136. Tomas, A., Futter, C. E. & Eden, E. R. EGF receptor trafficking: consequences for signaling and cancer. *Trends Cell Biol.* **24,** 26–34 (2014).

137. Thien, C. B. & Langdon, W. Y. EGF receptor binding and transformation by v-cbl is ablated by the introduction of a loss-of-function mutation from the Caenorhabditis elegans sli-1 gene.

138. Shtiegman, K. *et al.* Defective ubiquitinylation of EGFR mutants of lung cancer confers prolonged signaling. *Oncogene* **26,** 6968–6978 (2007).

139. Sabet, O. *et al.* Ubiquitination switches EphA2 vesicular traffic from a continuous safeguard to a finite signalling mode. *Nat. Commun.* **6,** 8047 (2015).

140. Francavilla, C. *et al.* Multilayered proteomics reveals molecular switches dictating ligand-dependent EGFR trafficking. doi:10.1038/nsmb.3218

141. De Donatis, A. *et al.* Proliferation versus migration in platelet-derived growth factor signaling: the key role of endocytosis. *J. Biol. Chem.* **283,** 19948–56 (2008).

142. Parachoniak, C. A., Luo, Y., Abella, J. V., Keen, J. H. & Park, M. GGA3 Functions as a Switch to Promote Met Receptor Recycling, Essential for Sustained ERK and Cell Migration. *Dev. Cell* **20,** 751–763 (2011).

143. Teis, D., Wunderlich, W. & Huber, L. A. Localization of the MP1-MAPK Scaffold

Complex to Endosomes Is Mediated by p14 and Required for Signal Transduction through the MAPK cascade. *Dev. Cell* **3,** 803–814 (2002).

144. Brown, G. C. & Kholodenko, B. N. Spatial gradients of cellular phospho-proteins. **457,** 452–454 (1999).

145. Good, M. C., Zalatan, J. G. & Lim, W. a. Scaffold proteins: hubs for controlling the flow of cellular information. *Science* **332,** 680–6 (2011).

146. Harding, A., Tian, T., Westbury, E., Frische, E. & Hancock, J. F. Subcellular localization determines MAP kinase signal output. *Curr. Biol.* **15,** 869–73 (2005).

147. Jones, S. M. & Kazlauskas, A. Growth-factor-dependent mitogenesis requires two distinct phases of signalling. *Nat. Cell Biol.* **3,** 165–172 (2001).

148. Zwang, Y. *et al.* Two Phases of Mitogenic Signaling Unveil Roles for p53 and EGR1 in Elimination of Inconsistent Growth Signals. *Mol. Cell* **42,** 524–535 (2011).

149. Atlas, E. *et al.* Heregulin is sufficient for the promotion of tumorigenicity and metastasis of breast cancer cells in vivo. *Mol. cancer Res.* **1,** 165–175 (2003).

150. Yang, C., Liu, Y., Lemmon, M. A., Marcelo, G. & Kazanietz, M. G. Essential Role for Rac in Heregulin β 1 Mitogenic Signaling : a Mechanism That Involves Epidermal Growth Factor Receptor and Is Independent of ErbB4. *Mol. Cell. Biol.* **26,** 831–842 (2006).

151. Tsai, M. S., Shamon-Taylor, L. A., Mehmi, I., Tang, C. K. & Lupu, R. Blockage of heregulin expression inhibits tumorigenicity and metastasis of breast cancer. *Oncogene* **22,** 761–768 (2003).

152. Maeder, C. I. *et al.* Spatial regulation of Fus3 MAP kinase activity through a reaction-diffusion mechanism in yeast pheromone signalling. *Nat. Cell Biol.* **9,** 1319–26 (2007).

153. Li, X., Huang, Y., Jiang, J. & Frank, S. J. ERK-dependent threonine phosphorylation of EGF receptor modulates receptor downregulation and signaling. *Cell. Signal.* **20,** 2145–55 (2008).

154. Dougherty, M. K. *et al.* KSR2 is a calcineurin substrate that promotes ERK cascade activation in response to calcium signals. *Mol. Cell* **34,** 652–62 (2009).

7 Abbreviations

°C	Degree Celsius
a.u.	Arbitrary units
Akt/PKB	Protein kinase B
ANOVA	Analysis of variance
ATP	Adenosine triphosphate
BFP	Blue fluorescent protein
C-terminus	Carboxyl terminus
CRISPR	Clustered Regularly Interspaced Short Palindromic Repeats
DMEM	Dulbecco's modified eagle medium
DNA	Deoxy ribonucleic acid
DTT	Dithiothreitol
DUSP	Dual-specificity phosphatase
EDTA	Ethylene diamine tetraacetic acid
EE	Early endosomes
EGF	Epidermal growth factor
eGFP	Enhanced green fluorescent protein
EGFR	Epidermal growth factor receptor
EphA2	Ephrin receptor type-A2
ER	Endoplasmatic reticulum
Erk	extracellular signal-regulated kinase
FBS	Fetal bovine serum
Fig.	Figure
FLIM	Fluorescence lifetime imaging microscopy
FRET	Förster resonance energy transfer
GEF	Guanine nucleotide exchange factors
GTP	Guanosine-5'-triphosphate

h	Hour
HRG	Heregulin
IP	Immunoprecipitation
kB	Kilo base pair
LAMP1	Lysosomal-associated membrane protein 1
LE	Late endosome
m	Meter
MAPK	Mitogen-activated protein kinase
MAPKK	Mitogen-activated protein kinase kinase
MAPKKK	Mitogen-activated protein kinase kinase kinase
mCherry	monomeric Cherry
mCitrine	monomeric Citrine
Min	Minute
ml	Milliliter
mM	Millimolar
n	Nano
N-Terminus	Amino-terminus
NA	Numerical aperture
NEAA	Non-essential amino acids
ng	Nanogram
NGF	Nerve growth factor
PAGE	polyacrylamide gel electrophoresis
PBS	Phosphate buffered saline
PCR	Polymerase chain reaction
PD03	Mek inhibitor PD0325901
PH	Pleckstrin homology domain
PI3K	Phosphoinositide-3-kinase
PIP3	Phosphatidylinositol (3,4,5)-trisphosphate

PM	Plasma membrane
pRb	Phosphorylated retinoblastoma protein
PTB	Phosphotyrosine-binding domain
PTP	Protein tyrosine phosphatase
PV	Pervanadate
pY	Phospho tyrosine
RE	Recycling endosome
ROS	Reactive oxygen species
RTK	Receptor tyrosine kinase
s	Second
s.d.	Standard deviation
s.e.m.	Standard error of mean
SDS	Sodium dodecyl sulphate
SH2	Src homology 2
siRNA	Small interfering RNA
SOS	Son of Sevenless
TAE	Tris-acetate-EDTA
TBS	Tris buffered salinetKRas
tKRas	Farnesyl tail of KRas
Ug	Micro
V	Volt
WT	Wild type
Y	Tyrosine
µ	Micro

8 Acknowlegements

First, I would like to thank Prof. Dr. Philippe Bastiaens for the opportunity to work on different interesting and exciting projects in his laboratory, but most importantly for his continuous guidance, motivation and encouragement during the last 1370 days.

I would also like to thank Prof. Dr. Andrea Musacchio for being the second examiner of this thesis and his valuable advice during my TAC meetings.

I convey a special thanks to Dr. Astrid Kramer, Tanja Forck, Christa Hornemann and Dr. Lucia Sironi for helping me with all kinds of administrative work.

Thank you, Jutta, Hendrike, Kirsten, Manuela, Lisaweta, Micha, Petra, Michelle and Michael for all your help and support in the lab. Also, thanks Sven for helping me numerous times with all our different microscopes.

Wayne and Amit!!!! Thank you for all the help and support along the way, working with you guys was amazing.

I would further like to thank all current and past members of Department 2, that are not mentioned by name, for all the good times, the help and discussions.

Finally, I would like to thank my parents for their continuous support during my PhD.

Thanks Jana, for always supporting me and especially for always being patient with me.

9 Publications and presentations

Results and methodologies presented in this thesis have contributed to the following peer-reviewed publications:

Yannick Brüggemann, Lisa Karajannis, Wayne Stallaert, Philippe I.H. Bastiaens. "Spatiotemporal modulation of Erk activity determines cell fate decisions". (In preparation).

Angel Stanoev, Amit Mhamane, Klaus C. Schuermann, Hernán E. Grecco, Wayne Stallaert, Martin Baumdick, Yannick Brüggemann, Maitreyi S. Joshi, Pedro Roda-Navarro, Sven Fengler, Rabea Stockert, Lisaweta Roßmannek, Jutta Luig, Aneta Koseska, and Philippe I. H. Bastiaens. "Interdependence between EGFR and phosphatases spatially established by vesicular dynamics generates a growth factor sensing and responding network". (Cell Systems, accepted in press).

Wayne Stallaert, Yannick Brüggemann, Ola Sabet, Lisa Baak, Marina Gattiglio and Philippe I.H. Bastiaens. "Contact inhibitory Eph signaling suppresses EGF-promoted cell migration by decoupling EGFR activity from vesicular recycling". (Science Signaling, accepted in press).

Martin Baumdick*, Yannick Brüggemann*, Malte Schmick*, Georgia Xouri*, Ola Sabet, Lloyd Davis, Jason W Chin, Philippe IH Bastiaens. "EGF-dependent re-routing of vesicular recycling switches spontaneous phosphorylation suppression to EGFR signaling". Elife, e12223 (2015) (*equal contribution).

Ola Sabet, Rabea Stockert, Georgia Xouri, Yannick Brüggemann, Angel Stanoev & Philippe I.H. Bastiaens (2015). "Ubiquitination switches EphA2 vesicular traffic from a continuous safeguard to a finite signaling mode". Nature Communications. 2015 (6).

The work was presented at the following conferences:

- IMPRS Symposium 2016 – "EGF-dependent rerouting of vesicular recycling switches spontaneous phosphorylation suppression to EGFR signaling" (Poster)
- ICSB, Barcelona, 2016 – "EGF-dependent rerouting of vesicular recycling switches spontaneous phosphorylation suppression to EGFR signaling" (Poster)